UNIVERSITY OF OKLAHOMA

GRADUATE COLLEGE

SYNTHESIS OF POLYMER NANOSTRUCTURES VIA THE USE OF SURFACTANT SURFACE AGGREGATES AS TEMPLATES

A DISSERTATION

SUBMITTED TO THE GRADUATE FACULTY

in partial fulfillment of the requirements for the

degree of

Doctor of Philosophy

By
MARICEL MARQUEZ
Norman, Oklahoma
2007

SYNTHESIS OF POLYMER NANOSTRUCTURES VIA THE USE OF SURFACTANT SURFACE AGGREGATES AS TEMPLATES

A DISSERTATION APPROVED FOR THE
SCHOOL OF CHEMICAL, BIOLOGICAL AND MATERIALS ENGINEERING

BY

_____
Dr. Brian Grady

_____
Dr. John Scamehorn

_____
Dr. Ian Robb

_____
Dr. Daniel Glatzhofer

_____
Dr. David Schmitdke

_____
Dr. Alberto Striolo

Dedicated to the Memory of my Brother, Jesus Enrique Marquez

Acknowledgements

Coming to OU as a part of the Study Abroad exchange program during my senior year at Simon Bolivar University was just the beginning of a life-changing experience. It was not only getting used to leaving far away from family and friends, but also adjusting to a new culture. Although not an easy process, I recall it as one of the best experiences in my life.

In my first year at OU, I met Heather and Bob Grimm, a wonderful couple who opened up their hearts, making me part of their lives and loving me as their true daughter. Thank you Mom and Bob for your love and support, without you this work would have not been possible.

Special thanks go to my graduate advisor Dr. Brian Grady, and to Dr. Lee Williams, vice president for research and dean of the Graduate College, for believing in me and for getting all the necessary paperwork filed expeditiously so that I could enroll at OU despite of all the inconvenience resulting from the political situation in Venezuela at the time. In addition, I would like to acknowledge Halliburton (especially Dr. Ian Robb), the Oklahoma State Regents, and the School of Chemical, Biological and Materials Engineering at OU for providing the financial support for my education and research projects. Thanks also to my graduate committee members for being willing to participate in this process and for their advice and technical guidance along the way.

Three key figures deserve much credit for this work; Dr. Andrew Carswell, the best mentor and friend anybody could ever have. Dr. Preston Larson for many fruitful discussions and help with SEM imaging, and Dr. Brian Grady for being a superb advisor, and for giving me the opportunity to grow both personally and academically. Special thanks to Soohyun Kim and Joomi Jung for much help with admicellar polymerization experiments, Krupa Patel and David Schmidtke for the protein adsorption work, and Nguyen Truong, and Dale Teeter for the electrical conductivity data. Working with people like you makes research fun and enjoyable!

I want to thank my husband Carlos for his loving patience and support along the way; especially during those times when my life seemed to be consumed by long hours of research and school. Thanks also for believing in me and for being my best friend. Your love Carlos truly gives direction to my life!

Finally, I am very grateful for my grandmother and my parents, for their love and all their many sacrifices. Without them I would not be the person who I am today. I want to dedicate this work to God, the source of everything, and to all of you who have touch my life in so many wonderful ways…Thank you very much!

Table of Contents

List of Tables

List of Equations

List of Figures

Abstract

The subject of this work is the synthesis of polymer nanostructures via the use of surfactant surface aggregates as templates, also termed Template Assisted Admicellar Polymerization (TAAP). The first chapter reviews some of the most current nanopatterning techniques (including both top-down and bottom-up approaches), with particular emphasis on the fabrication of organic and inorganic patterned nanostructures via particle lithography. In chapter 2, highly ordered hexagonal arrays of latex spheres were prepared on highly ordered pyrolytic graphite (HOPG) from a variation of the Langmuir Blodgett technique, using an anionic surfactant (SDS), and a low molecular weight (ca. 10000) polyacrylamide as spreading agents. When a nonionic polyethoxylated (EO = 9) surfactant was used as the spreading agent, no ordered arrays were observed. Based on the correlation found between the surface tension in the presence of the latex particles and the critical concentration at which hexagonal arrangements of latex spheres occurs; a model was proposed to explain the role of the spreading agent in forming stable monolayers at the air/liquid interface, which in turn are necessary for the formation of well-ordered monolayers on a solid substrate from the LB technique. According to this model, solid-like regions of small numbers of latex spheres form at the liquid-air interface, which are then transferred to the substrate. These ordered regions then act as nuclei for the formation of 2D arrays of latex

spheres on the surface upon water evaporation. The role of other factors such as relative humidity, substrate and solvent choice, and pulling vs. compression speed were also found to affect the quality of the monolayers formed. Finally, a simple, easy to automate, yet effective surface tension method was proposed to predict the optimal conditions for the formation of ordered monolayers using a variation of the LB deposition method from any monodisperse set of spheres.

In chapter 3, a novel method for the formation of nanometer-scale polymer structures on solid surfaces via template assisted admicellar polymerization (TAAP) is described. Admicellar polymerization uses a surfactant layer adsorbed on a surface to localize monomer to the surface prior to polymerization of the monomer. TAAP refers to nanostructures that form by restricting adsorption to the uncovered sites of an already-templated surface. In this case, the interstitial sites between adsorbed latex spheres were used as the template. Unlike most other process that form polymer nanostructures, polymer dimensions can be significantly smaller than the interstitial size because of sphere-surfactant-monomer interactions. As a proof of concept, nanostructures formed via TAAP were compared to structures prepared by others via adsorption of three different proteins (Bovine serum albumin, fibrinogen, and anti-mouse IgG) in the interstitial sites of colloidal monolayers. The size and shape of the nanostructures formed (honeycomb vs. pillars) was dependent upon the size of the spheres

utilized and the method of polymer deposition (i.e. admicellar polymerization vs. polymer adsorption). Thinner honeycomb walls, and larger separation distances between the template and the nanostructures were consistently found for TAAP.

In chapter 4, an in-depth study of the factors affecting TAAP is presented for three different monomers: aniline, pyrrole and methyl methacrylate; and three different surfaces: highly ordered pyrolytic graphite (HOPG), gold, and SiO_2. Among the parameters discussed are the effect of monomer and surfactant concentration, surfactant chain length, polymerization time and temperature, solution ionic strength, substrate choice and surface treatment. Control over these parameters allowed the synthesis of polymer nanopillars, nanorings, honeycombs, and "honeytubes." Experimental results showed that the nanostructures' morphology can be effectively modified by changing the length of the hydrophobic chain of the surfactant. Nanostructures with fewer defects were found for surfactants with the longest hydrophobic tails (i.e. 12 carbon atoms). The hydrophobic nature of the monomer also seemed to affect the morphology of the nanostructure; poly(methyl methacrylate) (PMMA) honeycombs showed thicker walls compared to polyaniline (PANI) and polypyrrole (Ppy). In general, HOPG seems to be a better choice of substrate for TAAP compared to gold-coated glass and SiO_2 wafers. Preliminary results on the formation of layered polymer nanostructures via multiple TAAP sequences were also presented.

Chapter 1. Patterned Nanostructures from Particle Lithography

I. Introduction

As the world advances into a new age of innovative technologies based on nanoscale machines and devices with potential applications in biology, medicine, catalysis, microelectronics and data storage, there is great demand for the development of nanoscale structures and arrays via efficient and reliable patterning methods, capable of producing arbitrarily shapes with high resolution and reproducibility. In particular, two-dimensional (2D) periodic nanometer structures on a solid surface exhibit interesting properties with applications in high performance microelectronic elements, optical and magnetic storage media, antireflective coatings, solar cells, molecular sensors, and physical masks for the fabrication of ordered nanostructure arrays via evaporation or reactive ion etching.

A number of methods have been developed to pattern 2D nanostructures on surfaces, most of which can be characterized as either "bottom-up" or "top-down" approaches. Bottom-up approaches rely on molecular or particle interactions to drive the nanostructure self-assembly. Top-down approaches

involve various lithographic methods to pattern micron and nanometer sized structures over large areas.[1] Conventional lithographic techniques are well-established and find wide use in industrial applications. Photolithography and its related analogues, x-ray or e-beam lithography, are by far the most widely used and highly developed of all technologies now practiced. The operational principle relies on the exposure of an appropriate material (resist) to electromagnetic radiation (e.g. UV or X-ray) to introduce a latent image, which is subsequently developed into relief structures through etching. In the case of writing with charged particles (electrons or ions) the task is accomplished using a beam or projected image of energetic particles rather than photons.[2] Diffraction limitation has been long recognized as the main disadvantage of photolithography with respect to other patterning methods; however, significant progress in high resolution photolithography has been achieved in the past decade by the so-called "next generation" lithographic methods: immersion lithography,[3,4] extreme ultraviolet (EUV) lithography,[5,6] and molecular glass photoresists,[7,8] among others. A review paper by Bratton et al.[9] discusses some of these techniques with special reference to the microelectronic industry.

In contrast to photolithography, scanning beam lithography is a serial process, which generally means longer processing times (this claim might be argued upon as photomasks required for photolithography are usually patterned

using scanning lithography); however, these techniques offer much higher resolution due to the fact that the de Broglie wavelengths of energetic particles are sufficiently short (< 0.1 nm) to minimize the effects of diffraction that typically limit photolithographic approaches.[10] In particular, e-beam and focused ion beam lithography allow the fabrication of arbitrary patterns with sub-50 nm resolution, but the main tradeoff of decreasing the beam size to achieve high resolution patterning is the decrease in beam current, which in turn increases the time necessary to achieve the same imaging dose.[1] X-ray lithography, on the other hand, has the advantage of parallel processing capabilities which significantly improves sample throughput, but requires substantially higher capital investment.[11]

Scanning probe techniques (SPL) including atomic force microscopy (AFM), scanning tunneling microscopy (STM), and dip-pen lithography have also been proved successful to fabricate high-resolution nanostructures and nanodevices on various substrates.[12-15] The technique resembles the stylus writing process in which a sharp edge (the tip of a cantilever) is used to draw patterns, to impart chemical functionality, and even to manipulate molecules and atoms with great precision. The ability to pattern features on a surface with atomic resolution makes SPL methods very attractive; however, the main drawback is the serial nature of the process, which results in long processing times. In order to

circumvent the problem of low throughput, semi-parallel approaches to SPL have been proposed where an array of probes is used instead of a single probe.[16,17] The problem with these approaches is that they significantly increase the complexity and the cost associated with the process.

In the past decade, molding and embossing techniques for nanopatterning have gained tremendous popularity as they provide an inexpensive way to pattern both inorganic and organic-based nanostructures over large areas of planar and non-planar substrates in a parallel fashion.[1,2,18,19] Molding and embossing techniques utilize either a hard or a soft elastomeric master (usually PDMS) for pattern generation and transfer. Molding techniques such as step-and-flash imprint lithography (SFIL),[20-23] replica molding (RM),[24,25] microcontact printing (uCP),[26] microtransfer molding (uTM),[27] and micromolding in capillaries (MIMIC)[28] involve curing a precursor (usually a monomer or prepolymer) against a topographically patterned master. Embossing, on the other hand, is the collective name for a set of lithographic techniques based on the imprinting of a topographically patterned mold into a flat polymer film. Nanoimprint lithography (NIL)[29] and solvent-assisted micromolding (SAMIM)[30] are examples of embossing.

In general, the briefly-discussed top-down techniques offer the ability to create very small feature sizes in complex shapes and arrays, with high-fidelity of

reproduction. Major drawbacks, however, are the high cost of the equipment and the need for highly skilled personnel, as well as the long processing times (sometimes tens to thousands of hours depending on the process and application). Bottom-up approaches based on self-assembly phenomena constitute an alternative to top-down approaches. Bottom-up approaches rely on the self-assembly of the so-called building blocks due to various forces (e.g. entropic interactions, electrostatic, hydrophobic, and van der Waals forces, hydrogen bonding, physical confinement, electromagnetic and gravitational fields, etc.) acting individually or collectively on the system. A number of articles have been published on the subject of self-assembly with particular interest in self-assembled monolayers (SAM's), phase-separated block copolymers, and particle lithography.[12,31-33]

The focus of this chapter is on the fabrication of organic and inorganic patterned nanostructures via particle lithography; an inexpensive, inherently parallel, high-throughput, and materials-general nanofabrication technique.[34] First, an overview of the history and evolution of particle lithography is presented, followed by a description of various methods developed to form 2D ordered arrays of colloidal particles on various surfaces. Next, the formation of patterned nanostructures from particle lithography is discussed with particular emphasis on

polymers, proteins, metals and semiconductor materials. Finally, the chapter is concluded with an overview of future challenges in particle lithography.

II. History and Development of Particle Lithography

In 1981, Fischer and Zingsheim[35] were the first to use a monolayer of polystyrene latex spheres on a substrate as a lithographic mask for surface patterning. They obtained colloidal monolayer domains of about 10 microns by drop-coating the sphere dispersion (10 wt %) on a glass slide. Platinum was then vacuum-deposited in the interstitial spaces between the spheres, and after removal of the latex spheres by sonication in benzene, an ordered platinum array was obtained. In a subsequent step, they infiltrated the platinum pattern with an epoxy resin (araldite). After polymerization and removal of the glass support with hydrofluoric acid, a conformable mask consisting of a metallic pattern embedded in a smooth polymer film was obtained. These masks were then used to demonstrate pattern replication capabilities with visible light on a negative photoresist and onto a molecular dye layer with nanometer resolution.

The work by Fischer and colleagues mainly focused on the imaging method and the resolution capabilities of visible light; however, not much emphasis was placed on the importance of particle lithography as a pattern

fabrication technique. A major breakthrough in the field of particle lithography took place a year later, in 1982, when Deckman and Dunsmuir proposed the so-called "Natural Lithography" technique, a form of microfabrication based on the use of spherical colloidal particles as etching or deposition masks.[36] In their work, the authors reported the fabrication of ordered arrays of silicon posts via reactive ion milling on a silicon wafer masked with a densely packed, spin-cast monolayer of 400 nm PS spheres. Triangular silver posts were also fabricated by metal evaporation in the interstices of the polymer mask followed by removal of the latex spheres in methylene chloride. The importance of controlling various fabrication parameters such as the concentration and rheology of the latex dispersion, and the spheres/substrate surface chemistry and charge was discussed in the paper. Particular emphasis was given to the requirement that the colloid wet the substrate, and that the spin speed be optimized so as to avoid multilayer or incomplete coverage of the surface. However, they did not provide a systematic study of the factors causing packing defects in the colloidal monolayer.

In later publications, Deckman and co-workers[37,38] continued to expand the scope of natural lithography by pursuing control over various parameters of the assembly process, as well as by exploring new applications of surface textures produced via natural lithography, such as sake cup and oyster-like etch profiles obtained through localized charging and self-shadowing effects on mosaic arrays

of 0.8 um polystyrene spheres. The resulting nanostructures showed potential applications as etching diagnostic tools to determine uniformity, selectivity and directionality in various etching processes. In addition, the authors monitored the time evolution of multiple layer colloidal aggregates and the ordering process by optically measuring the intensity of a HeNe laser beam specularly reflected from the spinning substrate. They observed a sudden increase in the viscosity of the colloidal dispersion and ordering when the fluid layer thickness was 1-2 um. Based on this observation, they hypothesized that micron sized surface patterns should produce graphoepitaxial effects. As a matter of fact, graphoepitaxial effects were indeed observed with deep and shallow groove gratings. Moreover, the effects were accentuated when the grating periodicity and groove width were an integral multiple of the sphere diameter. This work constitutes an important contribution to the field of particle lithography as it laid the foundation for what is known today as template-assisted particle lithography. This topic is further discussed in a later section of this chapter.

Almost a decade later, inspired by the seminal work of Fischer[35] and Deckman,[39] Van Duyne and co-workers[34] introduced the concept of "Nanosphere Lithography" (NSL), a more operationally descriptive term that extended the capabilities of natural lithography, making possible the fabrication of periodic particle array (PPA) surfaces having nanometer scale features from single and

double layer colloidal masks. Van Duyne's group demonstrated the flexibility of NSL as a material general fabrication process by varying both the substrate and the particle materials used. They successfully patterned metals, inorganic ionic insulators, and an organic pi-electron semiconductor on various substrates including metal insulator, and semiconductor materials. Moreover, they introduced for the first time the use of atomic force microscopy (AFM) for studies of single and double layer masks formation via NSL.

Another key contribution to the development of particle lithography is the work by Nagayama's group which resulted in a better understanding of the mechanism driving the formation of 2D hexagonal arrays of micron, and sub-micron size latex particles on various surfaces.[40-47] By using an optical microscope, Nagayama and collaborators followed the self-assembly process that takes place when a droplet of a colloid dispersion is let to evaporate slowly on a flat substrate encircled by a Teflon ring. From their observations, they concluded that a nucleus consisting of a few spheres packed in an ordered fashion starts to form when the thickness of the liquid film approaches the diameter of the colloidal particles, and that more particles are subsequently incorporated into the colloidal arrangement by convective transport due to attractive capillary forces acting laterally on the particles as the liquid layer evaporates.

A comprehensive study of the role of various parameters affecting the particle array formation was presented in 1992 by Denkov et al.[40] Among the factors discussed are the effect of particle size and concentration, liquid evaporation rate (proportional to temperature and relative humidity), meniscus shape, presence of surfactants and ionic strength of the solution, and surface wettability. In 1999, a similar study by Dushkin et al.[41] evaluated the effect of growth conditions (i.e. evaporation rate, meniscus profile, particle size and concentration, and substrate quality) on the structure of 2D latex crystals by means of various microscopic methods: optical microscopy, transmission and scanning electron microscopy, surface plasmon resonance microscopy, and atomic force microscopy. The study suggested that the onset of the nucleation process was the thinning of the suspension film and the consequent increase in particle concentration as water evaporated from the substrate. Then, once the nucleus is formed, the crystal growth is mainly governed by the evaporation rate and the meniscus profile. Experimental observations by Dushkin et al. concerning the nucleation and growth of 2D colloidal crystals on a solid substrate were successfully modeled by Maenosono et al.[42] using a discrete element simulation approach. A schematic of the mechanism of 2D colloidal crystal formation as proposed by Nagayama's group is shown in Figure 1.1.

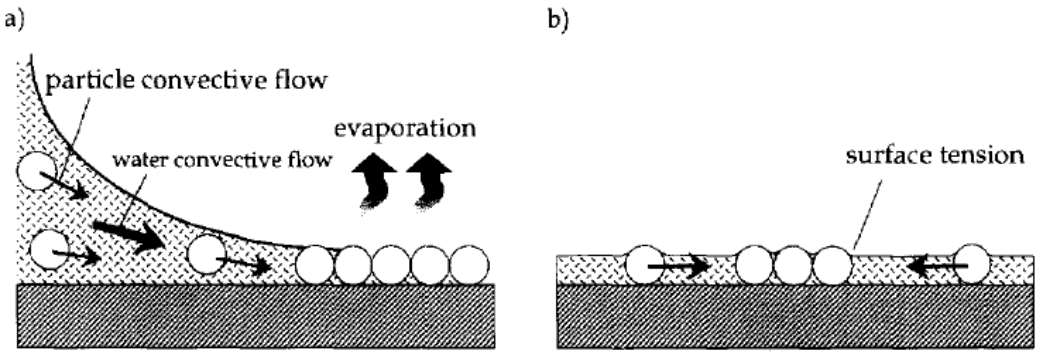

Figure 1.1. Schematic of 2D colloidal particle assembly driven by: a) convective flow, and b) lateral capillary forces resulting from surface tension and deformation of the water surface. Reprinted with permission from Ref.[43] Copyright @Elsevier Ltd.

Early work in particle lithography brought forth its tremendous potential as a nanofabrication technique. Since its origins, new methods have been developed to form large (in the order of cm^2), 2D ordered arrays of colloidal particles on different substrates with very few defects. In the following section we describe some of these deposition techniques.

III. Methods to Form 2D Ordered Arrays of Colloidal Particles

3.1. Convective Assembly of Colloids

As proposed by Nagayama et al.,[48] when a droplet of a colloidal dispersion is allowed to evaporate slowly on a flat substrate, under the right conditions lateral capillary forces acting on the particles cause them to self-assemble into 2D close-packed hexagonal arrays exhibiting polycrystalline domains of the order of a few hundreds of microns. Denkov et al.[40] were the first group to employ the controlled evaporative method to study the mechanism of formation of 2D colloidal arrays on a flat substrate. Specifically, they used a crystallization cell equipped with a Teflon ring tightly secured onto a glass substrate by an annular brass plate. A drop of the colloid dispersion of known volume and concentration was spread over the glass substrate encircled by the Teflon ring, and the water evaporation rate was controlled by adjusting the temperature of an upper glass cover plate. The crystallization process was followed by direct imaging with a light microscope fitted underneath the crystallization device. Relatively large PS latex particles (0.8 um and 1.7 um) were used in this study. Sodium dodecyl sulfate (SDS) and hexadecyltrimethylammonium bromide (HTAB) surfactants were used to enhance the wettability of the substrate by the sphere dispersion, and to slow down the liquid evaporation rate. Crystalline arrays with fewer defects were found for an optimum surfactant concentration.

A slight variation of Nagayama's radial evaporation method was recently employed by Tessier et al.[49] to form colloidal crystals consisting of a mixture of

latex and gold particles. The modified version of the crystallization cell used a thin piece of reinforced fluoroelastomer instead of a Teflon ring, mounted on a glass slide clamped between two steel plates. In both devices, the formation of a meniscus that is thinnest in the center of the cell is the key parameter for the nucleation of the colloidal crystal at the center of the cell.

Another variation of Nagayama's method was proposed by Micheletto et al.[50] In this technique, a droplet of the sphere dispersion is allowed to evaporate slowly onto a flat substrate, but instead of confining the dispersion to the boundaries of a Teflon ring, the substrate is tilted about 9^{o}. The quality of the monolayers was found to be a strong function of the tilt angle and the water evaporation rate, which was controlled by adjusting the temperature of the substrate resting on a Peltier cell. The whole system was enclosed in a small plastic box to prevent sample contamination and instabilities in the evaporation rate due to external air flow. This work deserves special recognition as the first to achieve ordered monolayers of nanometer size colloidal particles (42 nm in diameter) on a substrate. Due to its simplicity, Micheletto's method has been widely implemented by several groups; however, it often results in very low monolayer coverage (about 50%), with incomplete coverage and multiple layers observed throughout the surface.

Recognizing the importance of the substrate tilting angle on the meniscus profile and the growth of thin particle arrays, Dimitrov and Nagayama[51] proposed a dipping technique in which ordered, thin particle arrays are formed on a substrate by submersion and subsequent withdrawal of a clean substrate from the colloidal dispersion at a constant rate. The driving force in this method is water evaporation, which pulls the particles from the bulk into the meniscus in the vicinity of the three-phase contact line. For this process to work effectively, not only the dispersion must wet the substrate, but also the wetting film must approach the diameter of the particles. In addition, the particles must have enough mobility to slide on the substrate and find their position within the growing crystal before the liquid evaporates completely. For this reason, strongly adsorbing particles must be avoided. The particles must be monodisperse, and sufficiently stable in the dispersion to avoid precipitation or agglomerate formation. Moreover, the evaporation rate must be sufficiently slow to provide enough time for the particles to find their position of minimum free energy which is typically done by water saturating the air in contact with the substrate.

At a glance, this technique resembles the well-known Langmuir-Blodgett (LB) technique, with the difference that the particle monolayer is formed directly on the substrate while in contact with particles in the bulk; whereas in the LB technique, the monolayer is first formed at the air-liquid interface and then

transferred onto the substrate. Practically, the bulk technique does not require that spheres are aggregated at the air-liquid interface; in the same manner, the concentration of spheres in the bulk must be large enough to cover the surface. Formation of the monolayer in the bulk rather than at the air-liquid interface eliminates the need for insoluble particles, or particles attached to an insoluble film. Another advantage is that infinitely large surfaces could be coated in theory, without the risk of particle depletion. This is not the case when monolayers are formed at the air-liquid interface, where the number of particles available is limited to the area of the interface. Using this approach, Dimitrov and Nagayama were able to form polycrystalline monolayers of PS latex particles on glass substrates for a wide range of particles sizes (80 nm to 2 um), over large areas (in the order of cm^2).

3.2. Colloidal Assembly via Spin-Coating

The evaporation process driving the self-assembly of colloidal particles in thin liquid films can be accelerated in a controlled fashion by placing a small amount of the particle dispersion on a substrate rotating at relatively high speeds (e.g. 3000-4000 rpm). In this manner, colloidal monolayers have been formed over large areas of a substrate (of the order of cm^2) in times as short as a few

seconds. The technique is relatively simple and does not require the use of expensive or complex equipment. However, in order to obtain optimum results, several parameters need to be controlled; in particular, the colloidal suspension must wet the substrate, for that reason surfactants and other surface active agents are mixed with the sphere dispersion. Also, there must be a strong electrostatic repulsion between the colloids and the substrate, otherwise particles tend to aggregate on the substrate. Another important variable is the spinning speed; if the speed velocity is too low a multilayer coating will be produced, and if the speed is too high, incomplete coverage and defects are usually observed. Other factors such as the rheology of the particle dispersion, particle size and concentration, and colloid substrate interactions must be optimized for each system. Given the number of variables playing a role in the assembly process, control over the process can be cumbersome. The spin-coating method has long been used to form colloidal monolayers on a solid substrate, in particular for lithographic mask applications.[34,36,37,52,53]

3.3. Colloidal Assembly at the Air-Liquid Interface

The formation of stable monolayers of colloidal particles at the air-liquid interface and subsequent transferring onto a solid support has been widely

implemented by a number of research groups as a mean to form 2D ordered colloidal arrays on various substrates. Although most processes involve some sort of dipping technique to transfer the monolayer initially formed at the air-liquid interface onto the substrate, this process must not be confused with the dipping technique reported by Dimitrov and Nagayama,[51] in which monolayer formation takes place directly on the substrate while immersed in the bulk solution. Furthermore, unlike the convective assembly of colloids in thin liquid films where the assembly process is driven by capillary forces and convective transport; colloidal assembly at the air-liquid interface is driven by long-range forces acting on dipoles induced by the asymmetry of the interface between the liquid surface and partially immersed particles. As expected from the nature of the process, the assembly of colloidal particles at the air-liquid interface is highly dependent on the surface chemistry and charge of the particles, as well as the electrolytic properties of the underlying liquid. In general, a spreading agent (e.g. alcohol, surfactant, polymer, etc.) is used to ensure not only the partition of the spheres to the air-liquid interface, but also the stability of the monolayer once formed. Other factors such as particle size and concentration, as well as the chemistry of the transferring substrate are also found to affect the quality of the monolayer formed.

A comprehensive study of the aggregation of silica microspheres (300 nm in diameter) at the air-water interface was conducted by Hurd and Schaefer[54]

using optical microscopy. Monolayers were prepared according to the spreading method proposed by Goodwin et al.,[55] in which a dispersion of latex particles in methanol is dispensed dropwise onto the surface of a calcium chloride solution (1.0 N) contained in a Langmuir trough.

Fulda and Tieke[56] employed the traditional Langmuir-Blodgett (LB) technique to form relatively close packed monolayers of 0.5 um latex particles consisting of a polystyrene core and a hydrophobic shell of poly(acrylic acid) or poly(acrylamide) on copper substrates, using ethanol as the spreading agent. Particle monolayers were also transferred using the sub-phase lowering method (SL) developed by Araki et al.,[57] in which the liquid level is lowered by means of a faucet until the particle monolayer contacts the substrate. Surface-pressure area isotherms of the monolayers at the air-water interface were correlated with SEM micrographs of the monolayers on the solid supports. Monolayers of higher quality resulted when the SL method was used to transfer the monolayer from the air-water interface to the substrate.

As demonstrated by Bardosova et al.,[58] and Kondo et al.,[59] ordered monolayers of colloidal particles can also be formed at the air-liquid interface by controlling the surface chemistry of the colloidal particles. In Bardosova's paper, silica particles were made hydrophobic by reacting them with 3-(trimethhoxysilyl)propyl methacrylate. A dispersion of the modified particles in

chloroform was spread at the air-water interface, and the LB technique was used to transfer a close-packed monolayer onto the substrate at an optimum surface pressure. On the other hand, Kondo and co-workers utilized the spreading technique proposed by Goodwin et al.[55] to study the effect of coating silica particles (1 um in diameter) with alkoxyl chains of different length, on the formation of ordered monolayers at the air-benzene interface. Using the LB technique, they transferred the monolayers onto mica substrates and assessed the quality of the monolayers with SEM. Experimental results indicate that large, polycrystalline monolayers result when silica particles are coated with dodecanol, whereas incomplete surface coverage and fractal films resulted when the particles were coated with butanol and decanol. The authors related the difference in monolayer structure to the interparticle forces at the air-liquid interface, which can be controlled by adjusting the degree of immersion or the range of the repulsive interaction. Moreover, the authors concluded that attractive forces among particles must be sufficiently weak to allow the formation of rearrangement of ordered domains during film drying.

The use of organic layers to assemble particles at the air-liquid interface has been reported by several groups. Aveyard et al.,[60,61] for example, carried out an in-depth study of the structure of monolayers of micron-sized polystyrene latex spheres at the octane-water, and octane-aqueous surfactant solution interface as a

function of compression using a Langmuir trough; however no attempt was made to transfer the monolayers onto a solid support. Goldenberg et al.,[62] on the other hand, successfully prepared close-packed arrays of latex and silica particles in the range of 0.74 um to 1.7 um, onto hexane or heptane thin layers on water. The monolayers were subsequently transferred onto glass slides by either lowering the liquid level in a fashion similar to the sub-phase lowering method (SL) developed by Araki et al.,[57] or by lifting up the substrate through the monolayer. The study involved a variety of colloidal particles including monodispersed polystyrene latex, core-shell particles of polystyrene-2-hydroxyethyl methacrylate (PS-HEMA), and polystyrene-2,3-epoxypropylmethacrylate (PS-EPMA), as well as plain silica particles. Experimental data confirms the presence of highly ordered hexagonal structures at the air-alkane interface, and points out the importance of the organic layer in providing the ground for strong repulsive interactions responsible for the formation of high quality monolayers.

Another popular method to assemble monolayers of colloidal particles at the air-liquid interface involves the use of surfactants as stabilizing agents. In a paper by Weitz et al.,[63] 2D colloidal crystals were formed when aqueous dispersions of negatively-charged polystyrene latex were combined with a mixture of cationic, didodecyldimethylammonium bromide (DDAB), and a neutral surfactant (Triton X-100). The surfactant mixture self-assembled into

positively-charged vesicles, which promoted particle adhesion via columbic interactions. In this manner, particle adsorption onto the vesicle's surface was driven by charge neutralization, and the overall process was self-limited by lateral charge migration, which reverses the vesicle's charge to prevent multiple layer adsorption.

Van Duffel et al.[64] have assembled ammonium-functionalized silica spheres into 2D colloidal arrays of at the air-chloroform interface using a mixture of sodium dodecyl sulfate (SDS) and ethanol as the spreading agent. They used the traditional LB technique to transfer the monolayers onto glass and SiO_2 wafers, and determined the lattice constant of the crystal array by atomic force microscopy and optical diffraction measurements. The authors stated that no films could be prepared in the absence of SDS; however, no explanation was given on the role of the surfactant in driving the assembly process.

More recently, Marquez and Grady[65] carried out a study of the formation of 2D hexagonal arrays of latex spheres on highly ordered pyrolytic graphite (HOPG) using a slight variation of the conventional LB technique, in which various spreading agents (e.g. polymers and surfactants), were used instead of floating barriers, to drive the assembly of colloidal particles at the air-liquid interface. More details on this study can be found in chapter 2.

3.4. Colloidal Assembly via the Use of Electric and Magnetic Fields

The phenomenon of electrophoresis, i.e. the ability to move particles via an electric field, was discovered in 1807 by Ruess[66] while experimenting with particle transport in aqueous dispersions of clay. Early experiments on electrophoretic deposition can be traced back to the work of Hamaker[67] in 1940, and the development of a theory for particle transport near a substrate in the presence of an external field, by Koelmans and Overbeek[68] in 1954. Thirty years later, Richetti and co-workers[69] reported the use of an electric field to assemble colloidal latex particles into 2D crystalline arrays. Since the seminal work by Richetti et al., many studies have been carried out on the formation of ordered monolayers of colloidal particles on conductive substrates using external electric fields. Giersig and Mulvaney,[70,71] for example, reported the preparation of 2D ordered gold colloid lattices via electrophoretic deposition of citrate-stabilized and alkanethiol-capped gold nanoparticles (14 nm in diameter) on carbon-coated copper mesh grids. Electrophoresis times in the range of 1-2 min, and small electric fields (less than +1 V cm^{-1}) were used in the preparation of monolayers with crystalline domain sizes of about 1-2 microns over a few hundred squared microns. Longer times or significantly higher applied voltages (> 50 mV) resulted in multiple layer coverage. In every case, a significant portion of the substrate

showed incomplete surface coverage due to tear and ripping of the monolayer during solvent evaporation.

Electron-beam diffraction measurements of the lattice spacing suggested that particle ordering is mainly determined by the size of the surface adsorbates (i.e. the citrate ions and alkanethiols), and that the crystallographic orientation of the colloids plays no significant role. These results are consistent with experimental results by Schmid et al.[72] for triphenylphosphine-capped gold monolayers.

In addition to the assembly of gold nanoparticles, submicron sized (0.44 um in diameter) negatively charged latex spheres were successfully arranged into hexagonal close-packed monolayer and bilayers using stronger electric fields (i.e. +2 V cm^{-1} and +5 V cm^{-1}). These results opened up an alternative to the use of air-liquid monolayers and the LB technique for the fabrication of optical devices based on 2D ordered arrays of semiconductor nanoparticles.[71]

In an attempt to better understand the mechanism of nucleation and growth of colloid lattices via electrophoretic assembly, Giersig and Mulvaney studied the evolution of aggregate formation in solution as a function of the polarization time for trisodium citrated stabilized gold nanoparticles. They found that after 5 s, only a small fraction of the carbon-coated copper grids had been

covered with randomly distributed isolated particles. The onset of particle aggregation took place at 10 s, and 5 s later, island formation was clearly evident. After 35 s, the small islands or domains had already coalesced, covering a significantly portion of the copper grid. The authors explained their observations in terms of the reduction of the diffuse layer repulsion between the negatively charged gold particles upon adsorption, due to shielding of the particles surface charge by the positive charge on the carbon electrode. Thus, the particles migrate over the grid surface until they find available sites with the highest positive electrostatic potential, which corresponds to the greatest gain in Gibbs free energy. As the small ordered domains coalesce, a polycrystalline monolayer results due to the inability of the particles to rotate or realign once they find their place within the colloidal lattice.

Important contributions to the field of electrophoretic assembly of colloids have been provided by the works of Bohmer[73,74] and Aksay[75,76] on particle clustering and pattern formation in the presence of external fields. A hydrodynamic model based on electroosmotic flow around charged particles near electrode surfaces has been proposed by Bohmer et al.[73] to explain the long range interactions responsible for cluster formation of equally charged particles during electrophoretic deposition. As explained by the authors, a charged particle near or on a flat conducting surface creates flow in the adjacent fluid due to

electroosmosis about the particle's surface. Fluid is drawn laterally toward the particle near the electrode and pushed outward from the particle farther away from the electrode above the particle. This electrokinetic effect resulting from the deformation of the equilibrium diffuse layer is responsible for the transport of other particles present in the flow field towards already deposited particle rafts. When the potential is reversed, the direction of the flow reverses also, resulting is disruption and deagglomeration of particle aggregates as evidenced experimentally.

Aksay et al.,[75] on the other hand, have explained particle aggregation in terms of an electrohydrodynamic flow theory based on concentration gradients arising from electrode reactions and ionic transport through the solution. Furthermore, they demonstrated that the assembly process could be modulated by adjusting the frequency or the strength of the applied electric field. Using this technique they were able to fabricate ordered monolayer and multilayer close-packed colloidal arrays of silica, polystyrene, and gold particles in the range of 16nm to 2 um, with both dc and ac fields.[76] More recently, Aksay et al.[77] have proposed a novel method to form ordered arrays of micon-sized colloidal particles with optically tunable patterns via electrophoretic deposition in the presence of an ultraviolet illumination motif made using photochemically sensitive semiconductor materials. As suggested by the electrodynamic and the

electroosmotic theories, particle mobility increases with an increase in the current density and the field strength; hence, illumination of an ITO electrode with UV light should result in enhanced particle migration from darkened areas into lighted regions on photolithographically patterned ITO substrates.

Dielectrophoretic assembly of oriented and switchable 2D colloidal crystals of polystyrene latex and silica particles (0.5 um in diameter) has been recently reported by Velev et al.[78] The technique involves the use of a cell in which both electrodes are placed on the same side of the suspension, such that the particles assemble in the planar gap between them as shown in the schematic in Figure 1.2. One of the advantages of this process is that colloidal arrays can be formed extremely fast (in most cases the assembly process takes only a few seconds). Additionally, the controlled modulation of the electrostatic repulsion via electrolyte concentration can be used to control the lattice spacing, i.e. the distance between adjacent particles, with a precision of approximately 10 nm.

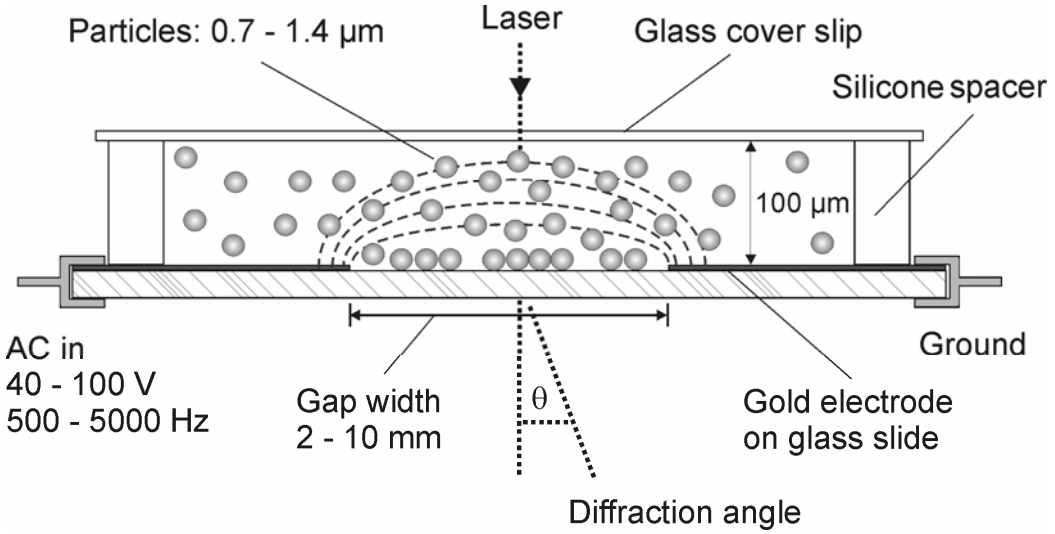

Figure 1.2. Schematic of set up for colloidal assembly using external electric fields. Reprinted with permission from Ref.[78] Copyright @American Institute of Physics.

A comparative study of the quality of colloidal monolayers formed via convective self-assembly in inclined planes, and under the influence of a periodic electric field, has been carried out by Schope.[79] The study revealed that higher quality monolayers can be achieved by applying a periodic shearing electric field perpendicular to the crystal growth direction. In particular, the area of the maximum monocrystalline regions was increased from 0.33 mm^2 to 1 mm^2 with respect to the convective self-assembly method. Also, the percentage of bad spots due to grain boundaries or missing spheres was decreased by an order of magnitude when an external electric field was used to direct the colloidal self-assembly. Moreover, Schope demonstrated that the number of dislocations

produced by polydispersity, aggregates, or even dust particles was slightly reduced, and that dislocations formed could be annealed during the growth of the monolayer, so their overall length can be substantially reduced.

The assembly of paramagnetic colloidal particles using magnetic fields has also been explored by Dimitrov et al.[80] When a magnetic field was applied normally to the interface (i.e. air-water or glass-water), non close-packed hexagonal arrays with interparticle distances ranging from 6 to 10 fold the diameter of the particles were observed at the interface. The interparticle distance was found to depend strongly on the distance between the interface and the magnet, the particle concentration and the concentration of added electrolytes. Experimental results were explained in terms of three main acting forces: 1) The magnetic field which attracted the particles toward the axis of symmetry at the interface; 2) Dipole-dipole magnetic repulsion forces between the particles; and 3) electrostatic repulsion forces due to the presence of negatively charged groups on the particles surface.[81]

3.5. Other Methods

Rapid assembly of colloidal particles and protein monolayers using a Dynamic Thin Laminar Flow (DTLF) apparatus has been proposed by Picard et

al.[82-84] The method relies on the hydrodynamic properties of thin laminar flow, and the assembly of particles at the air-liquid interface due to Brownian motion and convective evaporation. The DTLF apparatus consists of a rotating glass cylinder and a PTFE hemicylindrical trough equipped with six channels designed to control the subphase volume input, the pH, and the thin liquid film carrying the suspended colloidal particles on the surface of the cylinder. The whole device is mounted on a microscope stage to allow for direct observation of the monolayer formation. In a typical run, a known volume of the particle dispersion is gradually injected until the surface of the cylinder is completely covered with particles. Then, a water film on a wet hydrophilic substrate is brought in contact with the liquid on the cylinder, and when the two water films converge due to capillary effects, the colloidal monolayer gets transfer onto the substrate of interest. As the liquid film on the substrate evaporates through the particle monolayer, the monolayer finally contacts the surface of the substrate. This method for monolayer transferring has been coined horizontal deposition.[84]

Experimental results with sulfate stabilized and carboxyl-terminated polystyrene latex particles with particle sizes in the range of 53 nm to 6 um, indicated that the ordering process in the DTLF method depends strongly on the electrostatic interactions among the particles in the bulk, which can be controlled by adjusting the pH or the salinity of the liquid subphase. As a matter of fact, at

neutral pH the strong repulsive forces on the particles surface prevented monolayer formation; while at pH 4.0, the net charge on the particles surface was such that particles effectively partitioned to the air-liquid interface on the cylinder surface, and ordered monolayers formed on the substrate. Further reduction of the pH to 3.5 caused the particles to agglomerate and fractal structures resulted. Similar effects were observed when varying the electrolyte concentration.

In order to expand the flexibility of the DTLF method as a mean to produce particle monolayers on various substrates (e.g. glass plates, plastic films and metallic surfaces), Picard[85] suggested an improved version of the DTLF apparatus which allowed automated control of the rotational and translational movement of the cylindrical rod over large areas (potentially in the order of m^2) using a set of electrical motors. In this respect, particle monolayers were fabricated using two main operating modes depending on whether the substrate was hydrophobic or hydrophilic: In the first mode (i.e. the hydrophilic mode), the cylinder rotates in a direction opposite to the horizontal translation, and the particle monolayer is transferred from the air-liquid interface to the solid support by surface pressure effects at the liquid meniscus. In the second mode, most applicable to highly hydrophobic surfaces, the rotational and translational directions are set equal so that the hydrophobic surfaces of the particles and the substrate are in close proximity (a 100 um gap between the monolayer and the

substrate is maintained to prevent disruption of the monolayer ordering). Multiple layers were also achieved by carefully combining both deposition modes. A schematic of the process is shown in Figure 1.3.

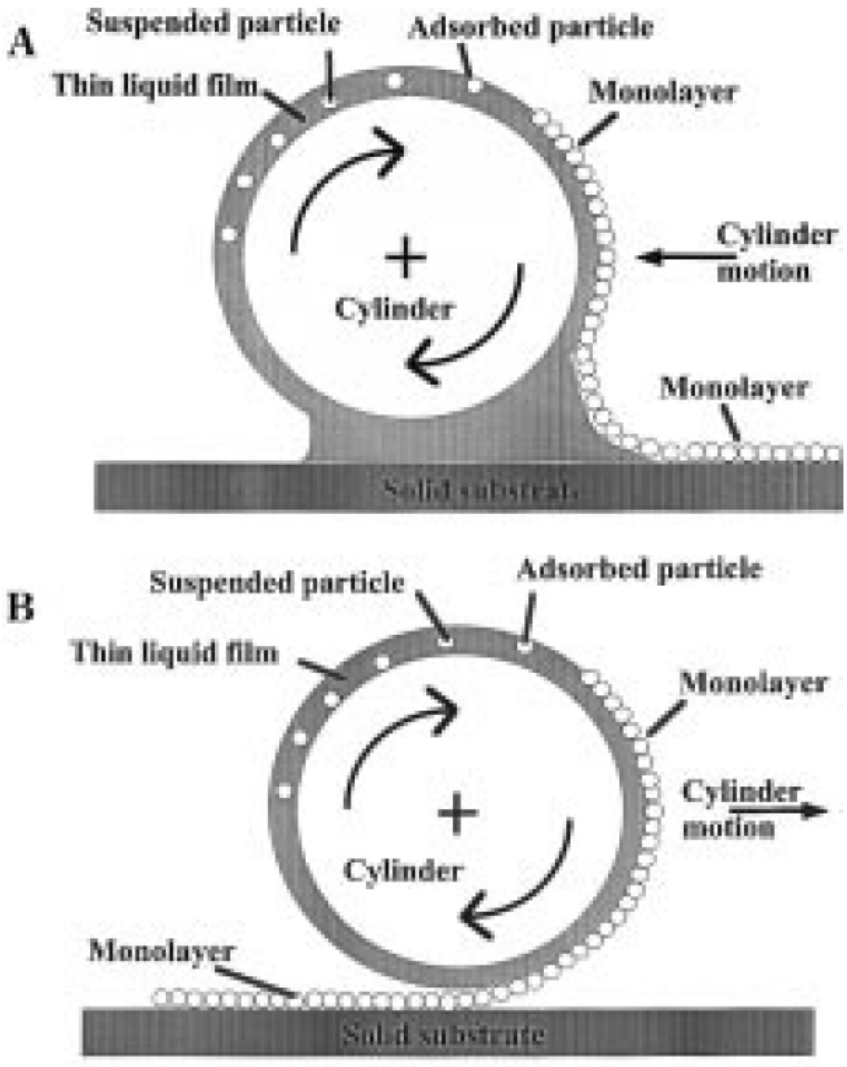

Figure 1.3. Schematic of the Dynamic Thin Laminar Flow (DTLF) apparatus working in: a) hydrophilic, and b) hydrophobic mode. Reprinted with permission from Ref.[85] Copyright @American Chemical Society.

It is important to note that although the modified version of the DTLF apparatus provided more control over the deposition process; the quality of the monolayers fabricated did not improve significantly with respect to earlier version of the DTLF device. As a matter of fact, fractal structures were observed in most cases, with a few exceptions in which 2D crystalline structures were obtained upon addition of glycerol. At the right concentration, glycerol served as a lubricant facilitating the sliding and rearrangement of particles on the surface. Concentrations other than the optimum resulted in fractal monolayers.

The use of a flow cell to fabricate close-packed arrays of mesoscale particles over large areas (ca. 1 cm^2) has been reported by Park and Xia.[86,87] The apparatus consists of a patterned photoresist material tightly sandwiched between two glass slides, and an opening fitted with a glass pipe connected to a rubber tube for the injection of the particle dispersion, and subsequent compression using a positive N_2 pressure. The cell is designed to have a number of channels with prefixed dimensions, which serve to direct the assembly of the colloids under the combined effect of the nitrogen flow and sonication. Once the assembly process has been completed, the system is dried in an oven at 65^oC for 4h approximately, and a close-packed array is left on the bottom surface of the cell. Using this method, Xia and co-workers were able to form crystalline arrays for a number of different colloids including silica, polystyrene and poly(methyl methacrylate)

particles with diameters in the range of 60 nm to 10 um. One of the advantages of the flow cell method is that the technique is relatively insensitive to the chemical composition and the surface properties of the colloids; however, other complications can take place such as the disruption of the particle array during opening of the flow cell, or defects arising from instabilities in the flow of the particles through the small grooves in the cell.

Another method for the rapid and controlled deposition of crystalline arrays of colloidal particles on flat surfaces has been proposed by Prevo and Velev.[88] In this technique, commonly referred to as the controlled spreading method, a small volume (i.e. 10 uL) of the particle dispersion is dispensed between two glass plates connected at a 30^{o} angle, and the close-packed array results when the particles are uniformly distributed on the bottom surface by the horizontal displacement of the upper plate at constant speed (in the range of 1-200 um/s) by means of an electric motor. A schematic of the process is shown in Figure 1.4.

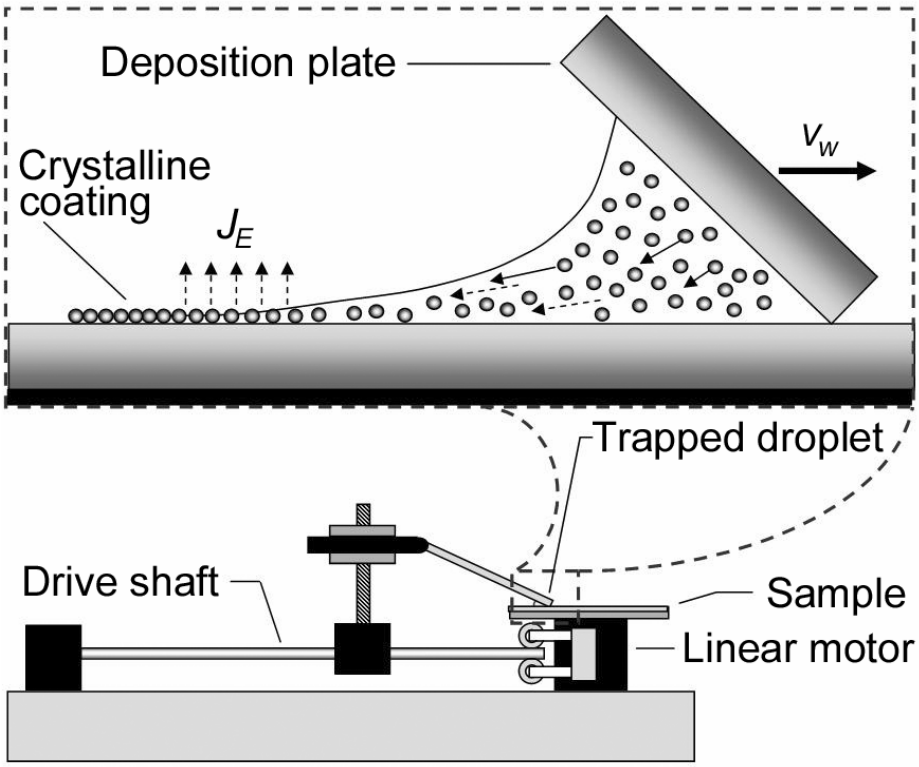

Figure 1.4. Schematic of particle assembly via the controlled spreading method. Reprinted with permission from Ref.[88] Copyright @American Chemical Society.

Velev's method resembles the convective assembly method first proposed by Nagayama et al.,[48] with the advantage that the deposition process is faster and it can be more precisely controlled by adjusting the angle and the traveling speed of the upper plate. Unlike Nagayama's method, the evaporation rate does not seem to have a significant effect on the quality of the arrays formed via the spreading technique. On the other hand, the deposition speed (i.e. the speed at which the upper plate moves relative to the bottom plate) was found to be the

most critical parameter in the process. Experimental results suggest that for a given particle volume fraction, there exists an optimum velocity, coined "the natural assembly speed of a monolayer," for which uniform polycrystalline monolayers with domain sizes in the range of 100-250 um form over large areas of the substrate (i.e. a few tens of squared centimeters). Higher deposition velocities result in incomplete monolayer coverage, whereas velocities much slower than the optimum deposition speed produce multiple layers of different thicknesses. Moreover, the deposition speed is convoluted with the particle volume fraction. In general, working at higher particle volume fractions allows the deposition speed to be increased, while preserving the quality of the monolayer produced. Operational diagrams relating the coating thickness and structure to the deposition parameters (particle volume fraction, and deposition speed), have been constructed from the experimental data thus making the process highly scalable for industrial applications.

More recently, Pan et al.[89] have proposed a novel method to assemble polystyrene latex particles into large area (of the order of cm^2), close-packed monolayers on a vortical water surface. The method is rather simple; it consists of a Teflon ring floating on the surface of a beaker filled with water. A magnetic stirrer is used to generate a vortex, and a small amount of the particles previously dispersed in ethanol is carefully dropped into the vortex. The combined effect of

the velocity gradient generated by the water motion and the centrifugal action of the stirring cause the particles to assemble into a close-packed monolayer at the vortex center. Once the monolayer is formed at the air-liquid interface, the underlying water volume is drained out of the beaker and replaced with clean water so that only the particles forming the monolayer are transferred onto the solid support by a simple dip-coating process as illustrated in the schematic in Figure 1.5.

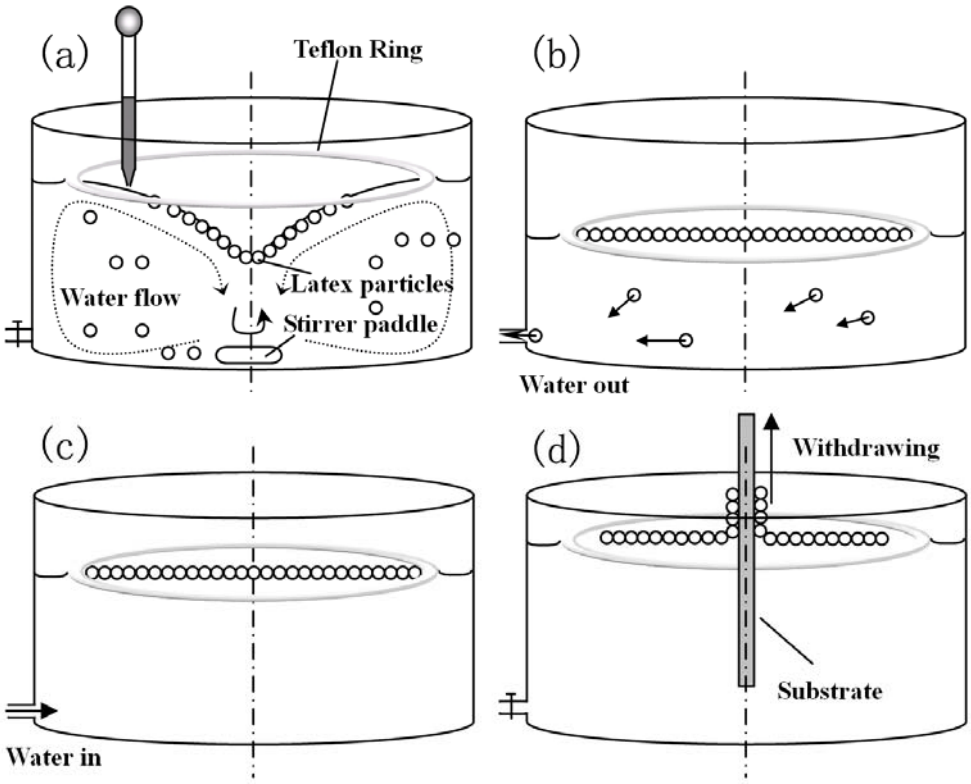

Figure 1.5. Schematics of colloidal assembly via the vortex method. Reprinted with permission from Ref.[89] Copyright @American Chemical Society.

The generality of the vortex method has been proved for different systems, including colloidal particles with different diameters in the range of 0.8-2 um, and substrates consisting of different materials (e.g. glass, silicon wafers and polystyrene), and different shapes (e.g. glass fibers, glass tubes, spherical surfaces, etc.). In addition to close-packed monolayers, multiple layers can also be fabricated by performing multiple dipping steps; however, the substrate must be dry prior to its immersion into the liquid in order to avoid the detachment of previously deposited layers. Another parameter of paramount importance in the vortex method is the rotation speed of the magnetic stirrer, which needs to be carefully controlled so as to avoid the collapse of the particle monolayer, and/or excessive turbulence of the water due to the migration of latex particles from the air-liquid interface into the bulk liquid. In this study the optimum stirring speed was found to be 120 rpm; however, this value is expected to change significantly depending on the water volume and the stirrer paddle size. Furthermore, care must be taken to avoid disruption of the monolayer during the water replacement step. This step is not trivial and may require a fair amount of trial and error to be performed adequately. In addition, all other considerations pertaining to the quality of the substrate (wetting characteristics, roughness, chemical and charge homogeneity, etc.), as well as the interaction between the colloids and the substrate, are applicable to the vortex method.

Non-close packed, 2D hexagonal arrays of colloidal particles have been achieved by Jiang et al.[90,91] by spin-coating a dispersion of silica colloids and a photopolymerizable monomer (ethoxylated trimethylolpropane triacrylate-ETPTA) onto a silicon wafer previously treated with 3-acryloxypropyl trichlorosilane (APTCS). As shown in Figure 1.6, the technique offers the flexibility of producing colloidal crystal-polymer nanocomposites or non close-packed hexagonal arrays of colloidal particles on a given substrate, after removal of the polymer film by oxygen plasma etching or dissolution in hydrofluoric acid. The non close-packed arrays are believed to form as the result of normal pressures produced by spin-coating and monomer photopolymerization, which push the particles against the substrate.[92] In addition to non close-packed arrays, colloidal patterns with more complex shapes have also been prepared via the so-called template-assisted particle lithography, a technique that relies on the use of lithographically-produced surface relief features to direct the assembly of highly structured colloids through capillary and electrophoretic forces, electrostatic interactions, and wetting effects, among others.[93-100]

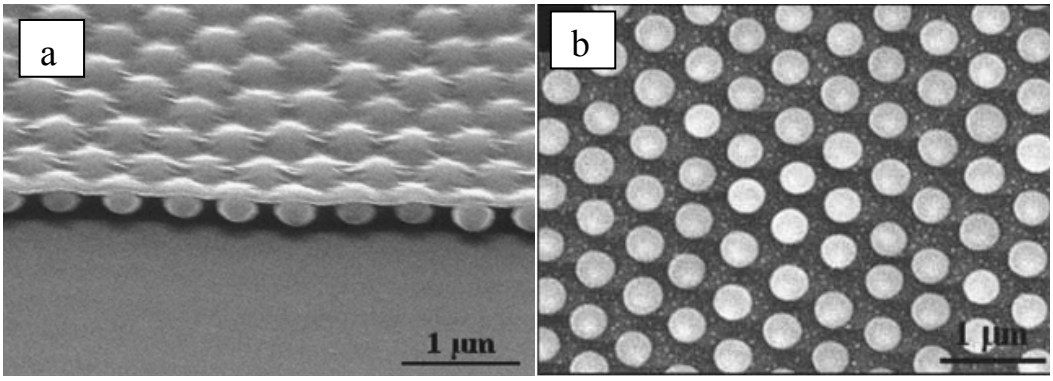

Figure 1.6. Typical SEM images a) cross-sectional view, and b) top-view of a non close-packed monolayer colloidal crystal-polymer nanocomposite made by spin coating. Reprinted with permission from Ref.[90] Copyright @American Institute of Physics.

IV. Two-Dimensional Patterning via Particle Lithography

4.1. Patterning of Metallic Materials

The pioneer work of Hulteen and Van Duyne[34] in 1995 demonstrated the potential of nanosphere lithography as a material general process for the fabrication of patterned nanostructures on a substrate. Well-ordered, 2D particle arrays were successfully obtained for a variety of materials including Ag, CaF_2, and cobal phthalocyanine (CoPc), on substrates such as mica, Si(100), Si(111), and Cu. The process involved three main steps: First, the mask (monolayer or double layer) was assembled on the substrate of interest by spin-coating a dispersion of polystyrene latex spheres in a mixture of non-ionic surfactant

(Triton x-100) and methanol. Second, the material was vacuum deposited on the surface in the interstitial spaces between the spheres. The amount of material and the deposition rate were followed using a quartz-crystal microbalance. In the final step the spheres were lifted off from the surface by sonicating in methylene chloride for a few minutes. When the deposited material (e.g. CoPc) was soluble in CH_2Cl_2, the spheres were lifted-off mechanically using tape.

In subsequent studies, Van Duyne and co-workers[101] demonstrated that size-tunable silver nanostructures can be fabricated by adjusting the sphere diameter and the thickness of the deposited layer, which determine the nanostructures in-plane diameter and out-of-plane height, respectively. Moreover, the shape of the nanostructures can be varied by choosing either a monolayer, or a bilayer mask. Based on the geometry of the interstitial sites, triangular-shaped nanoparticles are typically formed when the material is vacuum-deposited through a closed-packed monolayer, whereas spheroids are observed when a bilayer mask is used. A good correlation was found between structural parameters measured by AFM (after correction for tip convolution effects) and theoretical predictions based on geometrical considerations and the assumption that the material is preferentially deposited on the surface through the line-of-site of the mask.

Using UV extinction spectroscopy, Jensen et al.[102,103] measured experimentally the surface plasmonic properties (i.e. the collective oscillations of

conduction electrons resulting from light excitation) of silver arrays fabricated via NSL. They found that the wavelength corresponding to the extinction maximum of the localized surface plasmon resonance (LSPR) can be precisely tuned throughout the visible, near-infrared, and mid-infrared regions of the electromagnetic spectrum by adjusting the nanostructure dimensions and morphology, and by dielectric encapsulation of the nanostructures with silicon oxide layers grown on their surface. As demonstrated by the authors, the size of individual silver nanostructures can be conveniently manipulated by adjusting the diameter of the spheres and the thickness of the layer deposited through the mask. The shape, on the other hand, can be controlled by the choosing the appropriate colloidal mask (monolayer or bilayers), or by thermal annealing of the nanostructures. Moreover, they proposed a theoretical model to predict the extinction maxima based on the discrete dipole approximation (DDA) method and electrodynamic considerations. A similar work has been carried out by Astilean,[104] who showed the formation of size-tunable periodic arrays of silver and gold nanodots and nanoholes using reactive ion etching to control the size of the interstitial sites of a colloidal mask formed via the drop-coating technique. In a subsequent publication, Astilean et al.[105] used visible-near infrared transmission and reflectivity spectroscopy to characterize the optical properties of gold films deposited on periodic colloidal arrays of latex particles. This work, together with the work of Van Duyne's group, has significantly contributed to advancing the

potential applications of metal nanoparticles in Surface Enhanced Raman Spectroscopy (SERS) and other biosensing applications.

Burmeister et al.[106,107] also contributed to early studies of colloid monolayers as lithographic masks. They added flexibility to Micheletto's method[50] for the formation of colloidal monolayers, initially proved successful only on flat, hydrophilic substrates with good wettability and smoothness; by proposing that a monolayer originally prepared on a glass substrate be floated on a water surface, and subsequently transferred onto the substrate of interest by simply touching it from above. Although this modification requires an additional step, and some additional complications may derive from the transferring of the monolayer from one substrate to another, the technique offers the advantage of transferring colloidal masks onto multiple substrate choices. As a proff of concept, Burmeister and co-workers showed that it is possible to fabricate ordered 2D gold nanopillars and honeycombs with in-plane dimensions of the order of 200 nm and out-of-plane heights of the order of 70 nm, on various substrates including ITO-coated glass slides, copper grids, and hydrophobic single crystal WSe_2 substrates.

Nickel nanostructures with different geometrical configurations have also been patterned using latex spheres as lithographic masks. In a relatively simple procedure by Kandulski et al.,[108] colloidal templates are first assembled at the air-

liquid interface using a mixture of ethanol and a non-ionic polyethoxylated surfactant (EO = 10) as the spreading agent, and subsequently transferred onto a silicon substrate. Following metal deposition via e-beam evaporation, and sphere lift-off by ultrasonication in toluene, Ni nanodots arrays with different geometrical configurations can be obtained by controlling the revolution angle between the layers in the colloidal mask. Rossi and co-workers[109] have also prepared triangular Ni nanostructures on silicon surfaces by dip-coating P-doped silicon wafers into a dispersion of monodispersed latex spheres (174 nm and 760 nm in diameter), under a controlled-humidity nitrogen environment. They were able to fabricate Ni nanostructures of different sizes, while keeping the total amount of Ni covering the surface relatively constant. These samples were further used as electrodes in methanolic electrochemical cells, and the measured dark current density as a function of voltage was found to be strongly dependent on the dimensions of the n-Si/Ni nanocontacts.

Bartlett and colleagues[110,111] have reported the patterning of other metals such as platinum, palladium and cobalt into ordered arrays of interconnected spherical voids with uniform sizes via electrochemical deposition of aqueous solutions of H_2PtCl_6, $(NH_4)_2PdCl_4$, and $Co(Ac)_2$ into the interstitial sites of 2D closed-packed latex spheres assembled on an evaporated gold substrate, followed by template lift-off in toluene or THF for 24h. They also proposed the use of these

nanostructures to fabricate more complex metallic spherical cavities by allowing monodispersed latex spheres to slowly self-assemble onto the previously formed honeycomb structures using a custom-built cell.[112] The structural arrangement of the spheres, as well as the fraction of honeycomb holes occupied by spheres can be manipulated by changing the ratio between the sphere size and the center-to-center pore distance in the metallic honeycomb structure. Once the spheres are positioned within the honeycomb voids, they are coated with a metallic layer via electrochemical deposition, and after dissolution of the latex core, metallic spherical cavities with fixed dimensions and spatial configurations can be formed on the substrate. An advantage of the electrochemical deposition technique relative to other methods is the ability to control the deposited film thickness by selecting the appropriate reduction potential for the complex ions in solution. In addition, highly dense metal films can be deposited with little or no shrinkage during template removal; however, the process is restricted to electrically conducting substrates.

Another popular technique for the patterning of metallic nanostructures via particle lithography is the sol-gel technique. Liu et al.,[113] for example, have recently fabricated 2D hexagonal arrays of Fe/SiO_2 magnetic nanodots with pyramidal tetrahedron shapes using a combination of spin-coating and the sol-gel method. They first spin-cast a close-packed colloidal monolayer of latex spheres

(1 um in diameter) on the substrate, and heated it up for a few minutes at 100^{o}C in order to increase the adhesion with the substrate. Then, the metal precursor solution was infiltrated through the interstitial spaces of the latex mask by spin-coating at 3500 rpm for 1 min, and dried at 90^{o}C for 1h. In order to prevent oxidation of the iron, tetraethyl orthosilicate (TEOS) was added to the precursor solution to form a protected SiO_2 shell on the surface of the Fe nanostructures. The template was removed by calcination in a two-step process consisting of sintering at 450^{o}C for 2h, and reduction in H_2 gas at 800^{o}C for 4h. The morphology of the SiO_2-coated Fe nanostructures was further controlled by adjusting the concentration of the precursor solution, the heating treatment, and the speed and time for the spin-coating step. The magnetic properties of the nanoparticles were confirmed by the observation of the magnetization direction, as well as higher remanence, coercivity, and lower saturated fields relative to featureless Fe/SiO_2 thin films deposited under the same conditions as the patterned Fe/SiO_2 nanopillars. However, the effect of nanoparticle size, shape, and geometrical configuration remained to be addressed. An obvious set-back of this method is the extremely high temperatures involved in the process.

A recent publication by Wright et al.[114] describes a procedure in which particle lithography, thermal evaporation, sputtering and template stripping processes are combined to fabricate ultraflat ternary metallic nanopatterns

consisting of cobalt circles and gold triangles embedded within a titanium mesh. The authors claim that this method is capable of producing nanostructures 60 percent smaller than the size of the original template. The process starts with the convective self-assembly of a close-packed monolayer of latex spheres on freshly cleaved mica substrates. In the second step, triangular-shaped gold nanostructures are formed by thermal evaporation through the interstices of the colloidal mask. These nanostructures are then buried under a titanium overlayer deposited on the surface via the less directional sputtering technique, so that a mesh-like nanostructure forms around the particle-substrate contact point. After removing the latex spheres by sonication in chloroform or toluene for 5 min, the exposed bare mica circular regions are filled with a sputtercoated cobalt layer. The entire assembly is glued facedown to a silicon wafer with low viscosity epoxy resin cured at 150^{o}C for 2h. After stripping off the mica template in THF at room temperature, a ternary metallic nanopattern results on the silicon surface. The main advantage of Wright's technique is the ability to pattern various materials on the same surface with nanometer scale precision by exploiting the directional characteristics of relatively simple, well-known deposition processes such as thermal evaporation and sputtercoating.

The work by Winzer et al.[115] proved to be another significant breakthrough in the field of particle lithography as they were the first group to

report the formation of mesoscopic gold rings from nanosphere lithography. Following Van Duyne's procedure,[34] they formed close-packed monolayers of latex spheres on freshly cleaved mica substrates, and after evaporating the metal through the colloidal mask, they lifted-off the spheres from the surface leaving behind periodic arrays of gold nanodots or nanorings as shown in Figure 1.7. The authors attributed the formation of ring nanostructures to the diffusion of gold from the interstitial space to the area where the spheres contact the substrate, and pointed out that whether triangular-shaped nanodots or nanorings form depends strongly on the choice of the solution containing the spheres. The flexibility of the method was confirmed using latex spheres of different sizes in the range of 140-895 nm, and by choosing a different metal for the evaporation step. In this respect, well-ordered cobalt nanodots were fabricated using 270 nm latex spheres. Their magnetic properties were evaluated by measuring the reversal of the magnetization direction in the presence of an external field (400 Oe.) using a magnetic force microscope. Single-domain cobalt nanoparticles such as the ones prepared by Winser and co-workers may find potential applications as quantum magnetic storage devices. Gold nanorings, on the other hand, may be useful in surface-enhanced spectroscopy and sensing applications,[116-118] given their highly tunable plasmonic properties and electromagnetic field enhancement effects depending on the ratio of the ring thickness to its radius, as demonstrated by Aizpurua et al.[119]

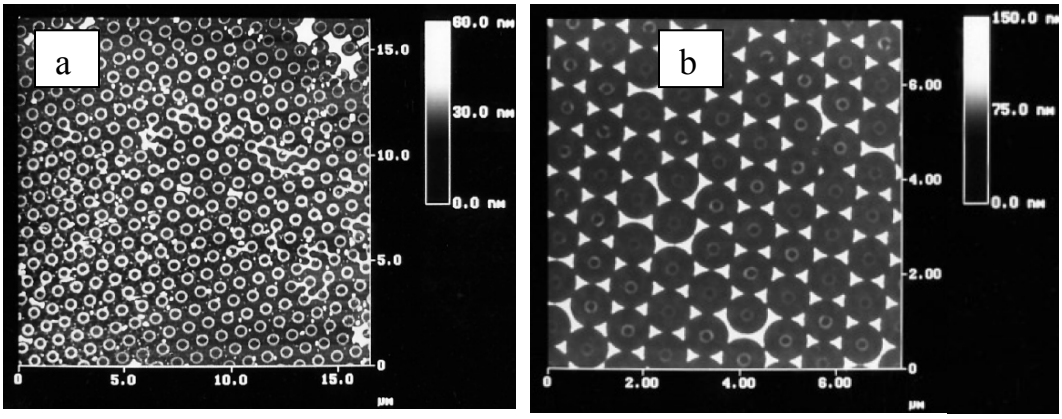

Figure 1.7. AFM images of periodic nanometer-scale gold a) nanorings, and b) triangular nanodots on mica substrates. Lattice periodicity is 895 nm. Reprinted with permission from Ref.[115] Copyright @ Springer Science and Business Media.

The interesting optical and electromagnetic properties exhibited by ring nanostructures relative to their solid analogues (nanodiscs and nanodots) have driven a significant research effort oriented towards the development of different avenues for the formation of ordered metal nanorings arrays. Aizpurua et al.,[119] for example, fabricated gold nanorings (120 nm in diameter, 40 nm in height and approximately 14 nm thick) by a combination of thermal evaporation and ion beam etching. In their method, the ring diameter is set by the size of the latex spheres used as a mask, whereas the thickness of the ring wall is determined by the thickness of the deposited gold film. Another method for the synthesis of gold nanorings based on the co-crystallization of submicron polystyrene latex and gold nanospheres, has been proposed by Velev's group.[49] The process is conceptually

simple; the substrate of interest is coated with a 9:1 dispersion of latex microspheres and gold nanoparticles. As the solvent evaporates, the particle volume fraction increases and the latex particles, present in a higher volume fraction relative to the gold nanoparticles, tend to crystallize first thus directing the crystallization of the much smaller gold nanoparticles in the interstitial sites of the latex mask. After the lattice is formed, the latex spheres are dissolved by dipping in toluene for about 15 min, and either non-connected gold nanorings or porous films remain on the substrate. Unlike thermal evaporation of the metal, this method renders highly porous nanostructures, as the metal structure itself consists of many colloidal nanoparticles. Whether rings or porous structures form depends primarily on the ratio of gold nanoparticles to latex microspheres in the colloidal dispersion.

Hexagonally-ordered isolated Fe nanorings (150 nm external diameter, and 20-30 nm thick walls) have been achieved by Giersig et al.[120] using a different approach. It involves a combination of thermal annealing and Angle-Resolved Nanosphere Lithography (AR-NSL) through a monolayer of latex spheres assembled on a silicon substrate via slow evaporation of the solvent. In this approach, the thermal annealing induced by microwave heating in a water/ethanol/acetone mixture (3:1:1) allows precise control of the size of the interstitial cavities in the range of 25 nm to 200 nm. Metal evaporation is done via

e-beam deposition with simultaneous control over the evaporation angle and sample rotation. In this method, the ring wall thickness can be controlled by the adjusting the size of the interstitial aperture via thermal annealing, and by controlling the evaporation angle (AR-NSL), which determines the amount of deposited metal.

Han and colleagues[121] have proposed an alternative route for the formation of isolated silver nanorings from colloidal lithography using polyelectrolyte hollow spheres prepared by layer-by-layer coating of polystyrene spheres (640 nm and 1000 nm in diameter) with poly(diallyldimethylammonium chloride)/poly(sodium 4-styrenesulfonate). In this method, the PE-coated spheres are assembled into close-packed monolayers on silicon wafers via the drop-coating technique, followed by extraction of the PS cores by dissolution in toluene for 12h. A precursor solution ($AgNO_3$) is then infiltrated into the negatively-charged PE shells through electrostatic interaction with the Ag^+ ions, and after reduction in a Tollen's reagent according to the following reaction, silver nanorings result.

$$RCHO + 2Ag(NH)^3OH \rightarrow RCOO^- + 2Ag(s) + NH_4^+ + NH_3 + H_2O$$

One of the advantages of Han's procedure to make metallic nanoarrays using PE hollow spheres is the fact that the size of the nanostructure can be easily

controlled by selecting the appropriate number of PE adsorption cycles. In addition, the method should work for a number of materials as long as the interaction between the precursor and PE shells is favorable.

Van Duyne's group have also reported the formation of magnetic nickel nanorings via e-beam deposition or pulsed laser deposition (PLD) of the metal through a monolayer of latex spheres (979 nm in diameter). Nanorings were never observed when the metal was thermally evaporated on the substrate. Based on this observation, they hypothesized that ring nanostructures form as the result of the bimodal kinetic energy distribution of gas-phase atoms produced by PLD and e-beam deposition. In other words, atoms with low kinetic energy (less than 1 eV) travel along the line-of-site of the mask and remain in the interstitial space, whereas atoms with higher kinetic energy (of the order of 1-10 eV), may have enough energy to reach the area where the spheres contact the substrate.[122]

In addition to nanodots and nanorings, other nanoparticle geometries are accessible from nanosphere lithography by changing the angle between the surface normal of the sample and the direction of material deposition. This technique, referred to as Angle-Resolved Nanosphere Lithography (AR NSL), not only increases the flexibility of particle lithography in terms of the nanoparticle shapes that can be created as a function of the deposition angle (θ_{dep}), and the azimuthal angle (ϕ) of a given crystalline domain within the mask; but also allows

a reduction of the in-plane nanoparticle size by up to a factor of 4 while using the same colloidal mask.[123] This is particularly important for the fabrication of nanopatterns in the 10-50 nm regime, where colloids' polydispersity significantly limits the formation of large area, 2D ordered colloidal arrays. An overview of different nanoparticle structural motifs fabricated via conventional NSL and AR NSL has been presented in a review paper by Haynes and Van Duyne.[122] In particular, the paper shows that silver nanostructures with varying degrees of overlap can be formed on mica substrates by changing θ_{dep} from 0^o to 20^o; whereas nanogaps with separation distances increasing with θ_{dep} can be obtained for $\theta_{dep} > 22^o$. A simple geometrical model has been proposed to determine the nanoparticle footprint as a function of θ_{dep} and ϕ has also been proposed.[123] Geometrically more complex nanostructures such as the nanochains and nanocontacts shown in Figure 1.8 can also be fabricated by performing multiple depositions with varied ϕ and θ_{dep} angles. These high aspect ratio nanostructures have shown strong dichroic contrast (varying by one order of magnitude) depending on whether the polarization of the exciting light is in direction parallel or perpendicular to the nanoparticle long axis, thus suggesting possible applications as dichroic filters.[124]

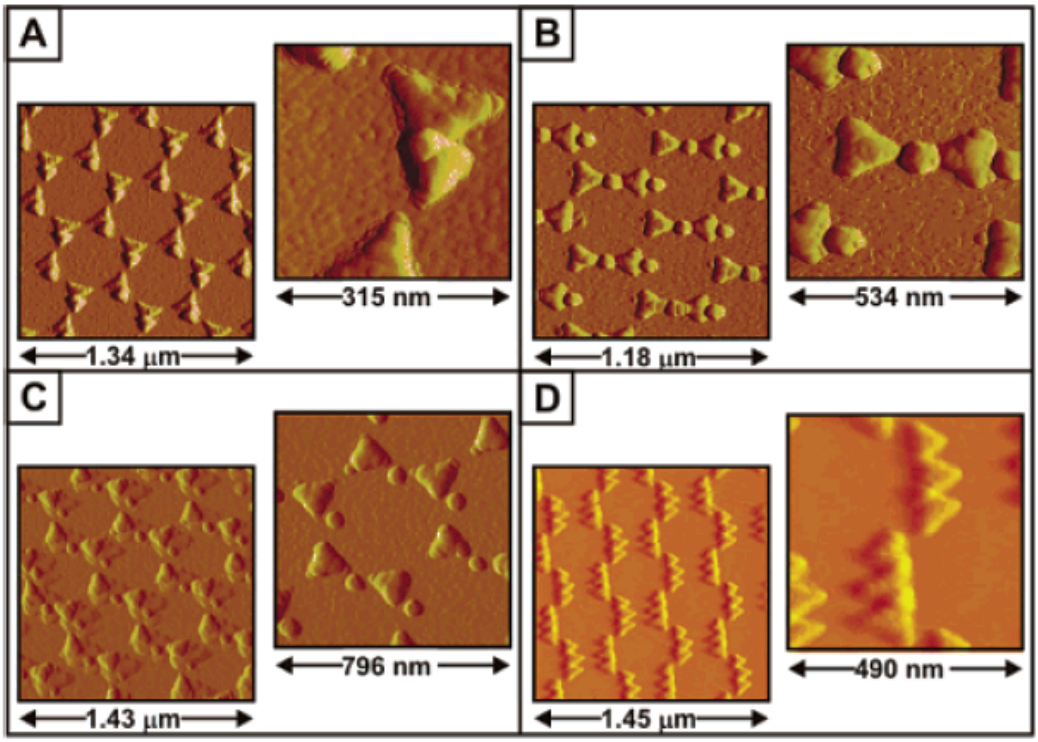

Figure 1.8. AFM images of nanostructures fabricated via multiple deposition angle-resolved nanosphere lithography with varied ϕ and θ_{dep} angles. Reprinted with permission from Ref.[124] Copyright @American Chemical Society.

Ordered iron nanorods have been achieved by Giersig et al.[120] via thermal evaporation of Fe through the rodlike interstices formed in a close-packed colloidal monolayer subjected to uniaxial stretching and thermal annealing. The stretched colloidal monolayer and the resulting Fe nanorods are shown in Figure 1.9. As suggested by the computer simulation results presented in Gersig's paper, more complex nanoparticle geometries could also be possible by combining uniaxially stretched masks and shadow NSL. Other structures such as 2D

hexagonal arrays of silver hollow spheres have been prepared by Chen and colleagues[125] via colloidal templating coupled with seeding and electroless deposition of the metal. The colloidal template was formed by confining the spheres between two parallel plates separated a fixed distance, in a procedure analogous to molding in microcapillaries.[126] In a subsequent step, the spheres were activated with a layer of Sn^{2+} ions in the form of SnCl(OH), $Sn(OH)_2$, or $Sn_2Cl(OH)_3$, followed by electroless plating in a mixture of potassium sodium tartrate and $AgNO_3$ in ammonia solution. The thickness of the silver shell was controlled by adjusting the time of electroless plating. Then, the latex cores were dissolved in a mixture of benzene and methanol, and an ordered array of hollow silver shells (45 nm thick approximately) was left on the surface. The presence of silver on the shells was confirmed with energy-dispersive X-ray analysis (EDX). These nanostructures are expected to find potential applications in Surface Enhanced Raman Spectroscopy.

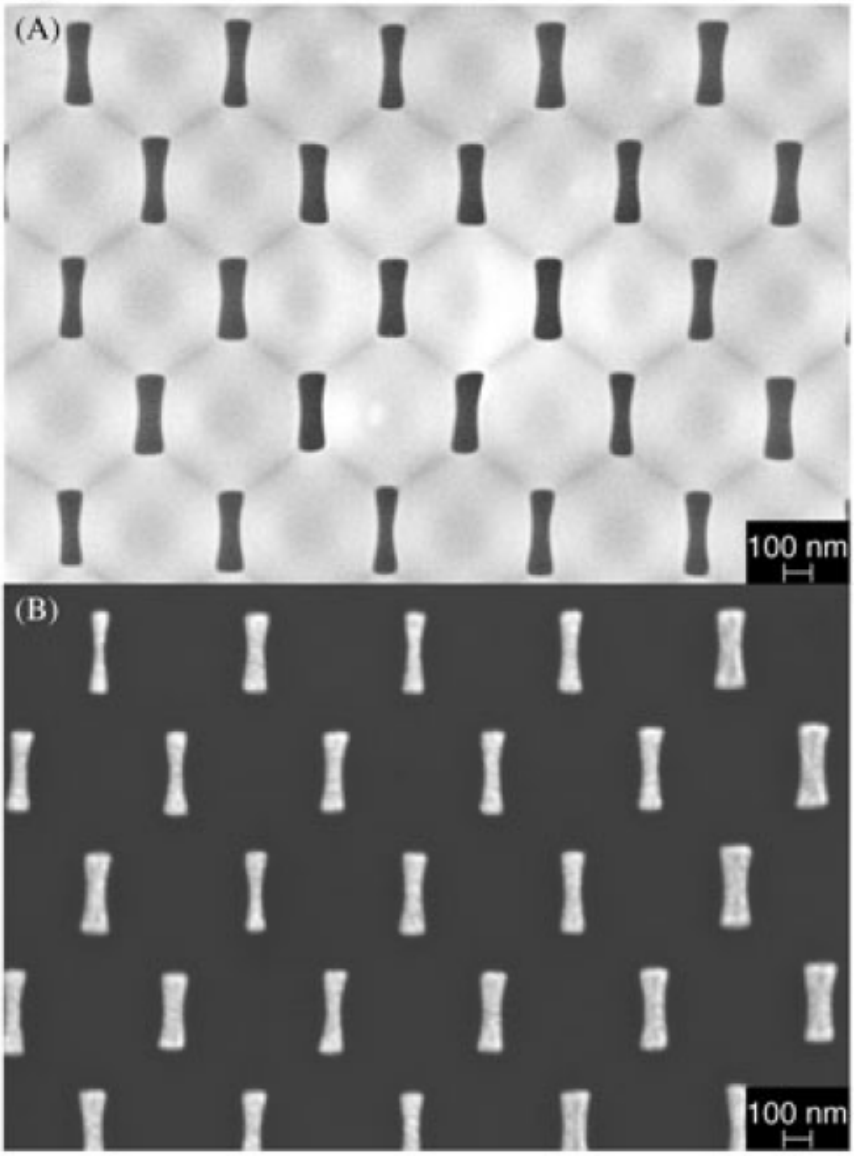

Figure 1.9. SEM images of a) rodlike apertures in stretched and subsequently annealed 540-nm PS latex mask, and b) hcp-ordered Fe nanorods evaporated through this mask. Reprinted with permission from Ref.[120] Copyright @Wiley-VCH Verlag GmbH & Co KGaA.

4.2. Patterning of Semiconductor Materials

Although not as large as the attention given to metals, the patterning of semiconductor materials via particle lithography has received some attention by the scientific community. Early work by Lenzmann et al.[127] in 1994, for example, showed that a monolayer of latex spheres deposited on a glass substrate using the LB technique can serve as a lithographic mask for the thermal evaporation of zinc sulfide nanostructures shaped as trigonal pyramids. Moreover, they demonstrated that the size and morphology of the nanostructures can be effectively modified by coating the surface of pre-existing ZnS nanopillars with thin metal films. In particular they showed that trigonal pyramids of ZnS transform into lentil-like nanostructures when a 0.2 um Y_2O_3 film is thermally overgrown the nanoparticle surface.

More recently, Li and Zinke-Allmang,[128] have proposed an alternative method to fabricate size-tunable highly-ordered Ge nanoparticle arrays on n-doped silicon substrates via NSL and thermal annealing. In their work, a monolayer of 300 nm polystyrene spheres previously dispersed in a solution of X-100 Triton surfactant and methanol (1:5000 by volume) was spin-coated on a silicon substrate, followed by e-beam evaporation of germanium through the mask. Following the deposition, the spheres were removed by sonication in methanol for 1 min, and a hexagonal array of triangular-shaped Ge nanoparticles

(with 70 nm in-plane, and 6 nm out-of-plane dimensions) was left on the surface. The size and morphology of the Ge nanostructures was further controlled by thermal annealing. As seen in Figure 1.10, spherical rather than triangular-shaped Ge nanostructures were obtained after thermal annealing in ultra-high vacuum at 650^{o}C for 25 min. This morphological change was usually accompanied by a reduction of the in-plane size by about 50 percent and an increase of the height by a factor of 5, while the overall volume of the nanostructure remained constant. Based on this observation, the authors proposed a new approach to tuning the dimensions of the nanostructures by varying the thickness of the deposited Ge layer, which in turn sets the individual nanoparticle volume when the same size latex spheres are used as the deposition mask. In this manner, Li and Zinke-Allmang demonstrated that keeping the annealing conditions constant with varying Ge particle volume allows control over the nanostructure size and shape, thus resulting in nanocrystals with various facets.

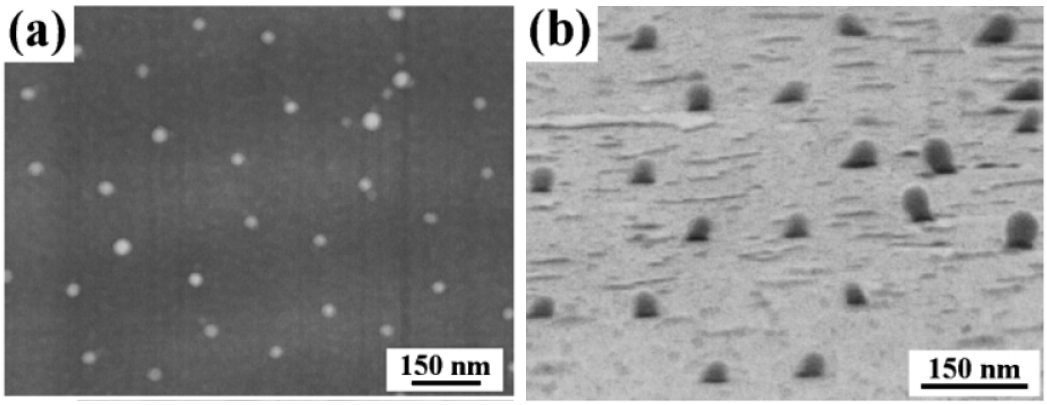

Figure 1.10. SEM images for the after-annealing Ge nanostructure/Si surface. a) normal view, and b) 45^{o} tilt angle. Reprinted with permission from Ref.[128] Copyright @Institute of Pure and Applied Physics, Japan.

Pacifico et al.[129] have reported the fabrication of 2D ordered arrays of quantum dots by a relatively simple procedure involving the formation of hexagonally packed silver triangular islands (30 nm thick) by thermal evaporation of the metal through the interstitial sites of a monolayer of latex spheres (3.2 and 4.9 um in diameter) initially assembled at the air-liquid interface, and subsequently transferred onto a glass substrate. A self-assembled monolayer (SAM) of aminoethanethiol is then adsorbed onto the silver islands with the mercaptant moiety preferentially bounded to the metallic surface and the amine groups exposed to the solution. In the final step, the functionalized glass substrates are contacted with a chloroform solution of core-shell CdSe@ZnS quantum dots, so that the dots link to the surface by reacting with the amine

functional groups. The result is a 2D hexagonal array of quantum dots with tunable luminescence. Other semiconducting nanostructures, such as crystalline titania nanorings (rutile-phase), have also been fabricated by sintering a close-packed monolayer of poly(styrene-co-divinylbenzene) latex spheres at 125^{o}C for 1h, followed by selective dissolution of the polystyrene cores in cyclohexane.[130] The resulting honeycomb structure is then used as the template for the infiltration of titanium isopropoxide, a TiO_2 precursor, which selectively adsorbs to the inner surface of the honeycomb wall via strong interactions with the phenyl groups on the honeycomb. After calcination at 900^{o}C, both interconnected and isolated titania rings with center-to-center distances relatively unchanged with respect to the original template, were obtained on the substrate. Energy-dispersive X-ray spectroscopy (EDX), and X-ray diffraction (XRD) were used to determine the atomic composition and the crystalline phase of the nanostructures. The merit of the technique relies primarily on the fact that polymeric honeycombs can be formed without the need of an infiltration step; however, it requires more complex (and perhaps more costly) colloids. In addition, when used as lithographic masks for the synthesis of other nanostructures such as semiconducting TiO_2 nanorings, the shape of the resulting nanostructures is somewhat distorted and does not exhibit long range ordering.

Cao et al.[131] have applied a potentiostatic electrochemical deposition (ECD) method to synthesize semiconducting ZnO honeycomb arrays with controllable morphology (hemispherical vs. well-like structures) by appropriately tuning the deposition potential. The procedure starts with the formation of a PS monolayer crystal on ITO-coated glass substrates via the spin-coating method. In order to promote a better adhesion with the substrate, the monolayer is subjected to a sintering step at 78^{o}C for 3 min. The ECD is carried out in an aqueous zinc nitrate solution for 2h, and then the spheres are ultrasonically removed in methylene chloride for 1 min approximately. The main limitation of this technique is the intrinsic need for conducting substrates.

Large area, size-tunable periodic silicon nanopillar arrays with sub-10 nm resolution have been created by Kuo and collegues[132,133] using a combination of NSL and Reactive Ion Etching (RIE). First, a close-packed monolayer of colloidal spheres (280 nm or 440 nm in diameter) was spin-coated on n-doped silicon wafers. Then, a thin chromium layer was sputter-coated through the colloidal template, followed by template removal via ultrasonication in CH_2Cl_2 for a few minutes. In the next step, uncovered areas were etched away via RIE and a hexagonal array of chromium-capped silicon nanopillars was formed on the surface. After removal of the chromium caps with a selective etchant (Transene), a SiO_2 layer of known thickness was grown on the pillars surface by thermal

oxidation at 800^{o}C. Upon removal of this external layer with an oxide etchant, the lateral dimension of the nanopillars was effectively reduced. The dependence of nanopillar size (lateral dimension) with oxidation time is illustrated in Figures 1.11a-c for nanostructures subjected to thermal oxidation at 800^{o}C for a) 60 min, b) 90 min, and c) 150 min, respectively. All the samples were prepared through a 50 nm thick chromium mask. Figure 1.11d, shows the result when chromium is replaced by a 100 nm thick aluminum mask. An advantage of the method proposed by Kuo and co-workers is that the separation distance and the size of the nanopillars can be tuned independently by adjusting the etching time, etching gas composition, the dimensions of the colloidal mask, and the metal used as a mask for the RIE step. Moreover, the resulting nanopillars have been shown to effectively serve as stamps for nanoimprint lithography.

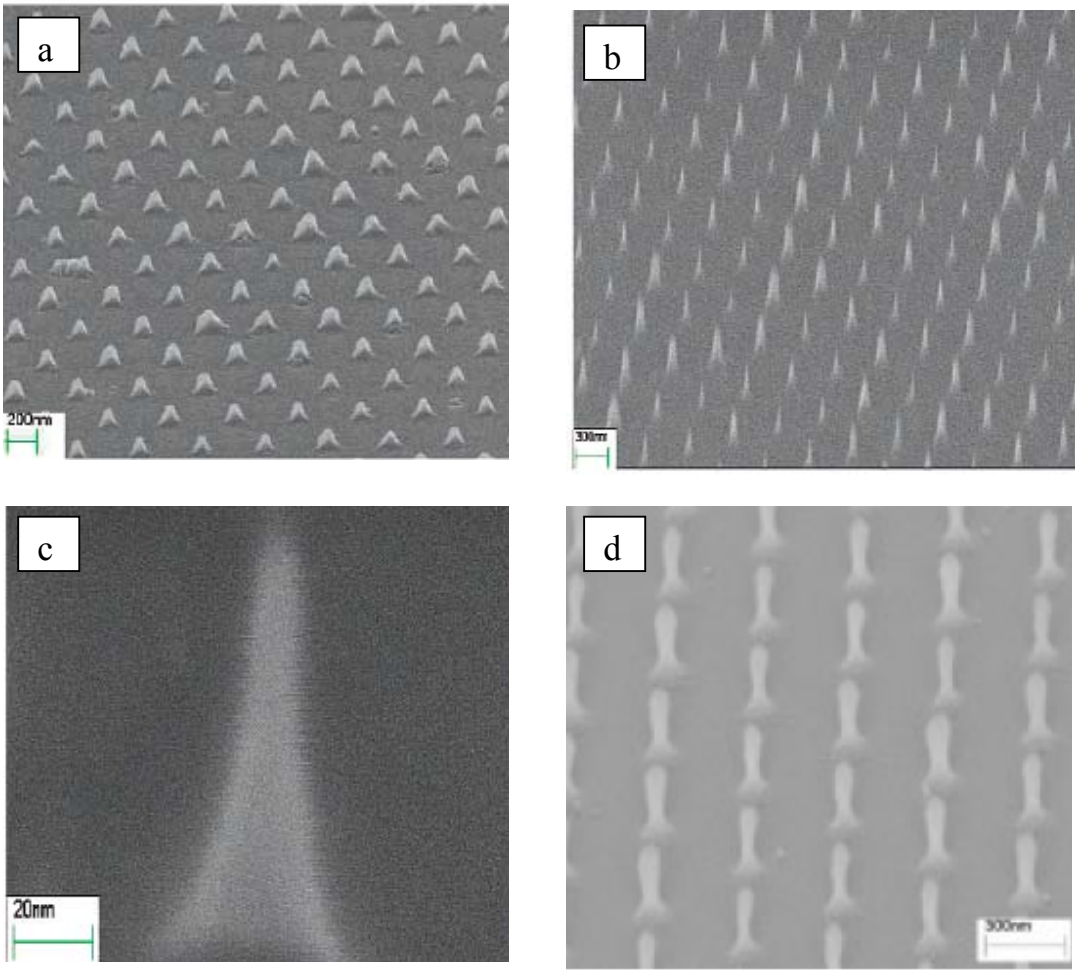

Figure 1.11. SEM images (45° tilt) of the size-reduced silicon nanopillar arrays formed using a 50 nm thick chromium mask prepared from a 440-nm double layer (DL) polystyrene template, after different oxidation times: a) 60 min, b) 90 min, c) Sub-10 nm pillar obtained using a 280 nm DL polystyrene template and 150 min of oxidation, d) Nanopillars formed when chromium is replaced by a 100 nm thick aluminum mask. Reprinted with permission from Ref.[132] Copyright @American Chemical Society; and Ref.[133] Copyright @Wiley-VCH Verlag GmbH & Co KGaA.

Given their potential applications as biosensors, field-emission and antenna devices to cite just a few, vertically aligned nanotubes and nanowires constitute another group of nanostructured materials studied by the scientific community. In particular, the formation of ordered nanotube and nanowire arrays of semiconductor materials via colloidal lithography has been explored by several research groups as an alternative to more expensive and time consuming methods such as e-beam lithography. Rybczynski et al.,[134-136] for example, have grown large periodic arrays of well-aligned, size-tunable carbon nanotubes onto n-doped Si wafers using hot filament plasma-enhanced chemical vapor deposition (PECVD), on an ordered array of Ni catalyst nanodots prepared via particle lithography from a monolayer of latex spheres previously assembled at the air-SDS solution interface. The formation of single-wall vs. multi-wall nanotubes was found to depend strongly on the size and shape of the catalyst particles. Single, free-standing nanotubes were most likely formed for Ni dots smaller than 300 nm. Well-defined instead of triangular-shaped nanoparticles were also more prone to rendering single tubes. As expected, the nanotube density was also found to correlate with the template size; in general, the larger the colloidal spheres in the mask, the lower the nanotube areal density. The problem with using larger spheres to decrease the array density is multiple nanotube growth for dot sizes greater than 300 nm. One way to circumvent this problem is by producing smaller catalyst particles via evaporation through a bilayer mask. The disadvantage of this

approach is that the formation of good quality bilayer masks tends to be operationally more challenging than their monolayer analogues. In this respect, Park and colleagues[137] have proposed two routes to decrease the size of the catalyst particle via angle-resolved NSL through a monolayer mask. One way is to deposit the catalyst at a high angle (e.g. 30^{o}); the other is to reduce the effective size of the catalyst particle by covering its surface with a non-catalytic metal (e.g. Cr) deposited at a different angle. Figure 1.12 shows the results obtained from these two approaches in comparison with the conventional deposition of Ni nanoparticle at 0^{o}. As deducted from the SEM images, Park's method can be effectively applied to control the areal density of the nanotubes array via AR NSL using a monolayer mask.

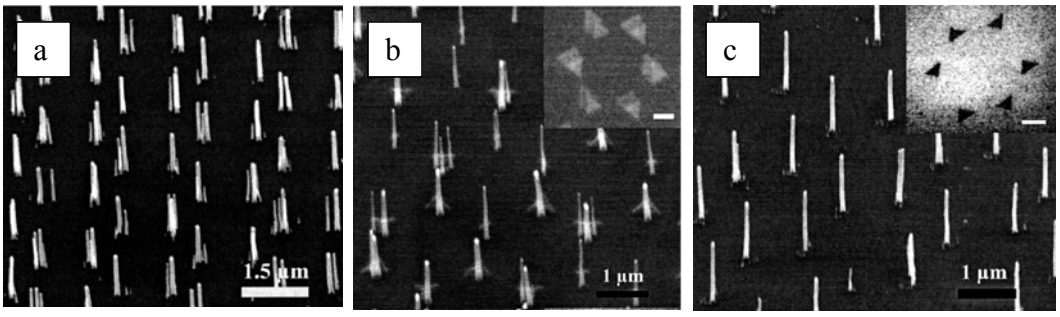

Figure 1.12. SEM images of CNT arrays grown on catalyst patterns formed at different deposition angles: a) Ni at θ_{dep}= 0°, b) Ni followed by Cr at θ_{dep}= 0° and 15°, respectively. c) Ni at a high deposition angle θ_{dep}= 30°. Reprinted with permission from Ref.[137] Copyright @American Institute of Physics.

The formation of hexagonal arrays of vertically aligned ZnO nanowires on single-crystal sapphire substrates has also been explored by Rybczynski's group using a vapor-liquid-solid (VLS) growth process with NSL-templated gold nanoparticles as the catalyst.[138] Similar results were obtained by Wang and colleagues,[139] although their experimental results showed denser nanowire arrays. As for the growth of aligned carbon nanotubes, whether single or multiple ZnO nanowires result from a single gold nanoparticle depends strongly on the size of the catalyst particle itself. In this respect, Rybczynski and collaborators suggested a threshold for single nanowire formation around 50 nm. They also found that multiple growth can be further reduced by a two-step annealing process whereby trace amounts of oxygen in the system can be effectively removed. In general, the main advantage of using particle lithography to fabricate ordered arrays of nanotubes and nanowires is that the size, shape, and areal distribution of the catalyst particles (and ultimately the nanotube array) can be controlled in a simple, efficient, inexpensive process.

4.3. Patterning of Ceramic Materials

The increasing demand for ever smaller integrated miniature devices including dynamic random access memories (DRAM), sensors, and

microelectromechanical actuators among others, has driven a significant research effort aimed at the development of new alternatives for the patterning of ceramic materials at the nanometer scale, as well as a better understanding of the size reduction effect on the ferroelectric/piezoelectric properties of the nanostructures as the result of crystalline phase transitions and other phenomena. Due to its simplicity and low cost, particle lithography has been widely implemented in conjunction with other methods such as the sol-gel technique, pulsed laser deposition (PLD), and inductive coupled plasma (ICP) etching for the patterning of ceramic materials at the nanometer scale. A very active group in this area is that of Ma and co-workers, who have successfully fabricated highly ordered arrays of pyramid-shaped $BaTiO_3$,[140,141] and $SrBi_2Ta_2O_9$[142] nanostructures on single-crystal Nb-doped $SrTiO_3$ substrates using a combination of particle lithography and pulsed layer deposition. In their method, the spheres are removed by dissolution in methylene chloride, and then the resulted nanostructures are annealed in air at 650^{o}C ($BaTiO_3$), and 950^{o}C ($SrBi_2Ta_2O_9$) for 1 h. Experimental results show that after annealing, the nanostructures lose their typical pyramid-like shape and break into nano-sized domains of high crystal anisotropy. As confirmed by their piezoresponse hysteresis loops, these nanostructures partially retain their ferroelectric behavior. The observed reduction in piezoresponse has been ascribed to crystalline defects in the colloidal mask used for the deposition step. In addition to the piezoresponse force measurements, the polycrystalline

nature and phase composition of the nanostructures was assessed by cross-sectional transmission electron microscopy, and selected area electron diffraction (SAED) analysis, respectively.

Highly-ordered nanopore arrays of ceramic materials have also been actively pursued due to their high surface area, which makes them suitable for sensing and catalytic applications, as well as for their interesting optical and electric properties which open up many potential applications as nanophotonic and optoelectronic devices, to name a few. By far the most common method for the synthesis of porous ceramic nanostructures via particle lithography is the sol-gel method, a technique that involves the hydrolysis and condensation of alkoxysilanes.[143] Kanungo and Collinson,[144] for example, have prepared ordered arrays of size-tunable cavities into a silica matrix by simultaneously spin-coating a 1:1 dispersion of latex spheres (500 nm in diameter) and the precursor solution onto glassy carbon substrates. They used a sol mixture consisting of tetramethoxysilane (TMOS), methanol, water and HCl. After film formation, the polystyrene spheres were removed by soaking in chloroform for 2-3h, and a honeycomb with well-ordered through-holes was obtained on the substrate. The diameter and depth of the cavities can be effectively controlled by adjusting the diameter of the latex spheres and by tuning the conditions of the sol-gel process. Nanostructures such as these, where non-conducting silica walls delimit the

fraction of an exposed underlying conducting substrate may find potential applications in electrochemical sensing, nanobatteries, and as nanosized reaction vessels for electrochemical deposition as recently demonstrated by Khramov et al.[145]

Ordered Fe_2O_3 nanopore arrays with controllable morphology have been fabricated by Cai and colleagues[146] via particle lithography and the sol-gel technique. The unique aspect of the solution-dipping template strategy implemented by Cai's group is the fact that the polystyrene colloidal template floats on the precursor solution due to surface tension. This confers great flexibility to the process as porous nanostructures can be engineered so that either through-holes or upper-end open cavities form, depending on the concentration of the sol mixture, $Fe(NO_3)_3$, and the treatment conditions (drying temperature and time, calcination vs. dissolution of the latex template, etc). In addition, the floating colloidal monolayer can be transferred onto another substrate prior to the drying step, thus making possible the formation of nanostructures even on substrates where the initial monolayer formation might be otherwise challenging. Moreover, the nanostructure morphology can be controlled by adjusting the concentration of the precursor solution as shown in the experimental results in Figure 1.13. At high $Fe(NO_3)_3$ concentrations (i.e. 0.8 M), complex nanostructure arrays such as the pore-hole/pore-particle morphology shown in Figure 1.13g tend

to form on the substrate. As the concentration is lowered through-pore honeycombs structures with thinner walls form instead. Ring-like structures are also observed at very low concentrations (i.e. 0.002 M). For a given concentration, the pore size can be controlled by changing the diameter of the latex spheres used as a template. The ability to control nanostructure size and morphology is further complemented by great flexibility in terms of precursor and substrate choices. Using the same technique, Cai and co-workers have been able to prepare similar porous nanostructures of other materials such as zinc, ZnO, NiO, Co_2O_3, CuO, CeO_2, Eu_2O_3, Dy_2O_3, and In_2O_3.[147] They have also demonstrated the fabrication of size-tunable hexagonally-ordered nanoparticle arrays from the partial dissolution of Fe_2O_3 and In_2O_3 porous films in 1M oxalic acid, and 10 wt% nitric acid, respectively.[148]

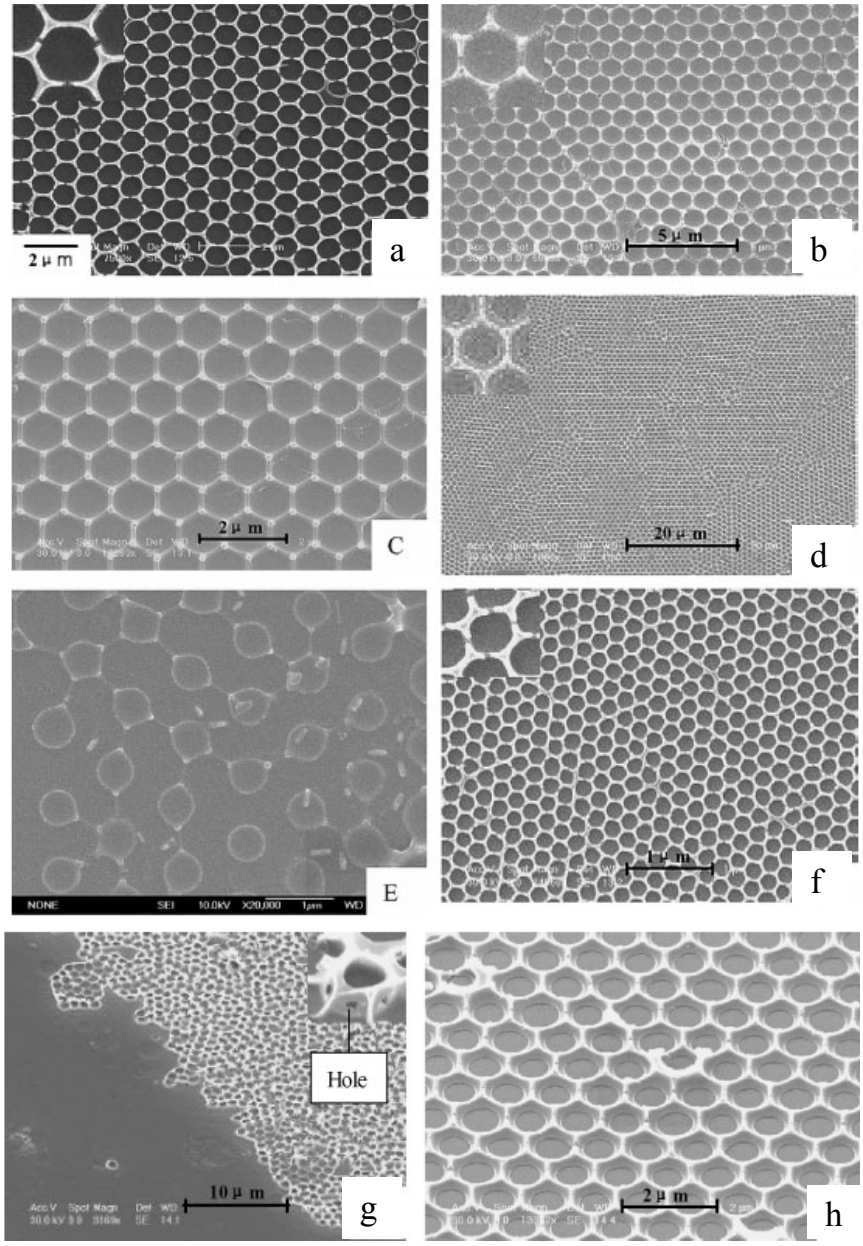

Figure 1.13. SEM images of ceramic nanostructures prepared with different precursor concentrations: a) 0.8 M, b) 0.08 M, c) 0.06 M, and d) 0.002 M. Samples a) to e) were prepared with 1 um PS latex spheres, whereas 200 nm spheres were used as a template for f). The panels in g) and h) correspond to the tilt views of samples a) and d), respectively. Reprinted with permission from Ref.[146] Copyright @Wiley-VCH Verlag GmbH & Co KGaA.

More recently, Cai and colleagues[149,150] have proposed a new strategy for the formation of honeycomb/nanopillar arrays based on a combination of the sol-gel technique and controlled heat-induced deformation of 2D close-packed polystyrene colloidal templates above the polystyrene glass transition temperature (Tg~100^{o}C). Both silica and Fe_2O_3 nanostructures with various morphologies have been prepared from this approach. In both cases experimental results confirm that the interstitial sites within a close-packed PS latex monolayer can be effectively manipulated by choosing the appropriate sintering time. Upon infiltration with the precursor solution, followed by template removal via calcination, morphologically controlled nanostructures form on the substrate as shown in Figure 1.14. 2D ordered arrays of silica nanostructures with complex shapes (e.g. ellipsoidal-shaped nanoholes) have also been fabricated by Wang and collaborators via particle lithography using a combination of selective inductive coupled plasma (ICP) etching and the sol-gel technique.[151]

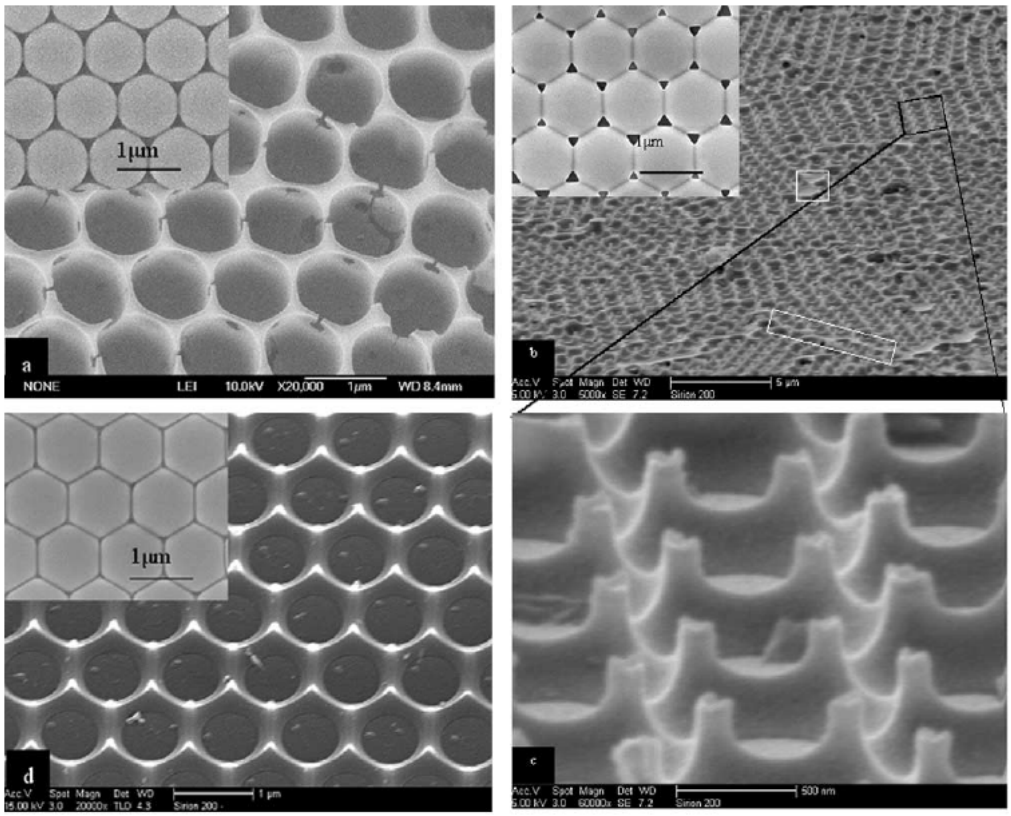

Figure 1.14. SEM images of Fe_2O_3 ordered nanostructures fabricated via the sol-gel technique with a 0.5 M $Fe(NO_3)_3$ precursor solution, and colloidal monolayers of 1 um PS spheres sintered at 120^{o}C for different periods of time: a) 0 min, b) 15 min, and d) 25 min. Figure c) is a zoom of sample shown in b). Reprinted with permission from Ref.[150] Copyright @Elsevier Ltd.

4.4. Patterning of Proteins and Polymeric Materials

This section deals with the patterning of proteins and their synthetic polymer analogues. As appropriately stated in the seminal work by Nagayama[152] on the formation of well-ordered protein arrays, both proteins and polymers are a

class of materials that result from a chemical reaction with different information inputs. In the case of proteins, the synthesis process is mainly directed by the translation of genetic information; whereas synthetic polymers are the result of a statistically controlled polymerization reaction, far less informative about the final fate of the synthesis. Surface-patterned proteins have been widely studied by the scientific community as a way to improve biological activity by the proper confinement of chemical functionality to specific sites, with just the right orientation. They have also been used for the study of cell growth and rolling behavior, as well as in biosensing, and molecular recognition.[153-159] Early works in protein and cell patterning have explored the self-assembly of protein monolayers at various interfaces including air/water, air/lipid/water, water/solid, and air/solid interfaces. Fromherz,[160] for instance, assembled a monolayer of ferritin on a lipid monolayer. Better quality 2D crystals of ferritin[161] and bacterial flagella[162] were achieved by Yoshimura's group using a metal liquid surface (e.g. mercury) instead of a lipid monolayer on water. The crystallization of antibodies and other proteins in the presence of ligand-introduced lipids, which enhance the specificity of protein-substrate interactions, has also been explored by other groups.[163-165] However, the quality and reproducibility of the crystalline arrays were not as desired.

More recently, Yi and co-workers[166] presented a novel approach to 2D cell patterning based on the use of polymer microstructures with controlled-geometries (rings, dots and honeycombs) to direct the assembly of bacterium, Serratia marcescens. The polymer nanostructures are formed by infiltration a siloxane elastomer precursor (polydimethylsiloxane-PDMS) into the interstitial sites of a close-packed array of PS spheres. Depending on the curing conditions, two different polymer patterns originated as the result of the temperature-dependent rheology of the PS colloids and the PDMS: At elevated curing temperatures (105^{o}C for 1h) the PDMS crosslinking rate is accelerated, and necking takes place in the PS colloidal template; as a result, the siloxane precursor can only fill in the interstitial sites, forming isolated polymer microrings and microdots. On the other hand, when curing is carried out at room temperature for long periods of time (50 h), the lower viscosity siloxane is able to penetrate further underneath where the spheres touch, forming PDMS honeycombs instead. Bacteria adsorption studies were carried out on both PDMS-honeycomb structures and non-templated, flat PDMS substrates. The results are shown in Figure 1.15. As evidenced by the strong contrast in Figure 1.15a, not only Serratia marcescens bacteria mimic the honeycomb template, but also they seem to adsorb with a higher packing density relative to the non-templated PDMS film (Figure 1.15b). The authors provided an explanation for this observation based on specific hydrophobic (PDMS)/hydrophilic (glass) interactions with the honeycomb-

templated substrate, which favor a more extended configuration as opposed to a flatter conformation in which the bacteria's long axis is parallel to the featureless PDMS film, as illustrated in the schematic in Figure 1.15c.

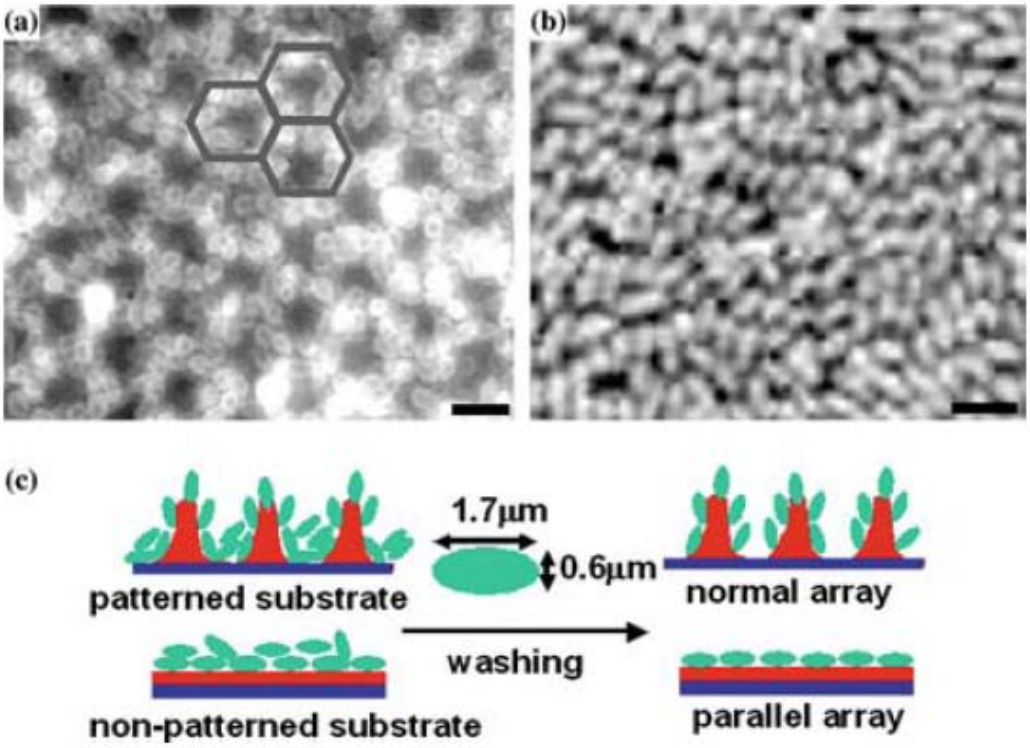

Figure 1.15. a) Optical micrograph of hexagonal patterned fluorescent bacterial cells, and b) bacterial cells on the non-patterned flat polydimethylsiloxane (bacteria are bright against a dark background). c) Schematic views of bacteria adsorption on the polydimethylsiloxane substrate; green ellipsoids, blue layer, and red layer represent bacteria, glass slide, polydimethylsiloxane, respectively. Reprinted with kind permission from Ref.[166] Copyright @Springer Science and Business Media.

An alternative approach for protein patterning based on 2D particle lithography has been proposed by Garno et al.[52,167] The procedure is relatively simple; a mixture of latex spheres and the protein solution (bovine serum albumin-BSA, rabbit immunoglobulin G-IgG, or staphylococcal protein A) is drop-coated on the substrate (mica, or gold thin films), and a hexagonal array of protein-coated latex spheres forms as the result of convective forces during drying. In the final step, the latex spheres are removed by rinsing with small volumes of water (about 0.5 mL water per 1 cm^2 surface). Moreover, the size and morphology of the protein arrays can be controlled by tuning the protein-to-latex ratio, and by changing the size of the latex spheres used as a template. Figure 1.16 shows three different BSA protein nanostructures prepared via particle lithography with 500 nm latex spheres, and various protein-sphere ratios corresponding to monolayer coverage (61000:1), half a monolayer (31500:1), and a lower sphere coverage fraction (26000:1). In every case, the height of the protein layer is about 4 nm, which corresponds well to the diameter of the BSA protein molecule as determined from X-ray crystallography measurements.[168] Similar results have been obtained by Marquez et.al.[169] from the adsorption of IgG (20 ug/mL) and fibrinogen (50 ug/mL) protein solutions onto a colloidal array of PS latex spheres with diameters in the range of 0.56-5.43 um. As demonstrated in chapter 3, the main difference between the nanostructures fabricated by Marquez and those by Garno is that the former's honeycombs

consist of through-holes, whereas in Garno's process the simultaneous drop-casting of the protein and the latex spheres allow protein penetration underneath the spheres.

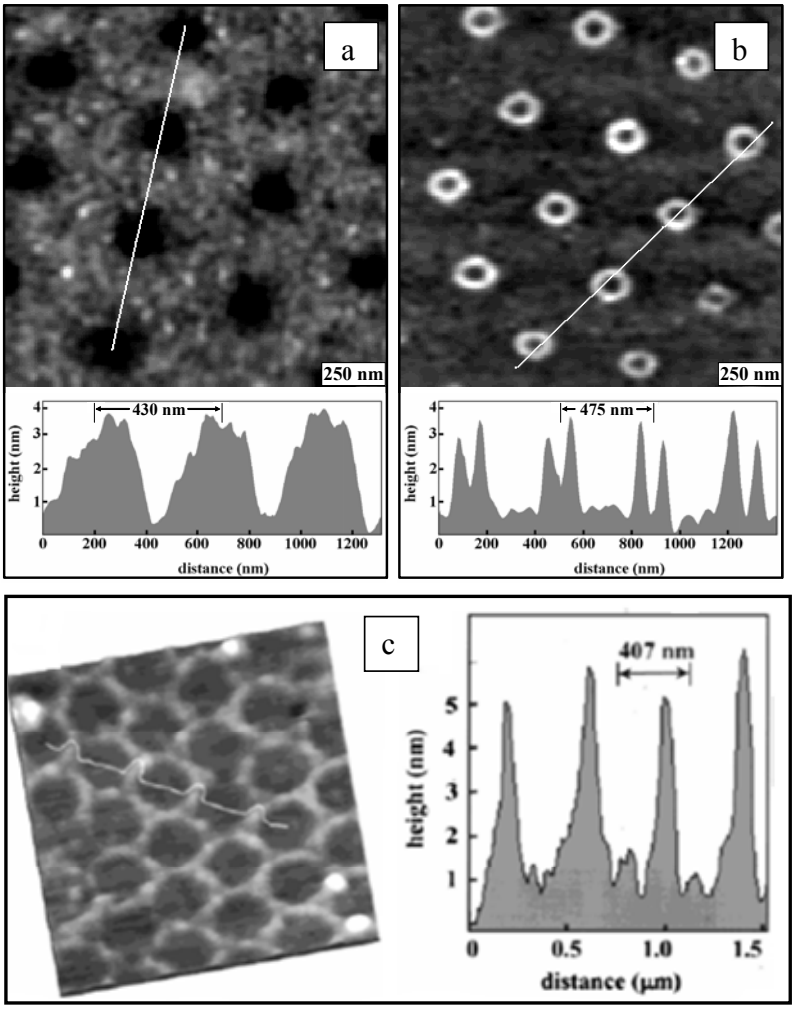

Figure 1.16. AFM topographs and corresponding cursor profiles of different arrays of BSA nanostructures produced with 500 nm latex particles at different protein/latex ratios: a) 61,000:1; b) 30,500:1; and c) 26,000:1. Reprinted with permission from Ref.[52] Copyright @American Chemical Society; and Ref.[167] Copyright @Royal Society of Chemistry.

Gleason and colleagues[170] have also explored the patterning of proteins and cells via colloidal lithography. They utilized a combination of gravimetric settling and applied electric fields (AC and DC) to drive the formation of fibronectin-coated colloidal particle arrays on gold-coated glass slides. The particle density in the final arrays was effectively controlled by varying the settling time, the particle concentration and the frequency of the AC field: closed-packed arrays were formed at low frequencies (i.e. 500-700 Hz), whereas arrays of decreasing particle densities resulted at higher frequencies (i.e. 2000-40000 Hz). After particle assembly, a DC field (2.5 V) was introduced to immobilize the particles on the substrate irreversibly. Then, the non-attached particles were removed by rinsing with a phosphate-buffered saline solution, and the uncovered areas of the substrate were made non-adhesive to other proteins and cells by incubating in a 2 wt% bovine serum albumin solution at room temperature for 30 min. These samples were further used for the study of fibroblast adhesion and spreading behavior as a function of fibronectin active sites. Experimental results revealed more compact cell morphologies on close-packed particle arrays, whereas a more extended cell conformation prevailed for the less dense arrays.

A general observation regarding the use of particle lithography for protein patterning is the fact that protein/sphere/substrate interactions must be optimized so that a strong adhesion exists between the protein and the substrate. The

interaction with the spheres, on the other hand, must be relatively weak in order to facilitate template removal without disruption of the protein nanostructure. In this respect, the combination of surfactant-free hydrophobic PS latex spheres and highly hydrophilic, flat substrates such as mica or glass have been found to work well for protein patterning via particle lithography.

Another approach to protein patterning has been presented by Valsesia and colleagues,[171] who demonstrated the selective immobilization of protein clusters on polymeric nanocraters of polyacrylic acid and polyethylene glycol (PEG) prepared via particle lithography and plasma-enhanced chemical vapor deposition (PECVD). The procedure employed is as follows: first a 350 nm thick PAA layer was deposited onto a silicon substrate via PECVD under optimum conditions for maximum concentration of surface carboxylic moieties. Then, a monolayer of PS latex spheres (500 nm in diameter) was spin-coated on the surface of the PAA layer, and subsequently exposed to oxygen-plasma etching so as to transfer the colloidal hexagonal pattern onto the underlying PAA layer. The residual PS spheres served as a mask for the PECVD deposition of a 30 nm thick PEG layer, highly resistant to protein adhesion. Then, the colloidal mask was removed by ultrasonication in water. The chemical composition of the surface after each treatment was addressed by FTIR, and chemical force microscopy. Finally, as confirmed by confocal microscopy, fluorescently-tagged BSA protein was

selectively immobilized onto the PAA-capped nanoposts through the reaction with activated carboxylic functional groups. Little or no protein was adsorbed inside the PEG pits.

Michel et al.[172] have also exploited the fabrication of biologically relevant chemical patterns and their use in surface protein patterning. The procedure is rather lengthy, involving as many as 10 steps. In the first step, a 12 nm TiO_2 layer was deposited on SiO_2 and quartz wafers. Then, the surface was rendered positively charged through layer-by-layer deposition of positively-charged poly(diallyldimethylammonium)chloride (PDDA), and negatively-charged poly(sodium 4-styrenesulfonate) (PSS). A monolayer of negatively-charged PS spheres (107 nm diameter) was drop-coated on the substrates, and subsequently subjected to thermal annealing for 60 s at 116^{o}C. The resulting colloidal array was used as a mask for the etching of the polyelectrolyte layers down to the SiO_2 substrate, protecting the TiO_2 layer right underneath the spheres. After removal of the colloidal mask by UV/ozone treatment for 1 h, nanostructured TiO_2 pillars on a SiO_2 background remained on the substrate. In the next step, these nanostructures were made biologically active by the selective adsorption of dodecyl phosphate (DDP) onto the TiO_2 pillars, and polycationic poly-L-lysine-grafted-poly(ethylene glycol) (PLL-g-PEG) adsorption on the SiO_2 background by a process known as Selective Molecular Assembly Patterning (SMAP).[173] The

SMAP-treated samples thus consisted of protein adhesive pillars on a non-adsorbing PLL-g-PEG background. Finally, protein patterning was carried out by incubation in 40 ug/mL fluorescently-tagged streptavidin, followed by immobilization of biotinylated phospholipid vesicles onto streptavidin. These biotinylated liposomes were used as markers for the streptavidin adsorbed to the adhesive TiO_2 nanopillars. Although the technique has been proved successful for the fabrication of biologically relevant surfaces at the nanometer scale, the patterns formed do not possess long range ordering.

The formation of polymer nanostructures via particle lithography has been the subject of an important research effort. In particular, the fabrication of ordered 3D macroporous polymer films has received great attention due to their potential applications as photonic band gap materials, porous electrodes, and filtration membranes, among others. Caruso and colleagues have been very active in this field; they demonstrated the fabrication of 3D polyaniline (PAni) and polypyrrole (Ppy) inverse opals using 3D colloidal arrays as the masks for the oxidative polymerization of aniline,[174] and the electrochemical polymerization of pyrrole.[175] Sumida et al.,[176] and Barlett et al.[177] have also prepared inversed opals of polythiophene, Ppy, and PAni via electrochemical polymerization. In addition, poly(methyl methacrylate), poly(urethane), poly(styrene), and poly(acrylate-co-methacrylate) have been templated by Colvin et al.,[178] and Xia et al.[179] Other

polymer nanostructures with more complex shapes have been prepared by reactive ion etching of multiple colloidal layers.[180-182] On the other hand, despite its many potential applications in biosensing, microelectronics and optoelectronics; the fabrication of 2D polymeric nanostructures has been less explored. A few articles have dealt with the fabrication of water-assisted 2D honeycomb structures from the casting of a polymer solution onto an interface (air-liquid, or air-solid) under highly humid condensing environments.[183-189] However, controlling the condensation and ordering of sub-micron sized water droplets on a polymer solution is not a simple task. It usually requires precise control over many process variables such as the polymer chemistry and rheology, and the condensing environment in order to avoid the collapse of water droplets. In this respect, the use of inorganic or polymer colloids instead of water droplets offers more stability. Hence, the remaining portion of this section highlights some of the most important contributions to the field of 2D polymer templating via particle lithography using inorganic or polymer colloids.

As shown in Figure 1.17, well-ordered PAni honeycombs and truncated eggshell nanostructures have been prepared by Briseno et al.[207,208] via electropolymerization of aniline monomer infiltrated within the interstices of a close-packed monolayer of polystyrene latex spheres precoated with poly(dialyldimethylammonium chloride) and poly(sodium 4-styrenesulfonate)

(PDADMAC/PSS) polyelectrolyte thin shells, followed by PS core removal in toluene. Consistent with well-known principles of kinetics of conducting polymer growth, polyelectrolyte (PE) layers were found to improve the homogeneity of the synthesized PAni layer by introducing a greater number of negative charges on the surface of the PS spheres, while preserving their hydrophobic nature.[209-211] The presence of PE layers also resulted in less pore shrinkage due to more rigid PE/PAni honeycomb walls. In addition, by varying the number of PE layers and the electropolymerization parameters, the loading fraction of PAni within the PE shells could be tuned, thus allowing systematic control over the honeycomb pore size, wall width and height. The main drawback of having the PE layers is the risk of causing a negative effect on the conductivity and ion mobility of the PAni nanostructures. In addition, this technique is limited to conducting monomers and substrates choices.

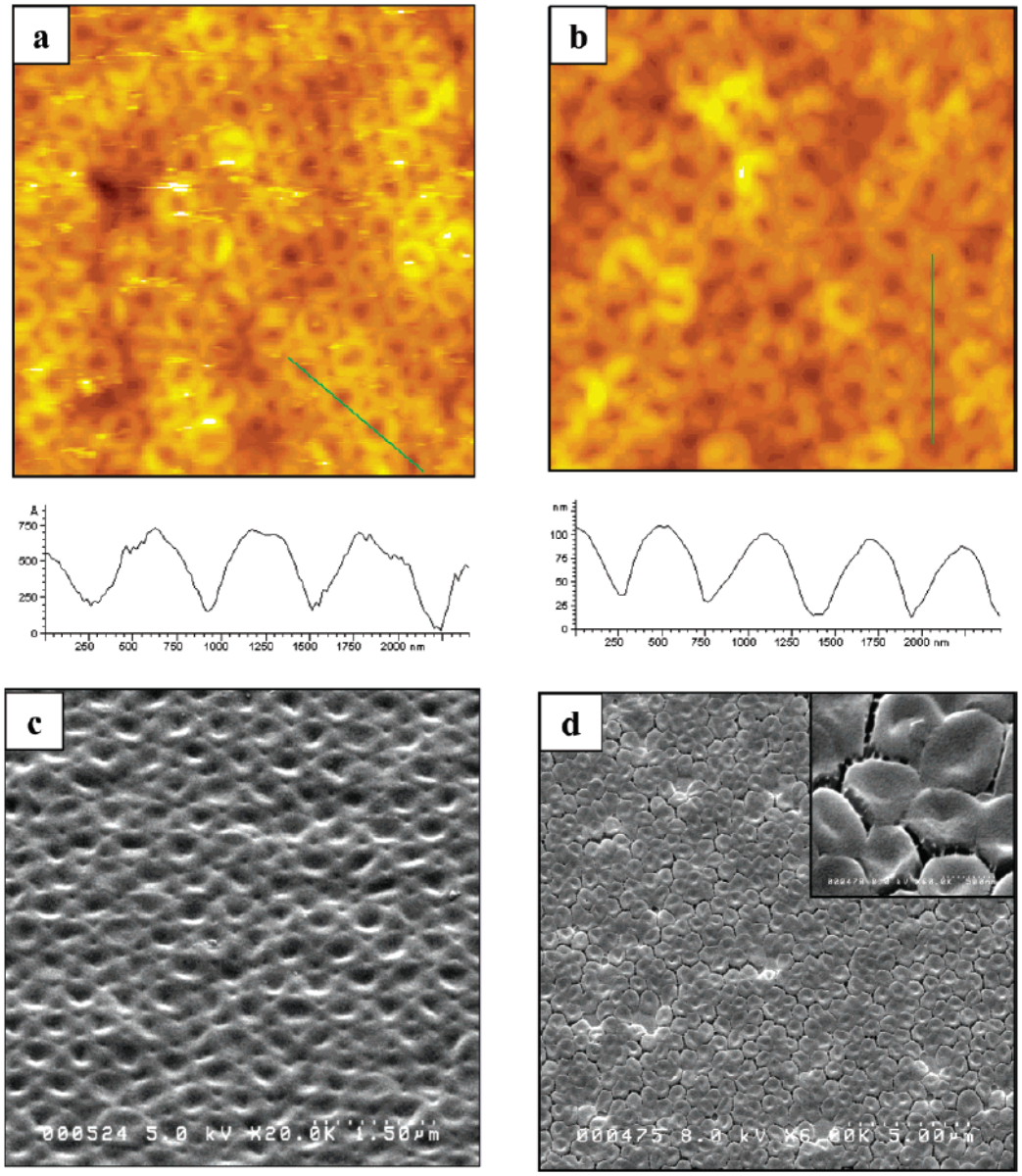

Figure 1.17. AFM images of PE*n*-PAni arrays produced via electropolymerization of aniline infiltrated inside the truncated eggshell structures produced by core extraction of a colloidal monolayer of PS latex coated with: a) 2, and b) 6 polyelectrolyte (PE) layers. Samples c) and d) are the SEM images of a and b, respectively. Reprinted with permission from Ref.[218] Copyright @American Chemical Society.

An alternative procedure, not involving electropolymerization or the use of PE layers, has been suggested by Zhou and collaborators for the fabrication of silanized polymer nanoring/nanoshell arrays and the subsequent attachment of DNA-capped gold nanoparticles.[212] In this procedure a 1 wt% 3-aminopropyltriethoxysilane (APTS) solution is infiltrated within the interstitial sites of a close-packed monolayer of PS spheres drop-cast on a silicon substrate. The resulting siloxane film is very robust and adheres strongly to the substrate through the silanol moieties on the SiO_2 wafer. Upon sonication in toluene for 15 s, only the PS cores were removed, leaving behind a mesoporous network of hexagonally ordered truncated aminosilane/polystyrene nanorings/nanoshells. The formation of polymer nanorings and nanodots as the result of partial detachment of PS spheres from glass substrates has also been reported by Boneberg and co-workers.[213] Moreover, Zhou et al. demonstrated the applicability of the synthesized nanostructures as high surface substrates for sensing applications, by further implanting the positively charged amino groups on the nanorings with negatively charged gold and DNA-capped gold nanoparticles via electrostatic interactions. XPS measurements confirmed the presence of anchored gold nanoparticles; however, the phosphorous peak associated with the DNA-capped gold particles could not be detected, possibly due to a small surface coverage of oligonucleotides capping the Au nanoparticles. The main limitation of this procedure is the need for silanol bearing substrates.

Xu and Goedel[214] have prepared free standing polyisoprene membranes via cross-linking of a monolayer of hydrophobized silica spheres (treated with polyisobutylene amphiphiles) embedded in a custom-prepared polyisoprene matrix bearing sulfonate and anthracene functional groups. The procedure starts by spreading the hybrid colloid-polyisoprene monolayer on a chloroform-water surface in a Langmuir trough. Upon compression of the monolayer, the polymer matrix is crosslinked via UV illumination, and the colloids are removed with hydrofluoric acid. The resulting 40 nm thick membranes consist of small, non-connected islands with uniform 55 nm-wide pores. Using a similar procedure, Xu and Goedel[215] have also prepared large area (in the order of hundreds of microns) polymer honeycombs by spreading a mixture of methacryloxypropiltrimethoxysilane-modified silica colloids and a nonvolatile photopolymerizable organic liquid (trimethylolpropane trimethacrylate-TMPTMA) on a water surface. Moreover, they demonstrated that these polymer honeycombs can be further utilized as templates in the sol-gel synthesis of morphologically tunable TiO_2, and ZnO nanostructures.[216] Figure 1.18 shows the SEM images of the hybrid silica-polymer monolayer, before and after removal of the colloidal template (Figures 1.18a-b); as well as the result after infiltration of the $Ti(OEt)_4$ precursor solution, before and after removal of the polymer honeycomb template (Figures 1.18c-d). As seen in Figures 1.18d-i, the morphology of the TiO_2 nanostructures can be controlled by adjusting the

precursor concentration. In general, hemispheres and cup-like nanostructures form at higher precursor concentrations (i.e. 10-20 wt%), whereas nanorings and web-like structures form at lower concentrations (i.e. 2 wt%).

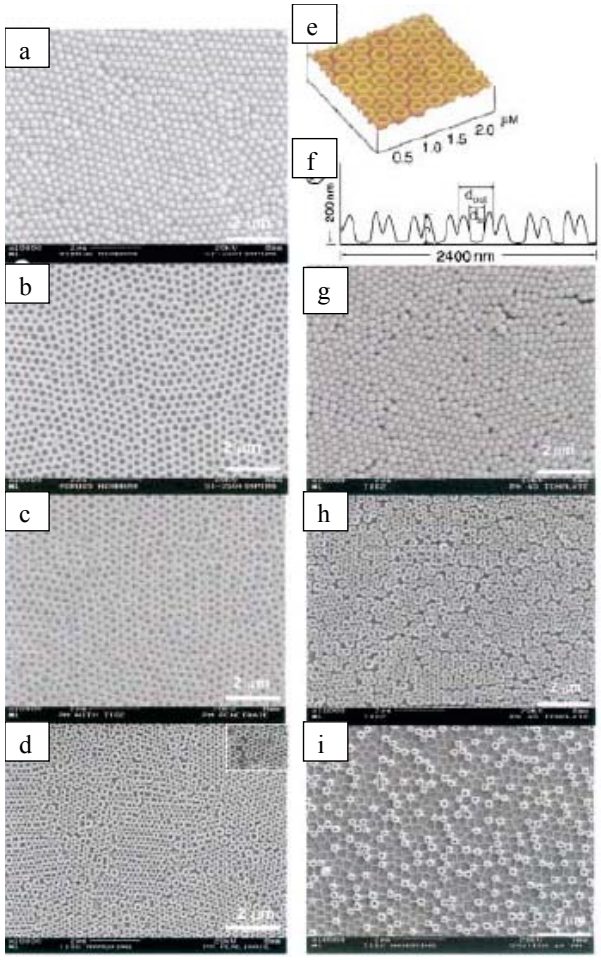

Figure 1.18. SEM images of: a) silane-modified silica colloids monolayer embedded in cross-linked organic polymer (TMPTMA). b) TMPTMA membrane after spheres removal. c) membrane supported on mica. d) TiO_2 nanorings on mica after removing the TMPTMA template. e) and f) SFM images and cross-section view of d). Effect of $Ti(OEt)_4$ concentration: g) 20 wt%, h) 10 wt%, and i) 2 wt%. Reprinted with permission from Ref.[215] Copyright @Wiley-VCH Verlag GmbH & Co KGaA.

Polymer microlens arrays with a plano-convex shape have been prepared by Nam and collaborators[217] via a double templating process in which poly(dimethylsiloxane) (PDMS) molds are cast on a monolayer of close-packed PS latex spheres, and subsequently used as templates for the UV photopolymerization of an urethane-based polyene mercaptoester prepolymer. A schematic of the process, as well as the SEM images of the PDMS mold and the polymer microlens array are shown in Figure 1.19. Other polymer nanostructures with controllable morphology have also been synthesized by Yi and Kim[218] from a technique that combines sintering rheology and partial dissolution of polystyrene-co-polydivinyl benzene (PS-co-PDVB) latex particles assembled into a hexagonal array on a flat surface. Trigonal isolated polymer nanoparticles and honeycomb-type structure are accessible depending on the sintering conditions. When colloid sintering is carried out at the glass transition temperature (Tg ~ 123^{o}C), the colloids simply adhere more strongly to the substrate; however, when sintering is performed at T > Tg (~140^{o}C), a necking effect is observed as the result of increased mobility in the uncrosslinked polymer fraction of the colloids. Then, as the PS soluble fraction of the colloids is selectively dissolved in cyclohexane, the insoluble PDVB fractions remain trapped either in the interstitial spaces, forming non-connected trigonal polymer nanostructures; or they adhere to the neck-area forming honeycomb-type structures. The key technological aspect

of this method is the fact that the colloidal particles serve not only as the template but also as the deposition material. The effect of the colloids crosslinked PDVB fraction, and the dissolution time on the morphology of the nanostructures is yet to be determined.

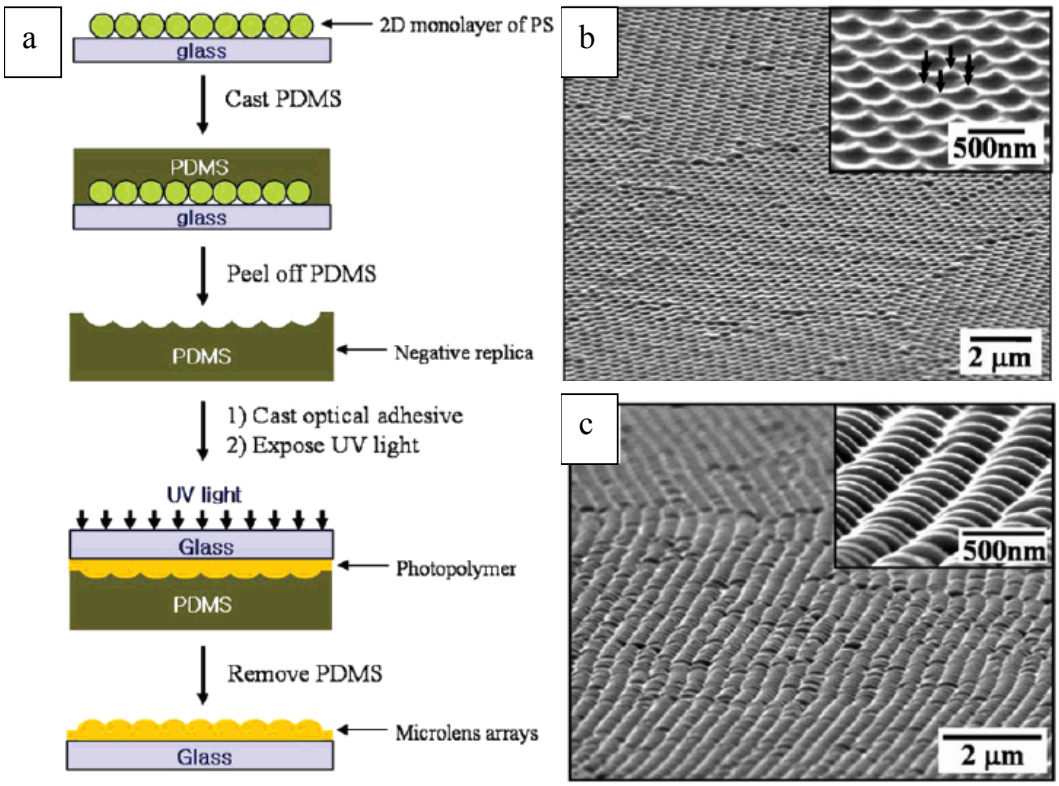

Figure 1.19. Fabrication of polymer microlens arrays via a double templating process in which poly(dimethylsiloxane) (PDMS) molds are cast on a monolayer of close-packed PS latex spheres, and subsequently used as templates for the UV photopolymerization of an urethane-based polyene mercaptoester prepolymer. a) schematic of the process, b) SEM images of the PDMS mold, and c) resulting polymer microlens array. Reprinted with permission from Ref.[217] Copyright @American Chemical Society.

Ordered arrays of hollow and truncated polymer spheres have been prepared by Li et al.[219] using a Fe_2O_3 honeycomb template prepared via particle lithography and the sol-gel technique.[146] In this relatively simple procedure, the holes of the honeycomb are infiltrated with a polymer solution (polyvinyl alcohol, polyvinyl pyrrolidone, or polymethyl phenylsilane), which evaporates and solidifies, adhering to the honeycomb walls. After the ceramic template is removed by selective dissolution in 1 M oxalic acid solution, an array of either hollow or truncated spheres (solid or hollow) result depending of the concentration of the polymer solution, the size of the holes in the ceramic honeycomb template, and the number of infiltration cycles. These nanostructures are expected to find applications as microreactor devices, and in controlled drug release.

Recently, Marquez et.al.[169] proposed a novel method for the formation of nanometer-scale polymer structures via template assisted admicellar polymerization (TAAP), a process that involves the use of surfactant surface aggregates to concentrate monomer at the surface prior to polymerization. More details on this process and the nanostructures formed can be found in chapters 3 and 4.

V. Emerging Technologies and Future Trends in Particle Lithography

Since its origins in the early 1980's, many fruitful achievements have been made in the field of particle lithography. A number of methods have been developed to organize polymeric, metallic, ceramic and composite colloidal particles into highly-ordered, close-packed and non close-packed hexagonal arrays, as well as other arrangements with more complex shapes. These achievements have been possible in part by a better understanding of the mechanism driving the self-assembly of colloidal particles at liquid interfaces, as well as the factors controlling the quality of novel particle arrays. An interesting review on this subject has been recently published by Velikov and Velev.[220] Another review by Sun and Yang[221] highlights current advances in the fabrication of non-conventional colloidal arrays, including the use of non-planar and pre-patterned substrates, non-spherical colloids, heterogeneous (i.e. different size and chemistry) colloids, and non close-packed, highly ordered arrays with different lattice symmetries, etc.

Advances in the fabrication of custom-tailored, well-ordered colloidal arrays with ease of production and high reproducibility have contributed tremendously to the advancement of particle lithography as an inexpensive, high

throughput, materials general nanofabrication technique. A recent review by Van Duyne and collaborators[222] revisits many of the advances in particle lithography, with particular emphasis to important contributions to the field by his group, such as the development of angle-resolved NSL as an alternative for the fabrication of nanoparticles with more complex morphologies, the use of reactive ion etching in combination with NSL for the production of ordered nanopores with more complex geometries, the electrochemical fine tuning of silver nanoparticles and their localized surface plasmon resonance properties, as well as the growth of ultra thin protective dielectric layers on Ag nanoparticles via atomic layer deposition, and their application in devices with nanosensing capabilities. Other groups have demonstrated the formation of patterned nanostructures via controlled sintering and partial dissolution of polymer colloids,[218] the formation of non close-packed colloids/polymer nanocomposites and nanoporous metallic arrays,[90,92] as well as the patterning of biological materials such as proteins and cells.[166,167,169]

Recognizing the tremendous advances in particle lithography in the past few years, the future ahead seems very promising, especially as many devices are currently being built and tested for commercial applications. Nonetheless, in order to further exploit the potential of particle lithography, many challenges still need to be overcome. For instance, new methods or even modifications of existing ones

must be evaluated in order to make possible the formation of defect-free, large colloidal monolayers with cm^2-sized monocrystalline domains. In this respect, particle size, particle size distribution and surface non-homogeneities have been recognized by the scientific community as some of the major limitations in advancing particle lithography. Hence, new synthetic routes for the reliable fabrication of monodisperse colloidal particles with homogeneous surface chemistries and charge distributions are much needed. It is also desirable to synthesize colloidal particles with a broad spectrum of surface chemistry choices, thus increasing their ability to interact with other substances and to carry out reactions in the interior and exterior surfaces of the particles. It addition, homogenous and atomically flat substrates facilitate the formation of more uniform, defect-free colloidal monolayers. The gradual fulfillment of the aforementioned requirements will not only contribute to move forward the field of particle lithography through the development of innovative contributions, but will significantly help the advancement of nanotechnology.

VI. Glossary

Admicellar polymerization: a technique that utilizes surfactant aggregates adsorbed on a surface to concentrate monomer at the surface prior to polymerization.

Angle-Resolved Nanosphere Lithography (AR NSL): A variation of nanosphere lithography in which the angle between the surface normal of the sample and the direction of material deposition is changed so as to allow for multiple geometries and nanostructure sizes.

Bottom-up assembly: a group of techniques that rely on molecular or particle interactions to drive self-assembly at the nanometer scale.

Chemical vapor deposition (CVD): a chemical process used to produce high-purity, thin film solid materials in which the substrate is exposed to a volatile precursor, and as the result of specific chemical reactions, the desired product is deposited on the substrate, while the undesired byproducts (usually in gaseous form) are removed by gas flow through the reaction chamber.

Dynamic Thin Laminar Flow (DTLF) device: an apparatus designed for the assembly of colloidal particles and protein monolayers. It consists of a rotating glass cylinder and a PTFE hemicylindrical trough equipped with six channels that

control the subphase volume input, the pH, and the thin liquid film carrying the suspended colloidal particles on the surface of the cylinder.

Electrophoresis: the ability to move particles via an electric field**.**

Embossing: a nanofabrication technique based on the imprinting of a topographically patterned mold into a flat polymer film.

Langmuir-Blodgett (LB) technique: A deposition technique that involves the formation of a monolayer at an interface and subsequent transfer onto a substrate.

Molding: a nanofabrication technique involving the curing of a precursor material (usually a monomer or prepolymer) against a topographically patterned master.

Nanosphere Lithography (NSL): a more operationally descriptive term that extended the capabilities of natural lithography, making possible the fabrication of periodic particle array (PPA) surfaces having nanometer scale features from single and double layer colloidal masks.

Natural Lithography: a form of microfabrication based on the use of spherical colloidal particles as etching or deposition masks.

Particle lithography: a nanofabrication technique based on the use of ordered arrays of colloidal particles on a substrate as a lithographic mask for surface patterning.

Photolithography: a technique that relies on the exposure of an appropriate material (resist) to electromagnetic radiation (e.g. UV or X-ray) to introduce a latent image, which is subsequently developed into relief structures through etching.

Photoresist: a light-sensitive material that exhibits significant changes in solubility when subjected to electromagnetic radiation, making it suitable for pattern transfer applications.

Scanning probe lithography (SPL): a nanofabrication technique that [13, 14]resembles the stylus writing process in which a sharp edge (the tip of a cantilever) is used to draw patterns, to impart chemical functionality, and even to manipulate molecules and atoms with great precision.

Self assembled monolayers (SAMs): An ordered array of single molecules on a surface.

Sol-gel method: a technique based on the hydrolysis of alcohol functional groups in a liquid precursor, and subsequent condensation of the resulting hydroxyl groups to form a continuous solid network.

Surfactants: surface-active agents that contain a hydrophilic head group and a hydrophobic tail.

Top-down assembly: a group of lithographic methods designed to pattern micron and nanometer sized structures over large areas.

VII. References

1. B. Gates, Q. Xu, M. Stewart, D. Ryan, C. Grant Willson and G. Whitesides. *Chem. Rev.* **2005**, 105, 1171.

2. Y. Xia, J. Rogers, K. Paul and G. Whitesides. *Chem. Rev.* **1999**, 99, 1823.

3. S. Owa, H. Nagasaka, Y. Ishii, O. Hirakawa and T. Yamamoto. *Solid State Technol.* **2004**, 47, 43.

4. M. Switkes, R. Kunz, M. Rothschild, R. Sinta, M. Yeung and S. Baek. *J. Vac. Sci. Technol. B* **2003**, 21, 2794.

5. R. Brainard, J. Cobb and C. Cutler. *J. Photopolym. Sci. Technol.* **2003**, 16, 401.

6. F. cerrina, S. Bollepalli, M. Khan, H. Solak, W. Li and D. He. *Microelectron. Eng.* **2000**, 53, 13.

7. T. Kadota, H. Kageyama, F. Wakaya, K. Gamo and Y. Shirota. *Mater. Sci. Eng. C* **2001**, C16, 91.

8. Y. Shirota. *J. Mater. Chem.* **2005**, 15, 75.

9. D. Bratton, D. Yan, J. Dai and C. Ober. *Polym. Adv. Technol.* **2006**, 17, 94.

10. T. Ito and S. Okazaki. *Nature* **2000**, 406, 1027.

11. H. Smith and M. Schattenburg. *IBM J. Res. Dev.* **1993**, 37, 319.

12. M. Geissler and Y. Xia. *Adv. Mater.* **2004**, 16, 1249.

13. D. Wouters and U. Schubert. *Angew. Chem., Int. Ed.* **2004**, 43, 2480.

14. S. Kraemer, R. Fuierer and C. Gorman. *Chem. Rev.* **2003**, 103, 4367.

15. D. Ginger, H. Zhang and C. Mirkin. *Angew. Chem. Int. Ed.* **2004**, 43, 30.

16. S. Minne, S. Manalis, A. Atalar and C. Quate. *J. Vac. Sci. Technol. B* **1996**, 14, 2456.

17. S. Minne, S. Manalis, A. Atalar and C. Quate. *Appl. Phys. Lett.* **1996**, 68, 1427.

18. Y. Xia and G. Whitesides. *Annu. Rev. Mater. Sci.* **1998**, 28, 153.

19. Y. Xia and G. Whitesides . *Angew. Chem., Int. Ed. Engl.* **1998**, 37, 550.

20. M. Dickey, R. Burns, E. Kim, S. Johnson, N. Stacey and C. Willson. *AICHE J.* **2005**, 51, 2547.

21. M. Colburn, S. Johnson, M. Stewart, S. Damle, T. Bailey, B. Choi, M. Wedlake, T. Michaelson, S. Sreenivasan, J. Ekerdt, C. Willson. *Proc. SPIE-Int. Soc. Opt. Eng.* **1999**, 3676, 379.

22. G. Jung, S. Ganapathiappan, D. Ohlberg, D. Olynick, Y. Chen, W. Tong and R. Williams. *Nano Lett.* **2004**, 4, 1225.

23. B. Smith, N. Stacey, J. Donnelly, D. Onsongo, T. Bailey, C. Mackay, D. Resnick, W. Dauksher, D. Mancini, K. Nordquist, S. Sreenivasan, S. Banerjee, J. Ekerdt and C. Willson. *Proc-SPIE-Int. Soc. Opt. Eng.* **2003**, 5037, 1029.

24. Y. Xia, J. McClelland, R. Gupta, D. Qin, X. Zhao, L. Sohn, R. Cellotta and G. Whitesides. *Adv. Mater.* **1997**, 9, 147.

25. Y. Xia, E. Kim, X-M. Zhao, J. Rogers, M. Prentiss and G. Whitesides. *Science* **1996**, 273, 347.

26. A. Quist, E. Pavlovic and S. Oscarsson, . *Anal. Bioanal. Chem.* **2005**, 381, 591.

27. X-M. Zhao, Y. Xia and G. Whitesides. *Adv. Mater.* **1996**, 8, 837.

28. E. Kim, Y. Xia and G. Whitesides. *Nature* **1995**, 376, 581.

29. E. Kim, Y. Xia, X-M. Zhao and G. Whitesides. *Adv. Mater.* **1997**, 9, 651.

30. S. Chou, P. Krauss and P. Renstrom. *J. Appl. Phys. Lett.* **1995**, 67, 3114.

31 B. Tieke, K-U. Fulda and A. Kampes. *Mono- and multilayers of spherical polymer particles prepared by langmuir-blodgett and self-assembly techniques,*. Marcel Decker: New york, 2002.

32. E. Bourgeat-Lami. *J. Nanosci. Nanotech.* **2002**, 2, 1.

33. Y. Xia, B. Gates, Y. Yin and Y. Lu. *Adv. Mater.* **2000**, 12, 693.

34. J. Hulteen and R. Van Duyne . *J. Vac. Sci. Technol. A* **1995**, 13, 1553.

35. C. Fischer and H. Zingsheim. *J. Vac. Sci. Technol.* **1981**, 19, 881.

36. H. Deckman and J. Dunsmuir. *Appl. Phys. Lett.* **1982**, 41, 377.

37. H. Deckman and J. Dunsmuir. *J. Vac. Sci. Technol. B* **1983**, 1, 1109.

38. H. Deckman, J. Dunsmuir, S. Garoff, J. McHenry and D. Peiffer. *J. Vac. Sci. Technol. B* **1988**, 6, 333.

39. H. Deckman, B. Abeles, J. Dunsmuir and C. Roxlo. *Appl. Phys. Lett.* **1987**, 50, 504.

40. N. Denkov, O. Velev, P. Kralchevsky, I. Ibanov, H. Yoshimura and K. Nagayama. *Langmuir* **1992**, 8, 3183.

41. S. Maenosono, C. Dushkin, Y. Yamaguchi, K. Nagayama and Y. Tsuji. *Colloid Polym. Sci.* **1999**, 277, 1152.

42. C. Dushkin, G. Lazarov, S. Kotsev, H. Yoshimura and K. Nagayama. *Colloid Polym. Sci.* **1999**, 277, 914.

43. K. Nagayama. *Colloids and Surf. A: Physicochem. and Engr. Aspects* **1996**, 109, 363.

44. E. Adachi, A. Dimitrov and K. Nagayama. *Langmuir* **1995**, 11, 1057.

45. P. Kralchevsky and K. Nagayama. *Langmuir* **1994**, 10, 23.

46. A. Dimitrov, C. Dushkin, H. Yoshimura and K. Nagayama. *Langmuir* **1994**, 10, 432.

47. c. Dushkin, H. Yoshimura and K. Nagayama. *Chem. Phys. Lett.* **1993**, 204, 455.

48. N. Denkov, O. Velev, P. Kralchevsky, I. Ivanov and K. Nagayama. *Nature* **1993**, 361, 26.

49. P. Tessier, O. Velev, A. Kalambur, A. Lenhoff, J. Rabolt and E. Kaler. *Adv. Mater.* **2001**, 13, 396.

50. R. Micheletto, H. Fukuda and M. Ohtsu. *Langmuir* **1995**, 11, 3333.

51. A. Dimitrov and K. Nagayama. *Langmuir* **1996**, 12, 1303.

52. J. Garno, N. Amro, K. Wadu-Mesthrige and G-Y. Liu. *Langmuir 2002* **2002**, 18, 8186.

53. D. Wang and H. Mohwald. *Adv. Mater.* **2004**, 16, 244.

54. A. Hurd and D. Schaefer. *Phys. Rev. Lett.* **1985**, 54, 1043.

55. J. Goodwin, R. Ottewill and A. Parentich. *J. Phys. Chem.* **1980**, 84, 1580.

56. K. Fulda and B. Tieke. *Adv. Mater.* **1994**, 6, 288.

57. T. Araki, S-I. Oinuma and K. Iriyama. *Langmuir* **1991**, 7, 738.

58. M. Bardosova, P. Hodge, L. Pach, M. Pemble, V. Smatko, R. Tredgold and D. Whitehead. *Thin Solid Films* **2003**, 437, 276.

59. M. Kondo, K. Shinozaki, L. Bergstrom and N. Mizutani. *Langmuir* **1995**, 11, 394.

60. R. Aveyard, J. Clint, D. Nees and V. Paunov. *Langmuir* **2000**, 16, 1969.

61. R. Aveyard, J. Clint, D. Nees and N. Quirke. *Langmuir* **2000**, 16, 8820.

62. L. Goldenberg, J. Wagner, J. Stumpe, B-R. Paulke and E. Gornitz. *Langmuir* **2002**, 18, 5627.

63. L. Ramos, T. Lubensky, N. Dan, P. NBelson and D. Weitz. *Science* **1999**, 286, 2325.

64. B. van Duffel, R. Ras, F. De Schryver and R. Schoonheydt. *J. Mater. Chem.* **2001**, 11, 3333.

65. M. Marquez and B. Grady. *Langmuir* **2004**, 20 , 10998.

66. F. Ruess. *Mem. Soc. Imp. Natu. Moscou* **1809**, 2, 327.

67. H. Hamaker. *Trans. Faraday Soc.* **1940**, 36, 279.

68. h. Koelmans and J. Overbeek. *Discuss. Faraday Soc.* **1954**, 18, 52.

69. P. Richetti, J. Prost and P. Barois. *J. Phys. Lett.* **1984**, 45, 1137.

70. M. Giersig and P. Mulvaney. *J. Phys. Chem.* **1993**, 97, 6334.

71. M. Giersig and P. Mulvaney. *Langmuir* **1993**, 9, 3408.

72. G. Schmidt, A. Lehnert, U. Kreibig, Z. Adamczyk and P. Belouschek. *Z. Naturforsch* **1990**, 45b, 989.

73. Y. Solomentsev, M. Bohmer and J. Anderson. *Langmuir* **1997**, 13, 6058.

74. M. Bohmer. *Langmuir* **1996**, 12, 5747.

75. M. Trau, D. Saville and I. Aksay. *Langmuir* **1997**, 13, 6375.

76. M. Trau, D. Saville and I. Aksay. *Science* **1996**, 272, 706.

77. R. Hayward, D. Saville and I. Aksay. *Nature* **2000**, 404, 56.

78. S. Lumsdon, E. Kaler, J. Williams and O. Velev. *Appl. Phys. Lett.* **2003**, 82, 949.

79. H. Schope. *J. Phys. Condens. Mater.* **2003**, 15, L533.

80. A. Dimitrov, T. Takahashi, K. Furusawa and K. Nagayama. *J. Phys. Chem.* **1996**, 100, 3163.

81. T. Takahashi, A. Dimitrov and K. Nagayama. *J. Phys. Chem.* **1996**, 100, 3157.

82. G. Picard. *Langmuir* **1997**, 13, 3226.

83 G. Picard. *High dilution effects on cells and integrated systems*., World Scientific: London, 1996.

84. G. Picard, I. Nevernov, D. Alliata and L. Pazdernik. *Langmuir* **1997**, 13, 264.

85. G. Picard. *Langmuir* **1998**, 14, 3710.

86. S. Park and Y. Xia. *Langmuir* **1999**, 15, 266.

87. B. Gates, D. Qin and Y. Xia. *Adv. Mater.* **1999**, 11, 466.

88. B. Prevo and O. Velev. *Langmuir* **2004**, 20, 2099.

89. F. Pan, J. Zhang, C. Cai and T. Wang. *Langmuir* **2006**, 22, 7101.

90. P. Jiang, T. Prasad, M. McFarland and V. Colvin. *Appl. Phys. Lett.* **2006**, 89, 011908.

91. P. Jiang and M. McFarland. *J. Am. Chem. Soc.* **2004**, 126, 13778.

92. P. Jiang and M. McFarland. *J. AM. CHEM. SOC.* **2005**, 127, 3710.

93. P. Maury, M. Escalante, D. Reinhoudt and J. Huskens. *Adv. Mater.* **2005**, 17, 2718.

94. Q. Yan, A. Chen, S. Chua and X. Zhao. *J. Nanosci. Nanotechnol.* **2006**, 6, 1815.

95. R. Schaak, R. Cable, B. Leonard and B. Norris. *Langmuir* **2004**, 20, 7293.

96. M. Allard, E. Sargent, P. Lewis and E. Kumacheva. *Adv. Mater.* **2004**, 16, 1360.

97. D. Wang and H. Mohwald. *J. Mater. Chem.* **2004**, 14, 459.

98. Y. Yin, Y. Lu, B. Gates and Y. Xia. *J. Am. Chem. Soc.* **2001**, 123, 8718.

99. Y. Yin, Y. Lu and Y. Xia. *J. Mater. Chem.* **2001**, 11, 987.

100. J. Aizenberg, P. Braun and P. Wiltzius. *Phys. Rev. Lett.* **2000**, 84, 2997.

101. J. Hulteen, D. Treichel, M. Smith, M. Duval, T. Jensen and R. Van Duyne . *J. Phys. Chem. B* **1999**, 103, 3854.

102. T. Jensen, M. Malinsky, C. Haynes and R. Van Duyne. *J. Phys. Chem. B* **2000**, 104, 10549.

103. T. Jensen, G. Schatz and R. Van Duyne. *J. Phys. Chem. B* **1999**, 103, 2394.

104. S. Astilean, M. Bolboaca, D. Maniu and T. Iliescu. *Romanian Reports in Physics* **2004**, 56, 346.

105. S. Astilean. *Romanian Reports in Physics* **2004**, 56, 340.

106. F. Burmeister, C. Schafle, T. Matthes, M. Bohmisch, J. Boneberg and P. Leiderer. *Langmuir* **1997**, 13, 2983.

107. F. Burmeister, C. Schafle, B. Keilhofer, C. Bechinger, J. Boneberg and P. Leiderer. *Adv. Mater.* **1998**, 10, 495.

108. W. Kandulski, A. Kosiorek, J. Rybczynski, D. Bauman and M. Giersig. *Acta Physica Polonica A* **2003**, 104, 495.

109. R. Rossi, M. Tang and N. Lewis. *Appl. Phys. Lett.* **2000**, 77, 2698.

110. P. Bartlett, P. Birkin and M. Ghanem. *Chem. Commun.* **2000**, , 1671.

111. P. Bartlett, J. Baumberg, P. Birkin, M. Ghanem and M. Netti. *Chem. Mater.* **2002**, 14, 2199.

112. M. Abdelsalam, P. Bartlett, J. Baumberg and S. Coyle. *Adv. Mater.* **2004**, 16, 90.

113. W. Liu, W. Zhong, L. Qiu, L. Lu and Y. Du. *Eur. Phys. J. B* **2006**, 51, 501.

114. J. Wright, O. Worsfold, C. Whitehouse and M. Himmelhaus. *Adv. Mater.* **2006**, 18, 421.

115. M. Winzer, M. Kleiber, N. Dix and R. Wiesendanger. *Appl. Phys. A* **1996**, 63, 617.

116. L. Levy. *Physica* **1991**, B169, 245.

117. L. Levy, G. Dolan, J. Dunsmuir and H. Bouchiat. *Phys. Rev. Lett.* **1990**, 64, 2074.

118. K. Shafer-Peltier, C. Haynes, M. Glucksberg and R. Van Duyne. *J. Am. Chem. Soc.* **2003**, 125, 588-593.

119. J. Aizpurua, P. Hanarp, D. Sutherland, M. Kall, G. Bryant and F. Garcia de Abajo. *Phys. Rev. Lett.* **2003**, 90, 057401-057401.

120. A. Kosiorek, W. Kandulski, H. Glaczynska and M. Giersig. *Small* **2005**, 1, 439.

121. S. Han, X. Shi and F. Zhou. *Nano Lett.* **2002**, 2, 97.

122. C. Haynes and R. Van Duyne. *J. Phys. Chem. B* **2001**, 105, 5599.

123. C. Haynes, A. McFarland, M. Smith, J. Hulten and R. Van Duyne. *J. Phys. Chem. B* **2002**, 106, 1898.

124. C. Haynes and R. Van Duyne. *Nano Lett.* **2003**, 3, 939.

125. Z. Chen, P. Zhan, Z. Wang, J. Zhang, W. Zhang, N. Ming, C. Chan and P. Sheng. *Adv. Mater.* **2004**, 16, 417.

126. E. Kim, Y. Xia and G. Whitesides. *J. Am. Chem. Soc.* **1996**, 118, 5722.

127. F. Lenzmann, K. Li, A. Kitai and H. Stover. *Chem. Mater.* **1994**, 6, 156.

128. N. Li and M. Zinke-Allmang. *Jpn. J. Appl. Phys.* **2002**, 41, 4626.

129. J. Pacifico, D. Gomez and P. Mulvaney. *Adv. Mater.* **2005**, 17, 415.

130. D. Yi and D-Y Kim. *Nano Lett.* **2003**, 3, 207.

131. B. Cao, W. Cai, F. Sun, Y. Li, Y. Lei and L. Zhang. *Chem. Commun.* **2004**, , 1604.

132. C-W. Kuo, J-Y. Shiu, P. Chen and G. Somorjai. *J. Phys. Chem. B* **2003**, 107, 9950.

133. C-W. Kuo, J-Y. Shiu, Y-H. Cho and P. Chen. *Adv. Mater.* **2003**, 15, 1065.

134. J. Rybczynski, Y. Wang, D. Banerjee, K. Kempa and Z. Ren. *Proc. of SPIE* **2005**, 6003, 60030Y-1.

135. Z. Huang, D. Carnahan, M. Sennett, D. Wang, J. Wen, K. Kempa and Z. Ren. *Appl. Phys. Lett.* **2003**, 82, 460.

136. Y. Wang, X. Wang, J. Rybczynski, D. Wang, K. Kempa and Z. Ren. *Appl. Phys. Lett.* **2005**, 86, 153120-153121.

137. K. Park, S. Lee, K. Koh, R. Lacerda, K. Teo and W. Milne. *J. Appl. Phys.* **2005**, 97, 024311-024311.

138. D. Banerjee, J. Rybczynski, J. Huang, D. Wang, K. Kempa and Z. Ren. *Appl. Phys. A* **2005**, 80, 749.

139. X. Wang, C. Summers and Z. Wang. *Nano Lett.* **2004**, 4, 423.

140. W. Ma, C. Harnagea, D. hesse and U. Gosele. *Appl. Phys. Lett.* **2003**, 83, 3770.

141. W. Ma and D. Hesse. *Appl. Phys. Lett.* **2004**, 84, 2871.

142. W. Ma and D. Hesse. *Appl. Phys. Lett.* **2004**, 85, 3214.

143 J. Brinker and G. Scherer : *Sol-gel science*. Academic Press: New York; 1989.

144. M. Kanungo and M. Collinson. *Chem. Commun.* **2004**, , 548.

145. A. Khramov, J. Munos and M. Collinson. *Langmuir* **2001**, 17, 8112.

146. F. Sun, W. Cai, Y. Li, B. Cao, Y. Lei and L. Zhang. *Adv. Funct. Mater.* **2004**, 14, 283.

147. Y. Li, W. Cai, G. Duan, F. Sun, B. Cao, F. Lu, Q. Fang and I. Boyd. *Appl. Phys. A* **2005**, 81, 269.

148. Y. Li, W. Cai, G. Duan, F. Sun, B. Cao and F. Lu. *Materials Letters* **2005**, 59, 276.

149. Y. Li, W. Cai, B. Cao, G. Duan, C. Li, F. Sun and H. Zeng. *J. Mater. Chem.* **2006**, 16, 609.

150. Y. Li, W. Cai, B. Cao, G. Duan and F. Sun. *Polymer* **2005**, 46, 12033.

151. B. Wang, S-J. Chua and J. Teng. *Proc. IEEE Conf. Nanotechnology* **2005**.

152. K. Nagayama. *Nanobiology* **1992**, 1, 25.

153. S. Zhang, L. Yang, M. Altman, M. Lassle, H. Nugent, F. Frankel, D. Lauffenburger, G. Whitesides and A. Rich. *Biomaterials* **1999**, 20, 1213.

154. M. Ravenscroft, K. Bateman, K. Shaffer, H. Schessler, D. Jung, T. Schneider, C. Montgomery, T. Custer, A. Schaffner, Q. Liu, Y. Li, J. Baker and J. Hickman. *J. Am. Chem. Soc.* **1998**, 120, 12169.

155. A. Blawas and W. Reichert. *Biomaterials* **1998**, 19, 595.

156. W. Scouten, J. Luong and R. Brown. *Trends Biotechnol.* **1995**, 13, 178.

157. A-S. Andersson, J. Brink, U. Lidberg and D. Sutherland. *IEE Transactions in Nanobioscience* **2003**, 2, 49.

158. T. Tatsuma, A. Ikezawa, Y. Ohko, T. Miwa, T. Matsue and A. Fujishima. *Adv. Mat.* **2002**, 12, 643.

159. J. Jones, N. Fell, T. Alexander, C. Tombrello and A. Fountain. *Proc. of SPIE* **2004**, 5269, 192.

160. P. Fromherz. *Nature* **1971**, 231, 267.

161. H. Yoshimura, S. Endo, M. Matsumoto, K. Nagayama and Y. Kagawa. *J. Biochemestry* **1989**, 106, 958.

162. T. Akiba, H. Yoshimura and K. Namba. *Nature* **1991**, 252, 1544.

163. E. Uzgiris and R. Kornberg. *Nature* **1983**, 301, 125.

164. S. Darst, E. Kubalek and R. Kornberg. *Nature* **1989**, 340, 730.

165. R. reed, J. Mattai and G. Shipley. *Biochemistry* **1990**, 26, 824.

166. D. Yi, M. Kim, L. Turner, K. Breuer and D-Y. Kim. *Biotechnology Lett.* **2006**, 28, 169.

167. J-R. Li, G. Henry and J. Garno. *Analyst* **2006**, 131, 244.

168 V. Rosenoer, M. Oratz and M. Rothschilde: *Albumin structure and function*. Pergamon Press, New York; 1977.

169. M. Marquez, K. Patel, A. Carswell, D. Schmidtkey and B. Grady. *Langmuir* **2006**, 22, 8010.

170. N. Gleason, C. Nodes, E. Higham, N. Guckert, I. Aksay, J. Schwarzbauer and J. Carbeck. *Langmuir* **2003**, 19, 513.

171. A. Valsesia, P. Colpo, T. Meziani, F. Bretagnol, M. Lejeune, F. Rossi, A. Bouma and M. Garcia-Parajo. *Adv. Funct. Mater.* **2006**, 16, 1242.

172. R. Michel, I. Reviakine, D. Sutherland, C. Fokas, G. Csucs, G. Danuser, N. Spencer and M. Textor. *Langmuir* **2002**, 18, 8580.

173. R. Michel, J. Lussi, G. Csucs, I. Reviakine, G. Danuser, J. Hubbell, M. Textor and N. Spencer. *Langmuir* **2002**, 16, 6305.

174. D. Wang and F. Caruso. *Adv. Mater.* **2001**, 13, 350.

175. T. Cassagneau and F. Caruso. *Adv. Mater.* **2002**, 14, 1837.

176. T. Sumida, Y. Wada, T. Kitamura and S. Yanagida. *Chem. Commun.* **2000**, , 1613.

177. P. Bartlett, P. Birkin, M. Ghanem and C-S Toh. *J. Mater. Chem.* **2001**, 11, 849.

178. P. Jiang, K. Hwang, D. Mittleman, J. Bertone and V. Colvin. *J. Am. Chem. Soc.* **1999**, 121, 11630.

179. B. Gates, Y. Yin and Y. Xia. *Chem. Mater.* **1999**, 11, 2827.

180. D-G. Choi, S. Jang, S. Kim, E. Lee, C-S Han and S-M. Yang. *Adv. Funct. Mater.* **2006**, 16, 33.

181. D-G. Choi, H. Yu, S. Jang and S-M. Yang. *J. AM. CHEM. SOC.* **2004**, 126, 7019.

182. H. Agheli and D. Sutherland. *IEEE Transactions on Nanobioscience* **2006**, 5, 9.

183. O. Karthaus, N. Maruyama, X. Cieren, M. Shimomura, H. Hasegawa and T. Hashimoto. *Langmuir* **2000**, 16, 6071.

184. H. Yabu and M. Shimomura. *Langmuir* **2006**, 22, 4992.

185. H. Yabu, M. Kojima, M. Tsubouchi, S-Y Onoue, M. Sugitani and M. Shimomura. *Colloids and Surfaces A: Physicochem. Eng. Aspects* **2006**, 284, 254.

186. H. Yabu, Y. Hirai and M. Shimomura. *Langmuir* **2006**, 22, 9760.

187. H. Yabu and M. Shimomura. *Chem. Mater.* **2005**, 17, 5231.

188. H. Yabu, M. Takebayashi, M. Tanaka and M. Shimomura. *Langmuir* **2005**, 21, 3235.

189. M. Barrow, R. Jones, J. Park, M. Srinivasarao, P. Williams and C. Wright. *Spectroscopy* **2004**, 18, 577.

190. W-L. Yuan, E. O'Rear, B. Grady and D. Glatshofer. *Langmuir* **2002**, 18, 3343.

191. S. Buofi and A. Gandini . *Cellulose* **2002**, 00, 1.

192. O. Matarredona, K. Mach, M. Rieger and E. O'Rear. *Corrosion Science* **2003**, 45, 2541.

193. L. Salgaonkar and R. Jayaram. *J. Colloid and Interf. Sci.* **2005**, 291, 92.

194. J. Wu, J. Harwell and E. O'Rear. *Langmuir* **1987**, 3, 531.

195. J. Dong and G. Mao. *Colloid Polym. Sci.* **2005**, 284, 340.

196. H. Castano, E. O'Rear, P. McFetridge and V. Sikavitsas. *Macromol. Biosci.* **2004**, 4, 785.

197. D. Le, M. Kendrick and E. O'Rear. *Langmuir* **2004**, 20, 7802.

198. N. Kuramoto and E. Genie. *Synthetic Metals* **1995**, 68, 191.

199. J. Wu, J. Harwell and E. O'Rear. *J. Phys. Chem.* **1987**, 91, 623.

200. G. Funkhouser, M. Arevalo, D. Glatzhofer and E. O'Rear. *Langmuir* **1995**, 11, 1443.

201. B. Kitiyanan, J. O'Haver, J. Harwell and S. Osuwan. *Langmuir* **1996**, 12, 2162.

202. L. Grant, F. Tiberg and W. Ducker. *J. Phys. Chem. B* **1998**, 102, 4288.

203. H. Patrick, G. Warr,S. Manne and I. Aksay. *Langmuir* **1997**, 13, 4349.

204. F. Tiberg, J. Brinck and L. Grant. *Current Opinion in Colloid and Interf. Sci.* **2000**, 4, 411.

205. N. Holland, M. Ruegsegger and R. Marchant. *Langmuir* **1998**, 14, 2790.

206. L. Grant and W. Ducker. *J. Phys. Chem. B* **1997**, 101, 5337.

207. S. Han, A. Briseno, X. Shi, D. Mah and F. Zhou. *J. Phys. Chem. B* **2002**, 106, 6465.

208. A. Briseno, S. Han, I. Rauda and F. Zhou. *Langmuir* **2004**, 20, 219.

209. M. Goren and R. Lennox. *Nano Lett.* **2001**, 1, 735.

210. A. Fou and M. Rubner. *Macromolecules* **1995**, 28, 7115.

211. Z. Huang, P. Wamg, A. MacDiarmid, Y. Xia and G. Whitesides. *Langmuir* **1997**, 13, 6480.

212. Y. Wang, S. Han, A. Briseno, R. Sanedrin and F. Zhou. *J. Mater. Chem.* **2004**, 14, 3488.

213. J. Boneberg, F. Burmeister, C. Schafle, P. Leiderer, D. Reim, A. Fery and S. Herminghaus. *Langmuir* **1997**, 13, 7080.

214. H. Xu and W. Goedel. *Langmuir* **2002**, 18, 2363.

215. H. Xu and W. Goedel. *Angew. Chem. Int. Ed.* **2003**, 42, 4694.

216. H. Xu and W. Goedel. *Angew. Chem. Int. Ed.* **2003**, 42, 4696.

217. H. Nam, D-Y. Jung, G-R. Yi and H. Choi. *Langmuir* **2006**, 22, 7358.

218. D. Yi, D. Kim. *Chem. Commun.* **2003**, , 982.

219. Y. Li, W. Cai, G. Duan, B. Cao and F. Sun. *J. Mater. Res.* **2005**, 20, 338.

220 K. Velikov and O. Velev. "Novel materials derived from particles assembled on liquid surfaces." *In Colloidal particles at liquid interfaces.* Ed. B. Binks, T. Horozov; University Press: Cambridge, 2006.

221. Z. Sun and B. Yang. *Nanoscale Res. Lett.* **2006**, 1, 46.

222. X. Zhang, A. Whitney, J. Zhao, E. Hicks and R. Van Duyne. *J. Nanosci. Nanotechnol.* **2006**, 6, 1920.

Chapter 2. Using Surface Tension to Predict the Formation of Colloidal Monolayers via the Langmuir-Blodgett (LB) Technique

I. Introduction

In the past few years, the development of highly ordered nanoscale and microscopic structures has drawn much attention, and a great deal of work has been done on the development of different alternatives for organizing materials with high degree of accuracy, reproducibility and efficiency. Chapter 1 reviews some of these techniques, focusing on the advantages and disadvantages of each method. Chapter 2, on the other hand, focuses on the formation of well-ordered, hexagonal arrays of latex spheres via the Langmuir-Blodgett technique, a method that exploits the well-known phenomenon of particle self-assembly at air-liquid interfaces, with subsequent transferring of the floating structure to a solid support through a simple dip-coating process.[1-8]

Despite the many advantages of the LB technique as a very simple, yet effective method to manipulate and control both particle and molecular organization, only a few studies have been conducted on the factors affecting the formation of highly ordered structures from this technique. In particular, the role

of the spreading agent in forming well-ordered, stable monolayers at the air-liquid interface has not been adequately explored. As a matter of fact, inconsistent results are usually obtained by different research groups due to a poor knowledge of the factors controlling particle aggregation and deposition at interfaces. In order to fully exploit the many potential applications of ordered particle arrays via the LB technique, a more thorough study needs to be conducted on the factors affecting the process. This chapter studies the interaction between submicron polystyrene latex spheres and the spreading agent (i.e. anionic SDS, nonionic polyoxyethylene nonylphenyl ether (EO = 9), and low molecular weight (Mw ~ 10000) water soluble polyacrylamide), as well as other factors such as humidity, and the effect of pulling vs. compression speed. The chapter also discusses the advantages of using the LB method not only because the process is relatively easy and inexpensive in comparison to some of the high-cost techniques reviewed in chapter 1, but also because it can be automated and scaled up to produce highly ordered 2D crystalline arrays in a continuous fashion. In particular, this work demonstrates that surface tension measurements can be used to identify the best set of conditions to form well-ordered colloidal monolayers via the LB technique, as long as the spreading agent/sphere/substrate interaction is favorable. The importance of the surface tension method here proposed is that it provides an effective tool to predict whether or not ordered arrays will form for a given colloid/substrate system from a very simple measurement that is easily automated.

II. Experimental

Materials. All reagents and materials were used as received. Dispersions of polystyrene latex microspheres (0.5 μm, and 2 μm in diameter), 2.5 wt % in water, stabilized with a slight anionic charge from surface sulfate groups remaining from the synthesis procedure, were purchased from Alfa Aesar. Sodium n-dodecyl sulfate (SDS) 98%, octylphenoxy poly(ethyleneoxy)ethanol (EO = 9, Igepal® CO 630), and polyacrylamide (PA), 50 wt % solution in water (Mw~10,000) were obtained from Aldrich Chemical Company. Highly ordered pyrolytic graphite (HOPG), monochromator ZYB grade (5 mm x 5 mm sheets) was purchased from Structure Probe Inc.

Film formation on HOPG via the LB technique. In order to form colloidal arrays of latex spheres on HOPG two different approaches were evaluated: The first approach is a slight variation of the conventional LB trough in which a glass cylinder with no floating barriers was used to contain the sphere dispersion. In this case, 5 mL of a dispersion containing PS microspheres and the spreading agent (SDS, octylphenoxy poly(ethyleneoxy) ethanol (EO = 9), or PA) was prepared by fixing the concentration of latex particles (1 wt %) and varying the concentration of the spreading agent in the range of 3.5 mM to 104 mM for SDS; 1.6 x 10^{-3} mM to 16.2 mM for Igepal® CO 630, and 5 x 10^{-4} wt % to 2 wt % for

PA. 18 MΩ nanopure water was used throughout the experiments. Based on the latex concentration (1 wt %), and the surface area of 0.5 μm and 2 μm spheres (i.e. 1.1 x 10^5 m^2/g and 2.8 x10^4 m^2/g respectively), the saturation concentration of the surfactant on the latex surface was estimated to be low enough so as not to affect the concentration of surfactant in solution, which indeed was found to be the case as determined by high pressure liquid chromatography. All dispersions were sonicated for 10 minutes prior to contact with the substrate. HOPG was cleaved and immediately dipped into 5 mL of the aforementioned sonicated dispersion; then, by means of a stepper motor, vertically withdrawn from solution at a rate of 5 μm/s. Roughly 15 min were required to coat the surface of a 25 mm^2 HOPG block at this rate.

The second approach resembles the first in the sense that a surfactant was also used to drive the formation of solid-like regions of spheres at the air-liquid interface, but the experimental set up is slightly different. It involves a rectangular chamber equipped with a pair of Teflon floating barriers which can travel along the surface of the liquid at a constant rate. The advantage here is that the concentration of latex spheres at the air-liquid interface can be increased by compressing the monolayer in the horizontal direction at a constant rate. In this study the pulling rate was fixed to 5 μm/s and the compression rate was varied from 0 to 20 μm/s. A schematic of the process is shown in Figure 2.1. All

experiments were carried out at room temperature (22 ± 1°C), and 45-50% relative humidity.

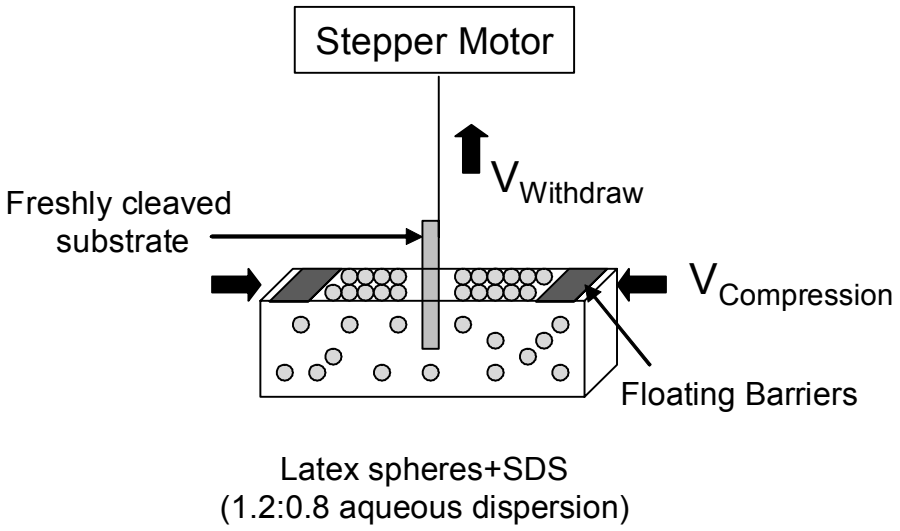

Figure 2.1. Schematic of the Langmuir-Blodgett deposition method. Not drawn to scale.

Instrumentation. Atomic Force Microscopy (AFM) imaging of the samples was performed with a Digital Instruments NanoScope III in tapping mode. High-resolution Scanning Electron Microscopy (SEM) images of hexagonal arrays of latex spheres on HOPG were obtained using a field emission scanning electron microscope (SEM, JEOL-6300F, Peabody, MA). The SEM was operated with an accelerating voltage of 15kV. Samples prepared for SEM were previously sputtered with thin films of gold (25-30 nm thick). A Nikon Eclipse E-800 optical

microscope was used to follow the arrangement of the latex spheres at the air-liquid interface as a function of surfactant concentration in solution. All images were recorded with a Universal Imaging Corp. software (MetaMorph 6.2r0).

Surface Tension Measurements. Surface tension as a function of surfactant/polymer equilibrium concentration was determined for solutions of SDS-only, PS/SDS, nonionic polyethoxylated (EO = 9) surfactant-only, PS/ nonionic polyethoxylated (EO = 9), PA-only and PS/PA using the Wilhelmy Plate method in a Kruss digital tensiometer, model 10 K-T. Two different readings were taken to estimate the surface tension of the solution: a first reading 2h after the plate had come in contact with the solution and a second reading upon film breakage during plate withdrawal from solution. Surface tension varied less than 0.5 mN/m after 2h. The reproducibility, including equilibration time and/or contamination effects, was 0.5 mN/m. Surface tensions measured on latex-free solutions of surfactants agreed with literature values.

III. Results

3.1. Atomic Force Microscopy and Scanning Electron Microscopy. The effect of SDS concentration on the ordering of latex spheres (i.e. 0.5 μm in diameter) on HOPG is shown in Figure 2.2 through the AFM imaging of films prepared from

1wt % PS spheres and varying concentrations of SDS in the range of 3.5 mM to 104 mM.

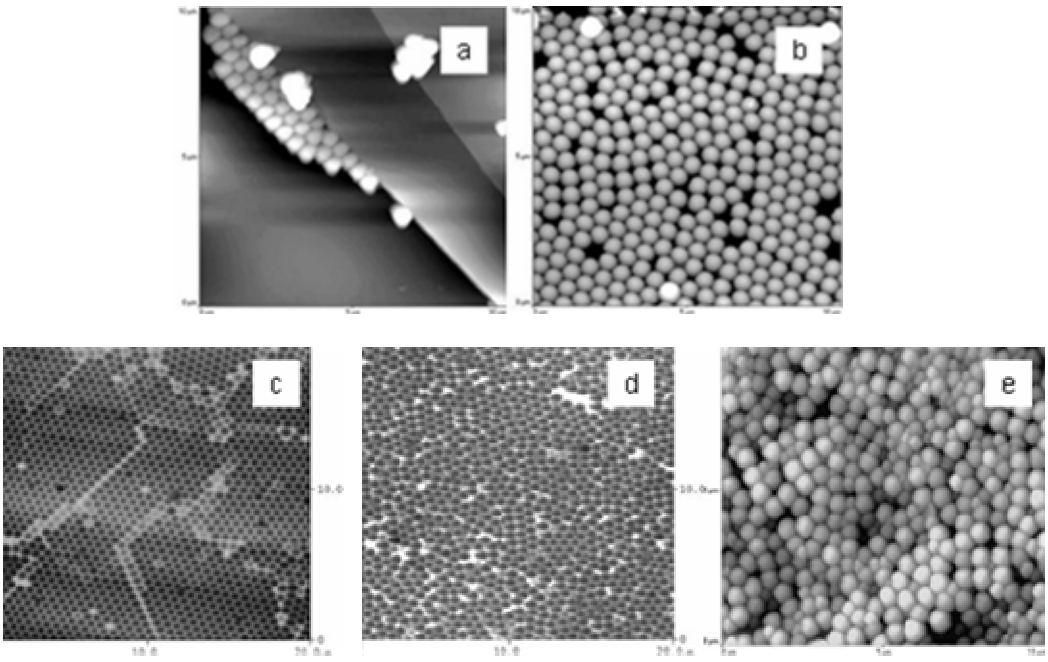

Figure 2.2. AFM micrograph of 500 nm latex spheres on HOPG prepared from LB technique with 1% spheres and a) 3.47 mM SDS, b) 8.68 mM SDS, c) 34.7 mM SDS, d) 69.4 mM SDS, and e) 104 mM SDS.

As represented by Figure 2.2a, surfactant concentrations below the CMC (i.e. 8.3mM) result in almost no spheres on the surface of HOPG. As the surfactant concentration is increased from 3.5 mM to 8.7 mM, spheres form small domains of hexagonally packed microspheres alternating with regions of loosely packed spheres and bare graphite. Indeed, Figure 2.2b shows what might be the onset of close packing of spheres in isolated regions. A further increase of the

surfactant concentration up to 34.7 mM SDS results in large domains of hexagonal arrays exhibiting only a few dislocations induced by surface irregularities as shown in Figure 2.2c. High resolution scanning electron micrographs of such highly ordered monolayers are shown in Figure 2.3

Increasing the SDS concentration from 3.5 mM to 34.7 mM renders a more stable, highly packed monolayer of latex spheres on graphite. However, as observed in Figure 2.2d, when the SDS concentration is further increased to 69.4 mM, the order of the monolayer is significantly disrupted, hexagonal arrays are quickly lost, and the spheres become appreciably deformed. At higher surfactant concentrations (SDS concentrations $\geq$ 104 mM), a transition from monolayer coverage of the surface to multiple layers of highly disordered latex spheres is observed.

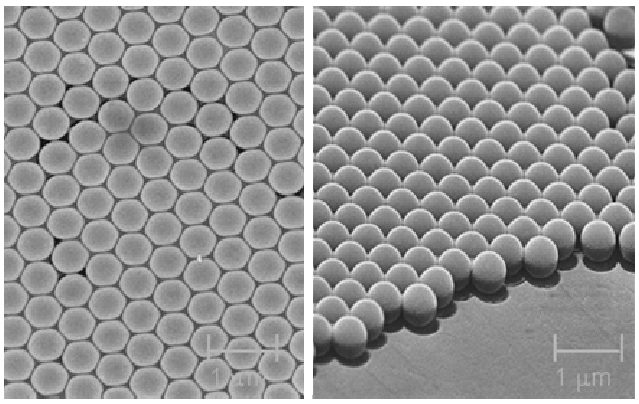

Figure 2.3. SEM micrographs of hexagonal arrays of 500 nm latex spheres on HOPG prepared from LB technique with 34.7 mM SDS as spreading agent and 1 wt% latex spheres.

The effect of SDS concentration on the ordering of larger latex spheres (i.e. 2 μm in diameter) on HOPG is shown in Figure 2.4 through the SEM imaging of films prepared from 1 wt % PS spheres and varying concentrations of SDS in the range of 3.5 mM to 104 mM. The same trend observed for the 0.5 μm spheres in Figure 2.2 is also observed for the 2 μm spheres in Figure 2.4, i.e. as the SDS concentration increases, the system transitions from an incomplete coverage of the surface (Figures 2.4a-b) to monolayer coverage (Figure 2.4c), and multiple layer coverage of the surface at SDS concentrations well above the CMC (Figure 2.4d).

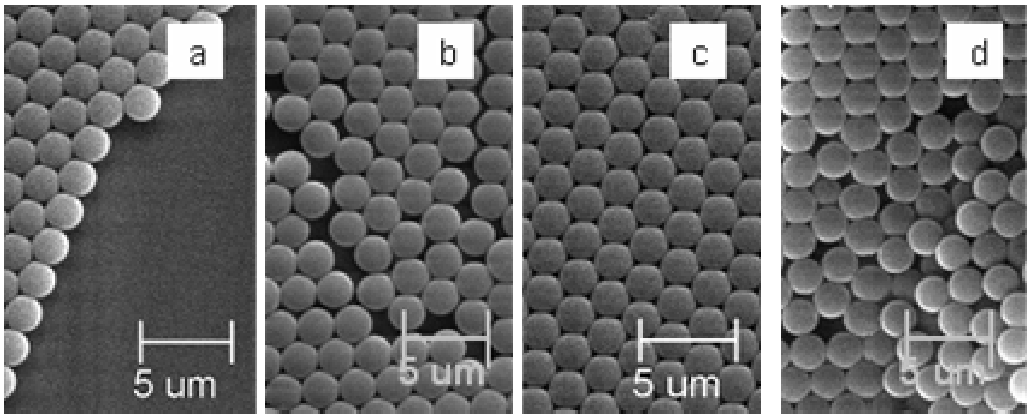

Figure 2.4. SEM micrographs of 2 μm latex spheres on HOPG prepared from LB technique with 1% spheres and a) 3.47 mM SDS, b) 8.68 mM SDS, c) 34.7 mM SDS, and d) 104 mM SDS.

Figure 2.5 shows the effect of polyacrylamide concentration on the ordering of 0.5 μm latex spheres on HOPG for polymer concentrations in the range of 0.001 wt % PA to 1 wt % PA. The images confirm the transition from incomplete coverage of the surface at very low polymer concentrations (Figure 2.5a) to a monolayer coverage (Figure 2.5b); eventually reaching a multilayer coverage of the surface at 0.01 wt % PA (Figure 2.5c). Instead of disordered multiple layers, at very high PA concentrations (i.e. 1 wt % PA) a few spheres are embedded in a polymer film adsorbed on the surface of HOPG (Figure 2.5d).

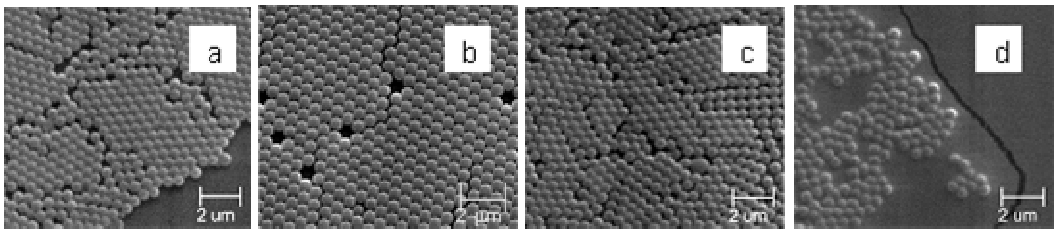

Figure 2.5. SEM micrographs of 500 nm latex spheres on HOPG prepared from LB technique with 1% spheres and a) 0.001 wt % PA, b) 0.005 wt % PA, c) 0.01 wt % PA, d) 1 wt % PA.

Figure 2.6 shows the effect of substrate choice on the wetting of 1:1 PS/SDS mixtures on different substrates: SiO_2, mica, glass, and HOPG.

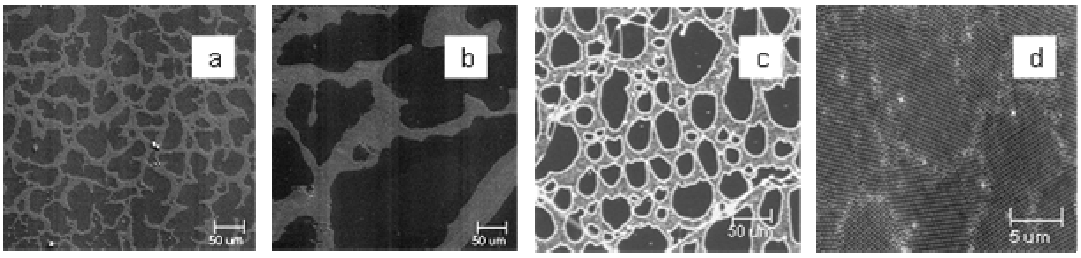

Figure 2.6. SEM micrographs of (1:1) PS/SDS mixtures on different substrates: a) SiO_2, b) mica, c) glass, and d) HOPG.

3.2. Surface Tension Measurements. Figures 2.7 to 2.9 show the results of surface tension measurements performed on solutions of SDS-only, PS/SDS, Igepal® CO 630-only, PS/Igepal® CO 630, PA-only, and PS/PA with the aim to detect any relationship between changes in the surface tension of the latex/surfactant or latex/polymer mixture at a given spreading agent concentration; and the formation of ordered arrays. In all cases, the measurements were made on systems containing 0.5 μm spheres.

In Figure 2.7, a relative minimum in the curve of surface tension as a function of surfactant concentration in the SDS-only solution (black symbols) is observed at 8.1 mM SDS, followed by a slight increase of the surface tension with increasing concentrations of SDS finally reaching a plateau around 43.5 mM. With pure surfactant, the curve should not show a relative minimum; rather the slope should be discontinuous at the CMC, and the surface tension should be constant above this concentration. This behavior shown in Figure 2.7 is very

common for SDS, because of the presence of dodecanol from hydrolysis. Our observations are in quantitative agreement with experimental results found in the literature[9] for SDS in aqueous solution at room temperature. The relative minimum at 8.1 mM SDS corresponds to the critical micelle concentration of SDS in water. For the PS/SDS solution, the CMC is slightly shifted to higher SDS concentrations (i.e. 8.3 mM), which is within the experimental error of the measurement.

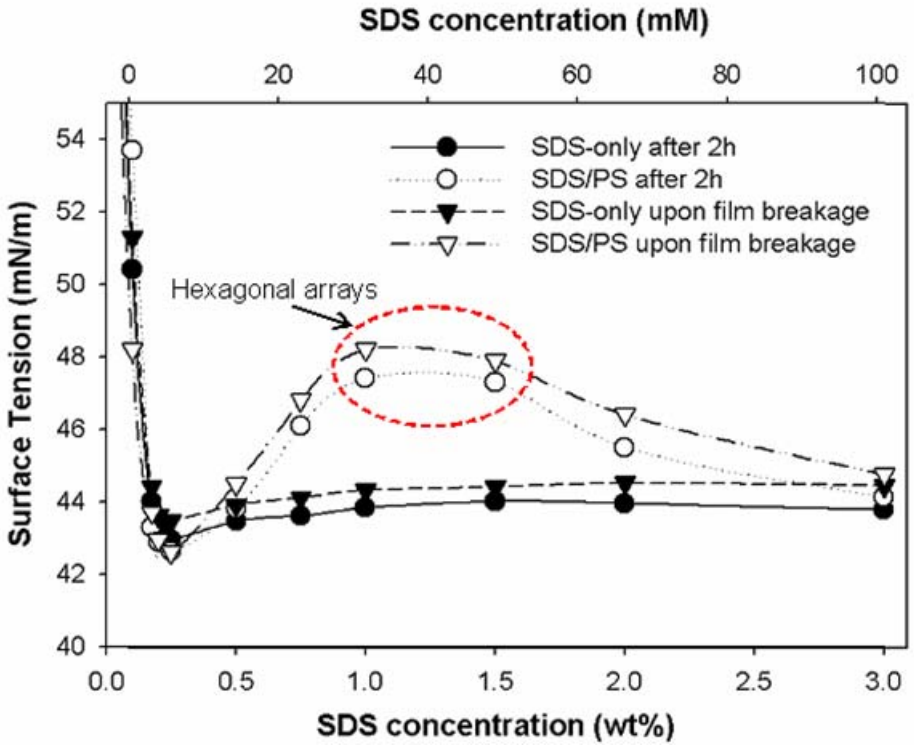

Figure 2.7. Surface tension curves for solutions of SDS-only (black) and PS/SDS (white) after 2h (circles), and upon film breakage (triangles). PS concentration in PS/SDS solutions is 1 wt %. The dotted oval encloses the range of surfactant concentrations at which ordered arrays of PS spheres are observed on the surface of HOPG.

The most striking and unexpected observation from Figure 2.7 is the sharp increase in surface tension in the PS/SDS solution at SDS concentrations between 17.4 mM and 34.7 mM. Although the presence of impurities, i.e. dodecanol in SDS, will cause a rise in surface tension above the CMC; the size of the increase in surface tension eliminates this possibility. *The relatively flat plateau region (dotted circle) corresponds to the range of surfactant concentrations at which ordered monolayers of latex spheres form on the surface of HOPG*. Above 69.4 mM, the surface tension drops, eventually returning to the surface tension of the SDS-only solution (i.e. 44.7 mN/m). Moreover, these solutions of 1 wt % PS and high SDS concentrations showed phase separation over short periods of time: 5 min after the solution was prepared in the case of the 69.4 mM SDS, and almost immediately after the 104 mM SDS solution was prepared. The cluster formation on the surface of HOPG is probably a reflection of phase separation. Phase separation of the 1 wt % PS and 34.7 mM SDS solution was not observed until after 12 hours.

Surface tension curves for the nonionic polyethoxylated (EO = 9) surfactant-only and PS/ nonionic polyethoxylated (EO = 9) surfactant are shown in Figure 2.8. As expected for a nonionic surfactant, the surface tension drops much more rapidly with added surfactant than for the anionic surfactant. The CMC for the nonionic polyethoxylated (EO = 9) surfactant-only solution is

observed at 0.081 mM (the CMC of SDS is around 8.1 mM), after which the surface tension reaches a plateau at about 32 mN/m. In the case of the nonionic polyethoxylated (EO = 9) surfactant/PS solution, the presence of solvated sulfate groups on the surface of the latex spheres increases the ionic strength of the solution, which results in a shift of the CMC toward higher surfactant concentrations (0.32 mM), and higher surface tension values relative to the nonionic polyethoxylated (EO = 9) surfactant-only solution. However, no evidence of any plateau maximum in the surface tension curve is found, and consistent with this observation no ordered structures were observed on HOPG when using the nonionic polyethoxylated (EO = 9) surfactant.

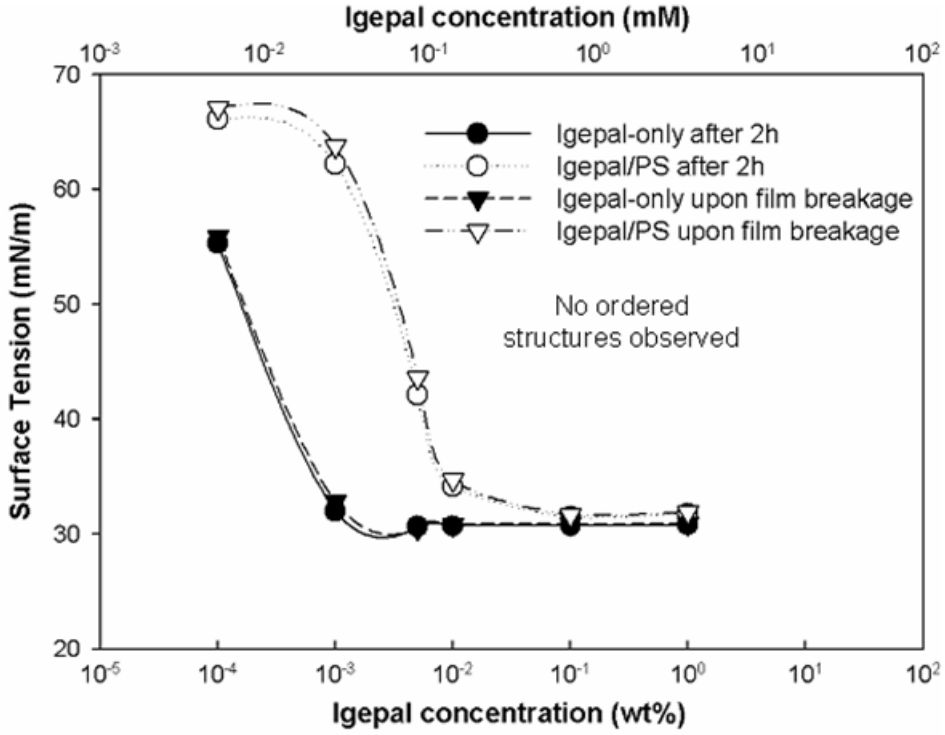

Figure 2.8. Surface tension curves for solutions of nonionic polyethoxylated (EO = 9) surfactant-only (black) and PS/ nonionic polyethoxylated (EO = 9) surfactant (white) after 2h (circles), and upon film breakage (triangles). PS concentration in PS/ nonionic polyethoxylated (EO = 9) surfactant (Igepal® CO 630) solutions is 1 wt %. No ordered structures were observed for this system.

Experimental results from surface tension measurements on the PA system are shown in Figure 2.9. As expected from the low surface activity of polyacrylamide, the PA-only solution (black symbols), shows only a slight reduction of the surface tension with increasing PA concentrations from 5 x 10^{-4} wt % to 0.02 wt %; beyond this point, the surface tension increases again. The existence of a minimum in the surface tension curve reflects the interaction forces between polyacrylamide and the water molecules at the air-liquid interface. At

concentrations higher than 0.02 wt % PA, attractive forces between polyacrylamide molecules become predominant and, consequently, PA migrates away from the air-liquid interface and the surface tension increases.

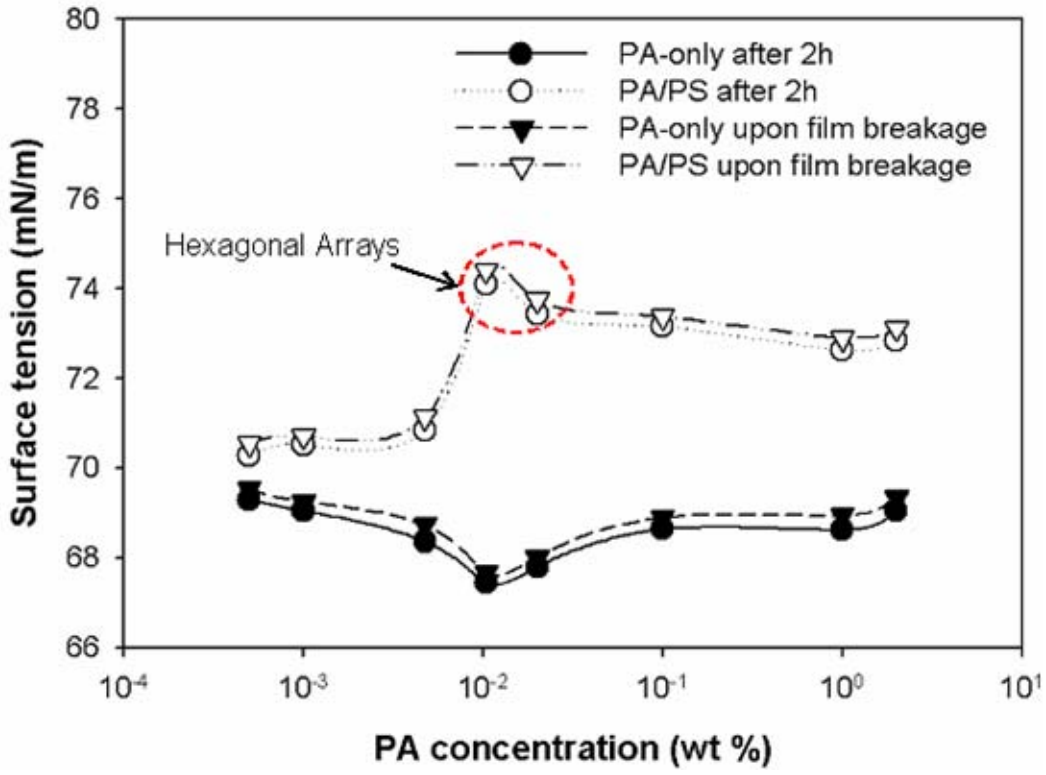

Figure 2.9. Surface tension curves for solutions of PA-only (black) and PS/PA (white) after 2h (circles), and upon film breakage (triangles). PS concentration in PS/PA solutions is 1 wt %. The dotted oval encloses the range of polymer concentrations at which ordered arrays of PS spheres are observed on the surface of HOPG.

On the other hand, the PS/PA system (white symbols) in Figure 2.9 shows a steep increase of the surface tension within a narrow range of PA concentrations

(i.e. 0.01 wt % to 0.1 wt % PA). This range of PA concentrations corresponds to the formation of ordered monolayers of latex spheres on HOPG. Beyond this range, either incomplete or multilayer coverage of the surface is observed. Again, the unique feature in the surface tension curve of the PS/PA system clearly points out the concentration range at which one should operate in order to obtain well-ordered hexagonal arrays of latex spheres. Further increase of the PA concentration in the PS/PA system does not seem to lower the surface tension to the value at very low PA contents (i.e. 70 mN/m), which is suggestive that spheres are at the air-liquid interface and hence should be on the surface of the solid after deposition. However, according to SEM of the films on the solid, only a few spheres are found and these are imbedded in a relatively thick polymer film. One possible explanation is that the high viscosity of the solution prevents some of the spheres from adsorbing to the solid substrate.

3.3. Optical Microscopy. Experimental results from AFM, SEM and surface tension measurements clearly suggest that the interaction between the latex spheres and the spreading agent is key to the formation of ordered monolayers on graphite. In order to have a better understanding of the mechanism of formation of such ordered arrays via the LB application; the air-liquid interface of latex dispersions consisting of 1 wt % PS and various surfactant concentrations in the range of 3.4 mM to 104 mM were investigated. Figure 2.10 shows optical

microscopy images of 2 μm latex spheres at the air-liquid interface as a function of SDS concentration.

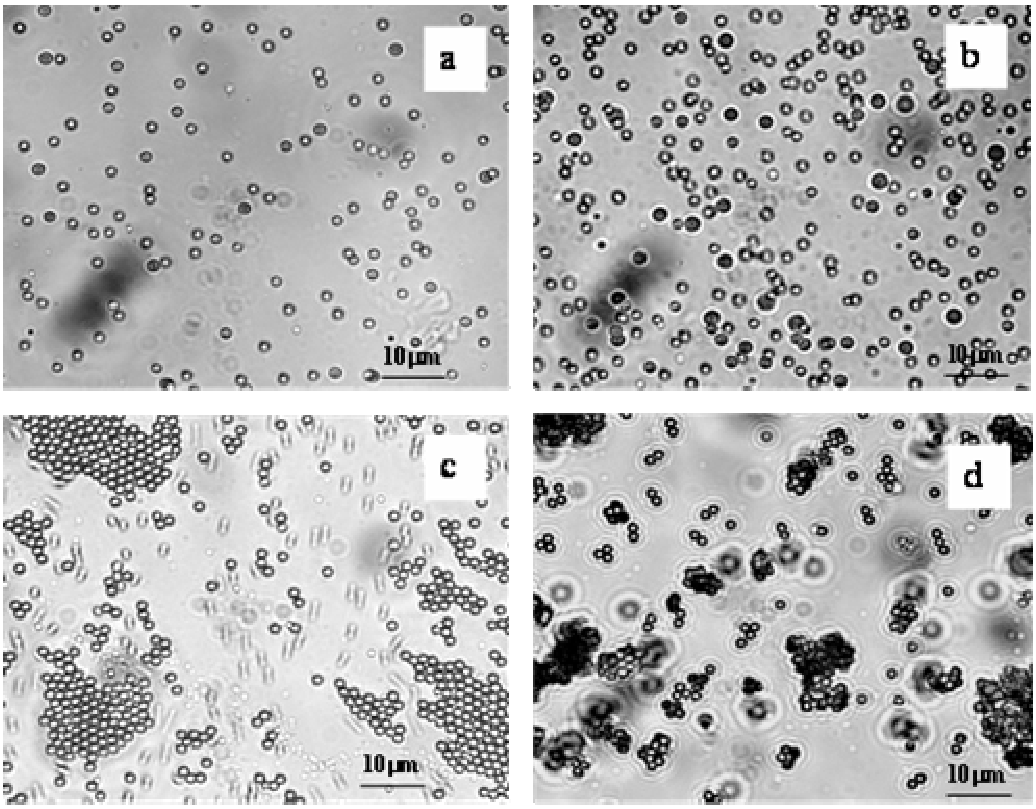

Figure 2.10. Optical microscopy of 2μm latex spheres at the air-liquid interface for dispersions of 1wt%PS in various surfactant concentrations: a) 3.47 mM SDS, b) 8.68 mM SDS, c) 34.7 mM SDS, and d) 104 mM SDS.

Microscopic observation of the air-liquid interface show a few latex spheres involved in intensive Brownian motion at low surfactant concentrations (Figure 2.10a), as the surfactant concentration is increased, more spheres are observed at the air-liquid interface with much slower Brownian motion (Figure

2.10b). When the surfactant concentration is 34.7 mM (Figure 2.10c), the spheres come closer together forming patches of monolayer coverage at the liquid surface. For SDS concentrations ≥ 69.4 mM, particle clustering is observed at the air-liquid interface (Figure 2.10d).

IV. Discussion

AFM and SEM images in Figures 2.2 to 2.5 clearly suggest a strong dependence between the formation of ordered monolayers of latex spheres on HOPG from the LB technique and the concentration of the spreading agent in solution. For the SDS system, there is a range of surfactant concentrations (i.e. 34.7 mM to 52.1 mM SDS) for which well-ordered arrays of latex spheres are observed on the substrate. As shown in Figures 1 and 3 for the 0.5 μm and 2 μm spheres respectively, surfactant concentrations beyond this range result in either loss of order or incomplete surface coverage. There are four possible roles of the surfactant in forming well-ordered arrays of latex spheres 1) The addition of SDS increases the ionic strength of the solution, constituting the driving force for the migration of the latex spheres from the bulk solution to the air-liquid interface 2) Well-known latex/surfactant interactions[10,11] are responsible for the formation of thermodynamically stable disordered monolayers with some well-ordered regions

at the air-liquid interface, by the balancing of steric repulsion interactions and the weakening of charge repulsion between solvated sulfate groups on the surface of the spheres. 3) Formation of a concave liquid surface upon addition of surfactant due to strong hydrophobic interactions between the hydrophobic portion of the surfactant and the substrate (HOPG); and, as a result, strong lateral forces (osmotic forces) push the latex particles together on the solid substrate; and 4) Surfactant molecules at the air-liquid interface slow the evaporation rate of the latex/surfactant solution with respect to the latex solution;[12] hence, the spheres have more time to rearrange and form ordered arrays on the substrate as the liquid film evaporates.[46]

Latex/surfactant interactions can be followed by observation of the experimental surface tension curves for SDS and nonionic polyethoxylated (EO = 9) surfactant in Figures 2.7 and 2.8, respectively. At low SDS concentrations, surfactant molecules at the air-liquid interface are rather far from each other and do not interact as in the case of a two-dimensional gas. This observation is in agreement with the optical microscopy image of the latex spheres at the air-liquid interface when the surfactant concentration is 3.5 mM (Figure 2.10a). Upon increasing SDS concentration, both the ionic strength and the surface compression of the solution increase, and as a result, latex spheres and surfactant molecules begin to interact as in a two-dimensional liquid (Figure 2.10b). As the surfactant

concentration is further increased, the lateral force (i.e. the horizontal component of the capillary force between spheres) increases proportionally and a patchy, two-dimensional solid-state phase forms at the air-liquid interface as shown in Figure 2.10c. In principle, the phase transition from a liquid-like phase to a patchy solid-like phase should encompass a sharp increase in surface pressure (i.e. a significant drop in surface tension). Instead, a sudden increase of the surface tension for the PS latex/SDS system is observed in Figure 2.7 for SDS concentrations in the range of 34.7 mM to 69.4 mM. This observation can be explained by considering the Gibbs surface tension equation (Equation 2.1):

$$d\gamma = -\sum_j \Gamma_j d\mu_j \qquad \text{(Equation 2.1)}$$

Which relates the change in surface tension ($d\gamma$) to the product of the surface excess (Γ) and the change in chemical potential ($d\mu$) of each species, j, present in the mixture. For diluted surfactant solutions, the change in chemical potential can be approximated by Equation 2.2:

$$d\mu_s = -RTd \ln C_s \qquad \text{(Equation 2.2)}$$

where R is the ideal gas constant, T is the absolute temperature, and C_s is the surfactant concentration in solution. Integration and rearrangement of Equations 2.1 and 2.2 yields:

$$\frac{d\gamma}{dC_s} = -\frac{RT\Gamma_s}{C_s} \qquad \text{(Equation 2.3)}$$

According to Equation 2.3, the change in surface tension with surfactant concentration is inversely proportional to the concentration of surfactant in solution. In other words, an increase in surfactant concentration up to the CMC (i.e. the maximum concentration of surfactant monomers in solution) should result in a reduction of the surface tension of the solution. This is the case for the surfactant-only solution as observed in Figure 2.7, but in the presence of negatively charged latex spheres (1 wt%), as the SDS concentration is increased from 34.7 to 69.4 mM, the ionic strength of the solution increases and the spheres adsorb preferentially at the air-liquid interface due to their large surface energy compared to the surfactant molecules. The displacement of surfactant molecules from the interface may explain the sudden increase in surface tension observed. Another possibility is that the increase in surface tension may be an artifact produced by latex spheres adsorbing to the Wilhelmy plate used to determine the surface tension as illustrated in the schematic shown in Figure X. As spheres adsorb to the roughened surface of the Pt plate, the wetted length is significantly increased by the surface area of the spheres, and as a result, the surface tension determined according to the Wilhelmy equation (Equation 2.4) is overestimated.

$$\sigma = \frac{F}{L\cos(\theta)} \qquad \text{(Equation 2.4)}$$

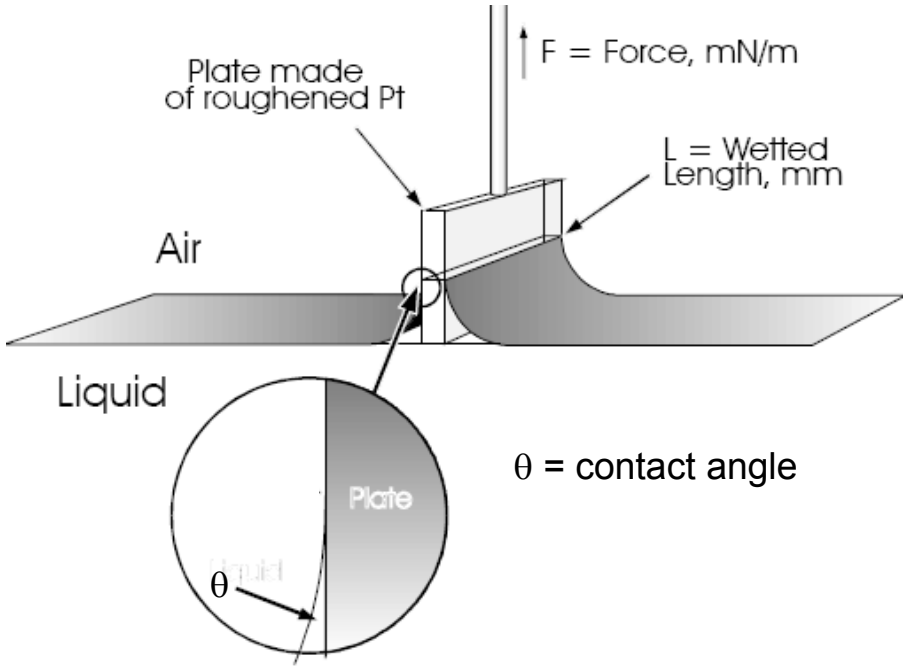

Figure 2.11. Schematic of Wilhelmy method for surface tension measurements.

Whether the surface tension increase observed in Figure 2.7 is a real thermodynamic phenomenon caused by the displacement of surfactant molecules from the interface by the preferential adsorption of latex spheres; or an artifice associated with the method used for the measurements, it provides a very simple, yet powerful tool to predict the formation of ordered arrays of latex spheres at the air-liquid interface for a given particle/spreading agent system.

As previously proposed by Bibette et al.,[13-15] the formation of solid-like regions of colloidal particles at the air-liquid interface can be explained in terms of strong attractive depletion forces resulting from the size asymmetry between

the micron-size spheres and the smaller micellar aggregates in solution at concentrations higher than the CMC. Moreover, as evidenced in Figure 2.10c, this organization process almost certainly occurs in the thin film of solution that is attached to the surface, and our surmise is that the well-ordered regions shown in Figure 2.10c might act as nucleation sites for the well-ordered monolayers observed in Figures 2.2c and 2.3 for the 0.5 μm spheres, and Figure 2.4c for the 2 μm spheres. However, the surfactant concentration must remain within the range for which a plateau in the surface tension is observed, otherwise particle coagulation and phase separation will occur as shown in Figure 2.10d for SDS ≥ 69.4 mM. Figure 2.12 shows the model proposed to explain the role of the surfactant in forming well-ordered monolayers on HOPG from the Langmuir-Blodgett-like technique.

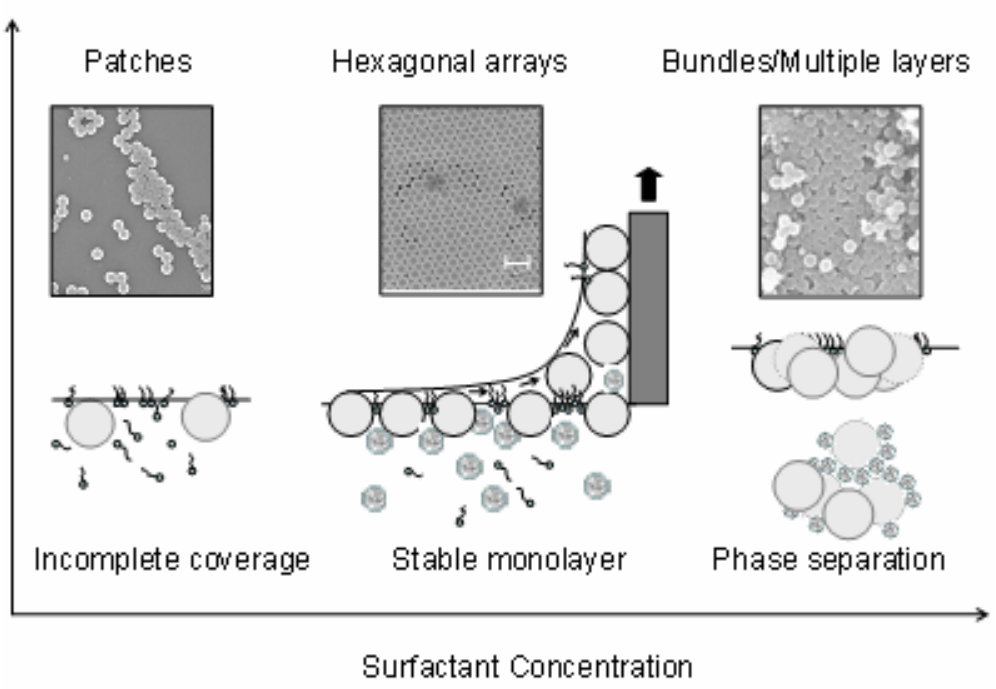

Figure 2.12. Schematic representation of the model proposed to explain the role of the surfactant in forming highly ordered, transferable monolayers of latex spheres at the air-liquid interface in LB technique.

The formation of highly ordered monolayers of latex spheres on HOPG when SDS is used as a spreading agent seems to be a balance between thermodynamic and kinetic driving forces. On the one hand, the surfactant concentration has to be above the CMC of the latex-surfactant mixture to form solid-like regions at the air-liquid interface; and on the other hand, the time for phase separation decreases as the surfactant concentration is increased. Experimental results from this work indicate that these effects are balanced for surfactant concentrations in the range of 34.7 mM to 52.1 mM when SDS is used

as the spreading agent in latexes of 0.5 μm and 2 μm in diameter. The difference between SDS and nonionic polyethoxylated (EO = 9) surfactant in driving spheres to the air-liquid interface might be due to the ability of the surfactant to stabilize the spheres in bulk; the nonionic surfactant is a much better stabilizing agent as evidenced by the absence of precipitation and perhaps this interaction prevents migration of spheres to the air-liquid interface.

With respect to the polyacrylamide as a spreading agent, Tsuneo[16] discusses the effect of neutral polymers on the ordering of monodisperse polystyrene spheres. In this work, the reflection spectrum technique is used to study subtle changes in the lattice constant of ordered structures on addition of neutral polymers. In the case of PA, the lattice constant was found to decrease as the result of strong dipole-dipole interactions between the latex spheres and the polymer. Thus, the effect is explained in terms of the changes in the magnitude and distribution of charges in the electrical double layer brought about by the adsorption of the polymer on the latex spheres. We believe this effect, in combination with steric repulsion due to adsorbed polymer, is the driving force for the migration of the spheres from the bulk to the interface. At higher concentrations, the viscosity of the medium probably becomes an issue for the migration of the spheres to the air-liquid interface.

The generality of the surface tension method was confirmed by results with PA and the nonionic surfactant. These results are very encouraging since the formation of ordered arrays can be predicted from a very simple measurement that is easily automated. Further, the surface tension method should not be restricted to latex spheres as it could be applied to any particle system (e.g. gold particles) as long as changes in the particle concentration at the air-liquid interface result in significant changes in the measured surface tension. The only real question is whether an interaction between an arbitrary set of particles and the extremely low energy surface platinum of the Wilhelmy plate might skew the surface tension measurement somehow. This question remains to be addressed.

The surface tension method should be used to determine the optimum conditions for forming a film, but is not an absolute predictive method because factors unrelated to the morphology at the air-liquid interface affect the organization of spheres on a solid substrate. One factor is the substrate itself; i.e. the energetic interaction between the surface and the spheres and/or the interaction between the surface and the solvent. In experiments with negatively charged mica, long-range ordered arrays were not formed as shown in Figure 2.6b except at very slow pulling speeds, which we attributed to the incompatibility between the negatively charged spheres/surfactant and the negatively charged substrate. Patchy coverages were also found with silicon wafers and glass slides

(Figures 2.6a and 2.6c). The second key variable is the pulling speed; even with HOPG, if the pulling speed is too fast, then the ordered morphology will not be present on the surface. In this study the pulling speed was fixed to 5 μm/s. The effect of varying the compression speed on the deposition of 500 nm PS spheres on HOPG in the presence of 34.7 mM SDS is shown in Figure 2.13.

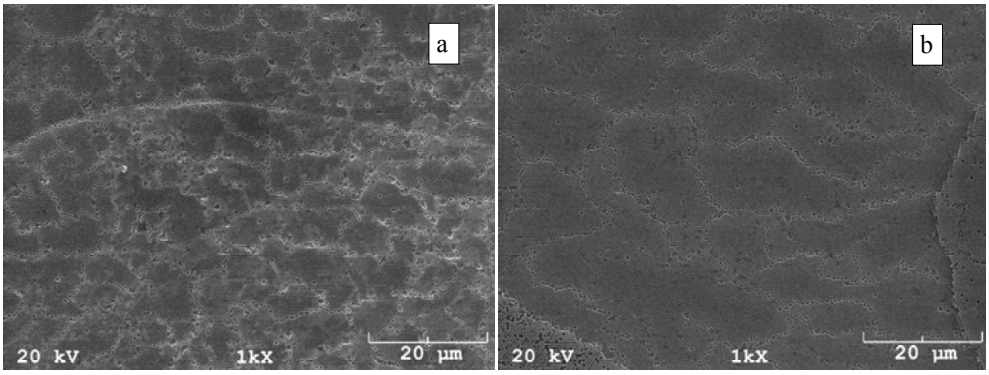

Figure 2.13. SEM micrographs of colloidal monolayers of latex spheres (500 nm in diameter) on HOPG showing high surface coverage, and crystalline domains of different sizes. The size of the domains can be controlled by adjusting the ratio of the compression speed (Vc) to the pulling speed (Vp): a) Vc/Vp = 3, and b) Vc/Vp = 1.

SEM images in Figure 2.13 confirm that monolayer surface coverage greater than 95 % can be achieved with the LB technique. Another variable of interest is the size of the crystalline domains. In this respect, large monocrystalline domains, with minimum crystalline boundaries and defects are usually desired for many commercial applications. This paper shows that the size of the crystalline domains can be controlled by tuning the compression and the pulling speed during the dip-coating process; however, it is important to note that

the largest crystalline domains obtained in this work (in the order of hundreds of microns squared) do not reach the sizes required for most industrial applications (i.e. of the order of mm^2).

Another important factor in the formation of ordered nanostructures via the LB technique is the choice of solvent. In this respect, the characteristics of the film formed on a particular substrate or at a particular pulling speed can be altered by changing solvent; replacing water with a 1:1 MeOH:H_2O mixture led to almost perfect films onto HOPG and reduced the patchiness onto SiO_2; however, the mixed solvent did not ameliorate the wetting onto mica or glass significantly. The importance of the surface tension method proposed here to all of these situations is that the method identifies the best set of conditions to perform experiments in order to obtain the highly ordered morphologies; and, in the case of the nonionic surfactant, also shows that under certain conditions forming the ordered morphologies is very difficult, if not impossible. Nevertheless, the surface tension condition is not by itself sufficient for obtaining ordered morphologies, and the results represented by Figure 2.6 support this conclusion.

V. Conclusions

Highly ordered hexagonal arrays of latex spheres on HOPG have been prepared from a variation of the LB technique with an anionic surfactant, SDS, and a water soluble polymer, PA as spreading agents; whereas no ordered arrays could be obtained when using a nonionic polyethoxylated (EO = 9) surfactant. Based on the correlation found between the surface tension in the presence of the latex particles and the critical concentration at which hexagonal arrangements of latex spheres occurs; a model has been proposed to explain the role of the spreading agent in forming stable monolayers at the air/liquid interface, which in turn are necessary for the formation of well-ordered monolayers on a solid substrate from the LB technique. According to this model, solid-like regions of latex spheres form at the liquid-air interface, which are then transferred to the substrate. These ordered regions then act as nuclei for the formation of 2D arrays of latex spheres on HOPG upon water evaporation. A simple, easy to automate, yet effective surface tension method has been proposed to predict the optimal conditions for the formation of ordered monolayers using a variation of the LB deposition method from any monodisperse set of spheres.

VI. References

1 Kumaki, J. *Macromolecule* **1986**, 19, 2258.

2 Kumaki, J. *Macromolecules* **1988**, 21, 749.

3 Yin, R; Cha, X; Zhang, X; and Shen, J. *Macromolecules* **1990**, 23, 5158.

4 Fulda, K; ans Tieke, B. *Adv. Mater.* **1994**, 6, 288.

5 Fulda, K; Piecha, D; Yarmohammadipour, H; and Tieke, B. *Progr. Colloid Polym. Sci.* **1996**, 101, 178.

6 Kondo, M; Shinozaki, K; Bergstrom, L; and Mizutani, N. *Langmuir* **1995**, 11, 394.

7 Du, H; Bai, Y; Zhui, L; Chen, Y; Tang, X; and Li, T. *Langmui.* **1997**, 13, 2538.

8 Iakovenko, S; Trifonov, A; Giersig, M; Mamedov, A; Naguesha, D; Hanin, V; Soldatov, E; and Kotov, N. *Adv. Mater.* **1999**, 11, 388.

9 Rosen, M. J. *Surfactants and Interfacial Phenomena.* 2nd ed.; John Wiley & Sons Inc: New York, **1989**; Chapter 3.

10 Brown, W and Zhao, J. *Macromolecules* **1993**, 26, 2711.

11 Brown, W and Zhao, J. *Langmuir* **1994**, 10, 3395.

12 Davies, J; and Rideal, E. *Interfacial Phenomena*, 2nd ed.; Academic Press: New York, **1963,** Chapter 7.

13 Mondain-Monval, O., Leal-Calderon, F., Phillip, J., Bibette, J. *Phys. Rev. Lett.* **1995**, 75, 3364.

14 Bibette,J., Roux, D., Pouligny, B. *J. Phys. II France* **1992**, 2, 401.

15 Bibette,J., Roux, D., Nallet, F. *Phys. Rev. Lett.* **1990**, 65, 2470.

16 Tsuneo, O. *J. Chem. Soc.; Faraday Trans. 1*. **1987**, 83, 2497.

Chapter 3. Synthesis of Polymer Nanostructures via Template Assisted Admicellar Polymerization (TAAP): A Comparative Study with Protein Adsorption

I. Introduction

In the previous two chapters it has been shown that the Langmuir-Blodgett (LB) technique can be use to produce well-ordered monolayers of latex spheres on a surface by allowing the particles to self-assemble at the air-liquid interface, and then transferring this structure to a substrate through a simple dip-coating process. Interstitial sites of adsorbed latex spheres have been used previously as templates to produce polymer nanostructures. Two approaches have been demonstrated in the literature. The first is to adsorb an already premade polymer in the interstitial sites as reported by Liu et al.[1] This method has the disadvantage of requiring adsorption to the underlying substrate for that particular polymer/solvent pair, which can pose significant restrictions on the type of polymer/substrate used. Further, there is a limitation on the smallest spheres that can be used, which depends on the radius of gyration of the polymer. The second approach is to use an electric field to concentrate monomer at the surface and polymerize.[2,3] Using an electric field to concentrate monomer has the

disadvantage that the monomers and surfaces that can be used are very limited. Both processes have the disadvantage that there is little, if any, separation distance between the template and the polymer. The ramification of having a substantial separation distance between the template and the polymer is that a pillar pattern is possible; no pillar-type patterns of polymers using latex-sphere interstitial sites have been reported in the literature (however carbon[4] and various metals[5,6] have been shown to form pillar-type structures with this type of lithography).

Other procedures described in the literature have been used to yield regularly arranged pillar-type patterns of polymers with sub 50 nm-scale dimensions. Most of these procedures used adsorbed block copolymers as the template; it is well-known that block copolymers can be adsorbed to form regularly arranged morphologies at a solid surface.[7] In one paper, the affinity of pyrrole for a hydrophobic component of a diblock copolymer was used to preferentially grow polypyrrole on top of the hydrophobic component.[8] A similar diblock copolymer approach was used by a different set of researchers, and the affinity of surfactant adsorption to different blocky components was used to selectively localize the monomer.[9] The disadvantage of both techniques is that the polymer does not make direct contact with the underlying surface, although through control of the process[10] and/or the use of etching techniques,[11] it is possible to produce patterns that have holes which in turn could be used in the

same manner as interstitial sites of latex spheres. Another disadvantage is that a block copolymer requires a great deal of time (i.e. a few days in most cases) to form well-ordered nanostructures.

In this chapter, a novel method for the formation of nanometer-scale polymer structures via template assisted admicellar polymerization (TAAP) is described. Admicellar polymerization uses surfactant aggregates adsorbed on a surface to concentrate monomer at the surface prior to polymerization. This phenomenon has been widely investigated for a number of systems including various monomer/surfactant combinations, as well as different substrates.[12-19] The basic steps involved in TAAP are illustrated in Figure 3.1. The first step is to mask the surface with a template such that polymer is synthesized only in selected areas. In this work a latex-sphere template has been chosen; however the process should work with nearly any type of template. The second and third steps, which may be carried out simultaneously, involve surfactant adsorption and monomer adsolubilization. Indeed, monomer-surfactant interaction is critical for the partition of monomer into the surfactant aggregate. This interaction has been studied for a number of monomer/surfactant pairs.[17,18,20-23] For the particular case of aniline monomer and sodium dodecyl sulfate (SDS) surfactant, the interaction is believed to resemble that of phenol at the oil-water interface, with the benzene ring of the anilinium cation oriented towards the hydrophobic portion of the SDS aggregate, and the NH^{2+} moiety side by side with negatively charged SDS head

groups in the palisade layer of the surfactant aggregate.[24-26] The polymerization proceeds via free radical propagation upon the addition of an initiator/oxidizer species, in this case ammonium peroxydisulfate (APS). In the fourth step, the substrate is washed with large amounts of water to remove residual monomer, surfactant, and initiator. Finally, the original template is removed and a patterned, thin polymer film is left on the surface. As shown in Figure 3.1, either polymer pillars or honeycombs can be formed depending on the size of the latex spheres and the conditions of admicellar polymerization.

An advantage of TAAP relative to other lithographic methods is the ability to form nanostructures with dimensions significantly smaller than the original template because of sphere-surfactant interactions. In order to illustrate this point, this work compares the morphology and dimensions of polyaniline (PANI) nanostructures synthesized via admicellar polymerization with structures formed via protein adsorption, for three different proteins (Bovine serum albumin, fibrinogen, and anti-mouse IgG). The protein patterning procedure here described also involves the use of sphere lithography for the masking of the substrate, allowing for a direct comparison between TAAP and polymer adsorption.

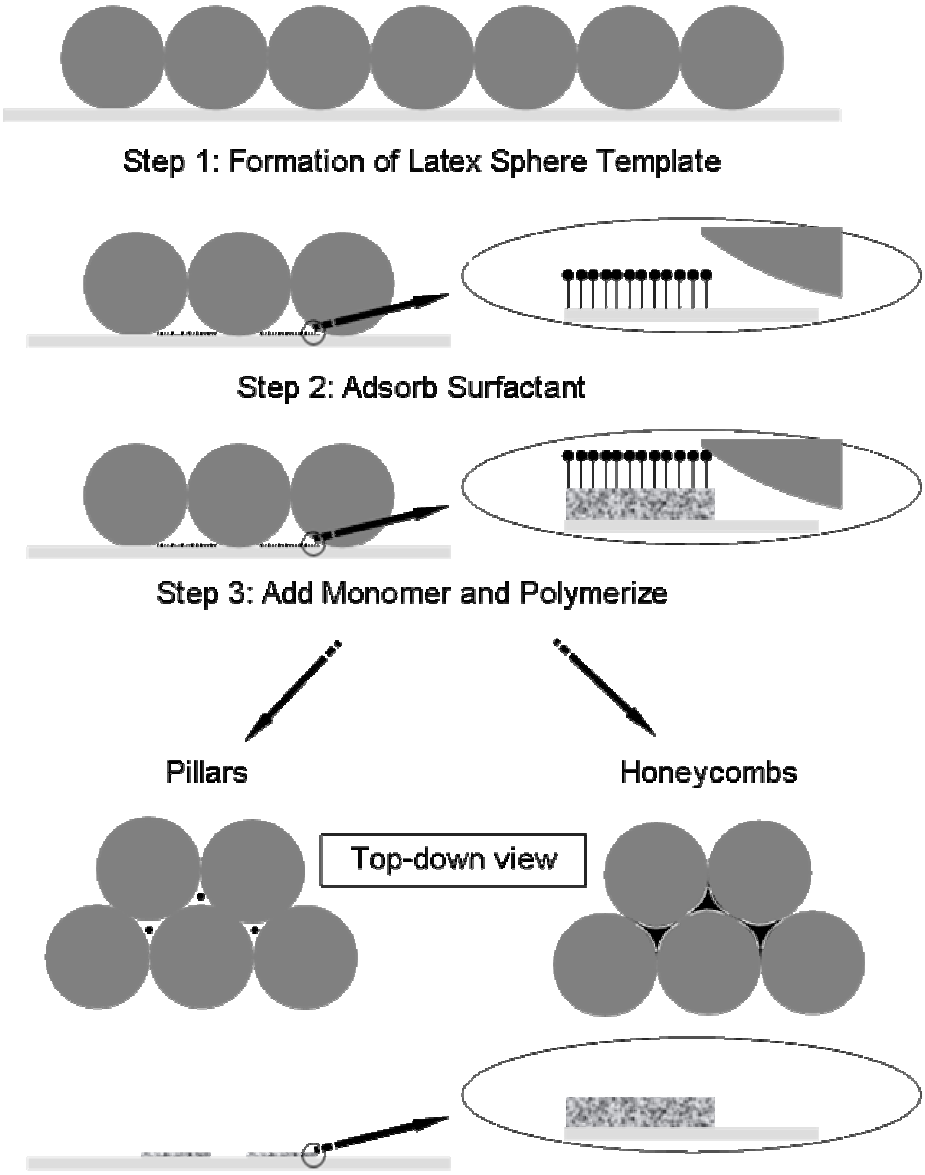

Figure 3.1. Schematic of Template-Assisted Admicellar Polymerization (TAAP) showing the difference in formation of polymer nanopillars and honeycombs. Figure not drawn to scale.

II. Experimental

Materials. Polystyrene latex spheres (2.5 wt% aqueous dispersion) stabilized with a slight anionic charge from surface sulfate groups, and nominal diameters of 55, 210, 504, 1016, and 2148 nm, were purchased from Alfa Aesar. 10 wt% aqueous dispersions of latex spheres (560 nm, 1011 nm, 1920 nm, and 5010 nm in diameter) were from Bang Laboratories Inc. Aniline (99%, distilled under reduced pressure), ammonium persulfate (APS, 98%), and sodium n-dodecyl sulfate (SDS) (98%, recrystallized once from ethanol), were obtained from Aldrich Chemical Company. Fluorescently tagged bovine serum albumin, fibrinogen, and anti-mouse IgG were purchased from Molecular Probes. HBSS-Ca^{2+} buffer and vectashield H-1000 were from Invitrogen Corporation, and Vector Laboratories, Inc. respectively. Highly-Ordered Pyrolytic Graphite (HOPG), monochromator ZYB grade (5 mm x 5 mm sheets) was purchased from Advanced Ceramics, and used freshly cleaved. Glass slides (1 x 1 cm^2) from Fisher Scientific were subsequently cleaned in tetrachloroethylene, acetone, methanol and DI water for 2 minutes each cycle, using an ultrasonic cleaner from Cole Palmer Instruments. Glass substrates were dried with an air stream prior to sphere deposition.

Substrate Masking. The choice of substrate was based on the mechanism driving the formation of the nanostructure. HOPG was chosen for TAAP because of two

reasons: First, the adsorption and formation of surface-induced SDS aggregates (i.e. hemicylinders) at the graphite-solution interface is well-understood.[27] Second, the hydrophobic nature of HOPG promotes aniline partition into surfactant aggregates on the surface due to hydrophobic interactions with the monomer. Partitioning of monomer into surfactant aggregates is a necessary condition for TAAP. Protein patterning, on the other hand, requires a strong interaction between the protein and the substrate. Glass substrates were chosen for the protein patterning experiments due to their excellent optical properties and compatibility with fluorescence microscopy techniques which allowed for in situ visualization and characterization of the protein patterns formed. In addition, several studies have demonstrated that proteins such as albumin, fibrinogen, and anti-mouse IgG readily adsorb onto glass and other silanol-containing substrates (e.g. silane-treated SiO2).[28-31] Finally, since the eventual use of these protein structures is to investigate the role of spatial patterning of proteins in cell adhesion, we wanted a substrate that could allow simultaneous imaging of the fluorescent protein patterns as well as adhering cells in real time.

Close-packed monolayers of latex spheres on HOPG were obtained by dipping the substrate in a 1:1 dispersion of latex spheres and the spreading agent (SDS) as described in chapter 2. Self-assembled monolayers of PS microspheres onto glass substrates were achieved by a conventional spin casting procedure using a spin coating device from Laurell Technologies Corporation (Model WS-

400A). The spin coating process was performed in two consecutive steps; first at the speed of 3000 rpm for 30 seconds and second at the speed of 1000 rpm for 30 seconds. No surfactant was used in the spin casting method.

Admicellar Polymerization. An aqueous solution of 5.4 mM aniline/SDS was prepared at pH 2 using HCl. All solutions were prepared with 18.2 $M\Omega\text{-}cm^{-1}$ nanopure water, and stirred for 1h at room temperature. The substrate, HOPG, previously coated with a monolayer of hexagonally packed latex spheres was contacted with 5 ml of the SDS/aniline solution for 1h at room temperature. After addition of 100 ul of 5.4 mM APS, admicellar polymerization was carried out with gentle stirring, at room temperature for 24h. Following polymerization, excess monomer and surfactant were rinsed thoroughly with pH 2 water (adjusted with HCl) and dried at room temperature. PS latex spheres were removed by soaking the samples in toluene for 5 days. All samples were kept in a desiccator for at least 12h prior to imaging.

In addition, two control samples were prepared: the first sample was synthesized following the same procedure described above, but no surfactant was added to promote the localization of aniline at the solid-liquid interface. The second control was prepared by dipping the substrate for 12h into a solution containing solution polymerized polyaniline that had been polymerized for 24h. HOPG substrates previously masked with a 504 nm latex sphere close-packed

monolayer were used for the control samples. PS latex spheres were removed by soaking the samples in toluene for 5 days.

Protein Adsorption. Protein patterns were achieved by adsorption of 100 μl of the protein solution (i.e. 20 μg/ml bovine serum albumin, 50 μg/ml fibrinogen, and 20 μg/ml anti-mouse IgG) onto glass substrates previously masked with a monolayer of PS latex microspheres. After 1h incubation, the substrate was washed with HBSS-Ca^{+2} buffer. PS latex spheres were subsequently removed by ultrasound in the HBSS-Ca^{+2} solution for 2 min. The substrates were then air dried for 15 min, and fixated prior to florescence imaging with vectashield H-1000.

Instrumentation. A confocal fluorescent microscope (Olympus Fluoview 504) was used to image fluorescently tagged honeycomb protein patterns on glass substrates. A Digital Instruments NanoScope III AFM was used in tapping mode to investigate the formation of polyaniline (PANI) structures on the surface of HOPG. MikroMasch Ultrasharp silicon nitride cantilevers were used with a backside aluminum coating and typical resonant frequencies of 325 kHz and force constants of 40 N/m. All images were captured at 0^{o} with minimal engagement forces and relatively high scanning rates. AFM calibration was carried out using grids with a pitch of 10 um and depth of 180 nm. High-resolution SEM imaging of PANI structures on HOPG was performed using a field emission scanning

electron microscope (SEM, JEOL-6300F, Peabody, MA). The SEM was operated with an accelerating voltage of 15kV. No coating of the polyaniline samples was necessary. X-ray photoelectron spectroscopy (XPS) data were recorded on a Physical Electronics PHI 5800ESCA System with a background pressure of approximately 2.0 x 10-9 Torr. An 800 mm spot size and 23 eV pass energy were typically used for the analysis. Voigt Amplitude curves using PeakFit® software from Systat Software were used for data fitting. Binding energies were corrected by reference to the C1s peak at 284.8 eV for hydrocarbon.

III. Results and Discussion

Polyaniline nanostructures synthesized on highly oriented pyrolytic graphite (HOPG) using the redox initiator ammonium persulfate at pH 2, and the surfactant sodium dodecyl sulfate at a concentration of 5.4 mM (2/3 of the critical micelle concentration) are shown in Figure 3.2.

Figures 3.2c-f show a series of honeycomb patterns, with the holes corresponding to the sites where latex spheres were originally present. If monomer were to completely fill the interstitial sites, all the spheres, regardless of nominal diameter, would yield honeycomb structures. However, pillars rather than honeycombs were formed for spheres with diameters less than 500 nm as

shown in Figures 3.2a and 3.2b, thus indicating that surfactant and/or monomer were not able to adsorb underneath where the spheres touch. The fully extended surfactant molecule has a length of about 2 nanometers; the fact that spheres of 210 nm nominal diameter did not yield a honeycomb pattern indicates that the sphere can significantly affect the ability of surfactant to adsorb at extremely large distances (i.e. on the order of hundreds of nanometers).

The dimensions of PANI nanostructures shown in Figure 3.2, including the separation distance between the polymer and the surface of the latex sphere, are tabulated in Table 3.1. These distances are calculated from the measured height of the structures and their characteristic diameters, as well as geometric considerations. As shown in the schematic accompanying Table 3.1, the distance *a* represents the height of the admicellar polymer directly underneath where the spheres touch; *b* is the shortest distance between the polymer at the center point of the interstitial site and the sphere, *c* is the distance between the polymer and the sphere directly underneath where the spheres touch, while *d* is the height of the admicellar polymer at the center point of the interstitial site.

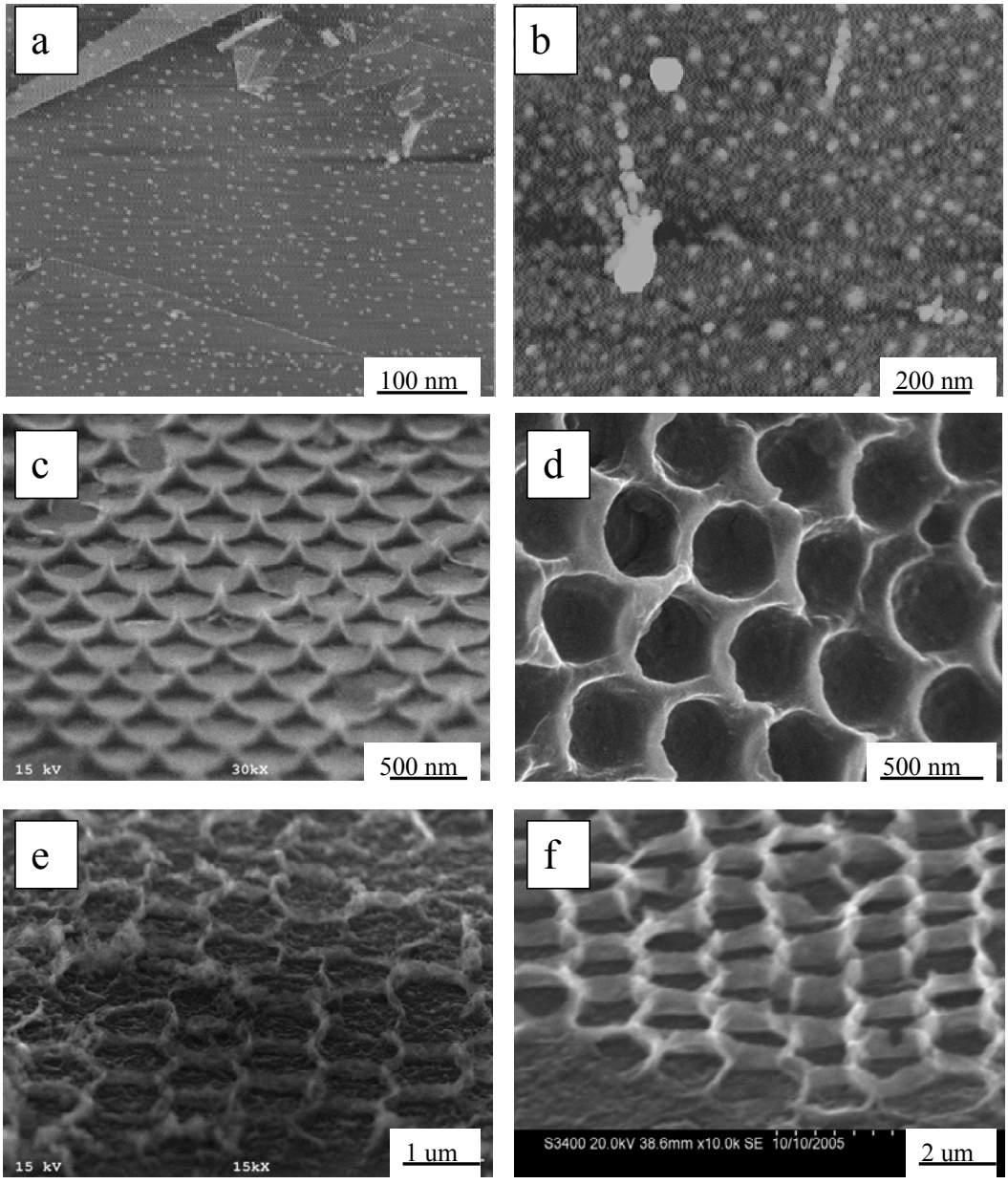

Figure 3.2. SEM and AFM micrographs of admicellar polymer on HOPG after removal of latex sphere template. AFM micrographs: a) 55 nm, and b) 210 nm spheres. SEM micrographs (60^{o} tilt angle): c) and d) 504 nm. e) 1016 nm, and f) 2148 nm spheres.

Table 3.1. Admicellar Polymer Characteristics.

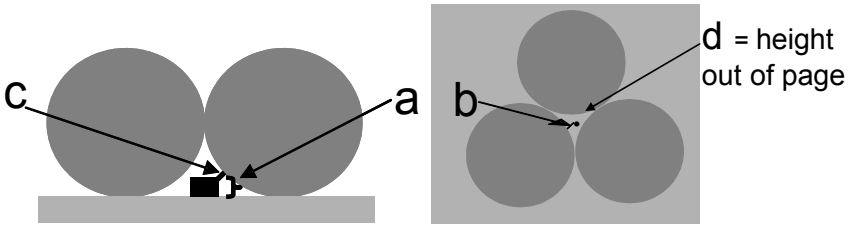

Sphere Diameter (nm)	Nanostructure Diameter (nm)	Nanostructure Height (nm)	Honeycomb Wall Thickness (nm)	Separation Distance[b] (nm)
55	20	25	n/a	4
210	45	60	n/a	24
504	350	30[a], 145[d]	65	58, 60[c]
1016	880	350	110	100, -28[c]
2148	1700	640	240	243, -22[c]

An interesting observation from Table 3.1 concerning the 504 nm spheres is the fact that the separation distance from the sphere to the center point of the interstitial site (*b*) is equivalent to the separation distance measured from the point directly underneath where the spheres touch (*c*). These two distances represent the closest approach distance of the polymer to the sphere, and should be equal if sphere-surfactant interactions are controlling the separation distance. On the other hand, negative values were obtained for the separation distance for the larger sphere sizes (1016 nm and 2140 nm in diameter). In principle, such values are not

possible if the spheres are serving as a template for the polymerization; however, a geometric reason for this apparent inconsistency can be provided by considering the morphology of the structures shown in Figures 3.2e and 3.2f. As seen in the figures, the wall heights do not have the expected parabolic shape as shown in Figure 3.2c; instead the height of the wall top is constant.

Similar results have been obtained for honeycomb structures synthesized from electropolymerization by Han et al. The honeycomb wall tops are not parabolic, and the separation distance calculated using the geometric parameters they report is also negative. One possibility for constant wall height is that the spheres lift off the substrate during the polymerization. Clearly the adhesion force between the spheres and the substrate depends sensitively on the spheres' surface charge and chemistry. This hypothesis is supported by the fact that both flat wall tops and parabolic shapes were obtained for 504 nm spheres from different batches from the same manufacturer. This observation points out the sensitivity of the TAAP method to slight variations (i.e. batch to batch variations) in sphere surface charge and chemistry.

Another possibility for the negative values in Table 3.1 is incomplete removal of polystyrene during the toluene wash. The presence of unremoved latex spheres in some images indicates that sphere dissolution is not complete in some cases. Unfortunately, using ultrasound to remove the spheres removed the PANI

nanostructure as well, indicating that PANI is not well adhered to the substrate. In fact, Figure 3.3 shows that sometimes the film can spontaneously lift off the surface and form "honeytube"-type structures; the fact that the film rolls up indicates residual stress in the structure possibly due to stresses formed during drying. The formation of these "honeytube" structures is revisited in Chapter 4.

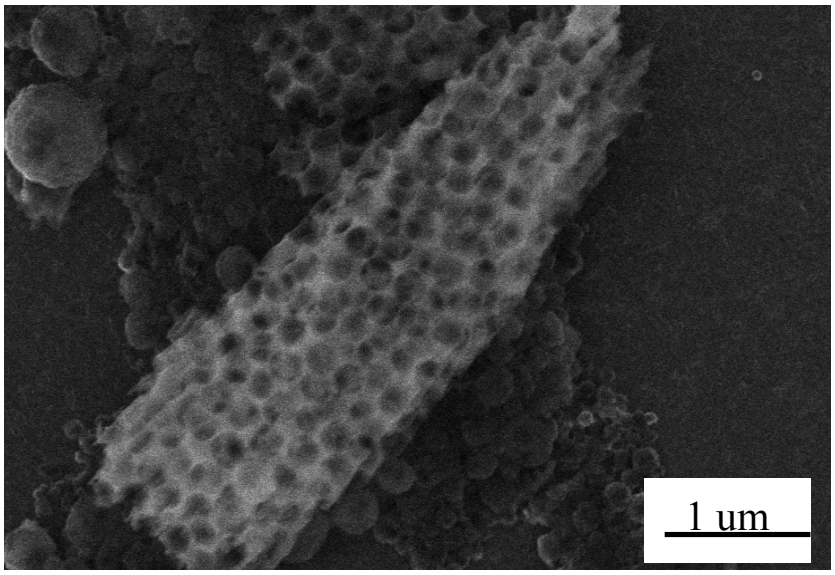

Figure 3.3. Polyaniline "honeytubes" caused by a spontaneous lifting off of the honeycomb film from the graphite surface.

To determine whether the synthesized nanostructures were effectively polyaniline, X-ray photoelectron spectroscopy (XPS) was carried out. PANI can be present in one of three oxidation states; leucoemeradine, emeraldine, and pernigraniline referring to reduced, reduced/oxidized, and oxidized states

respectively. Thus, the particular form of PANI can be characterized from XPS by means of three different nitrogen environments with specific N_{1s} binding energies: <399, 399-400, and >400 eV representing –N=, –NH–, and –$N^{+\bullet}$– respectively.[32] As deduced from the two positively charged (>400 eV) N_{1s} peaks observed in the XPS spectra of both PANI nanopillars and honeycomb structures (Figure 3.4), two different PANI species may be present: polaron and bipolaron states, with correspondingly increasing binding energies.[33] Moreover, evaluation of the relative area under these positively charged peaks with respect to the total nitrogen content (i.e. N^{+}/N) shows doping degrees of ca. 42 % and 61 % for pillars, and honeycomb nanostructures, respectively. Although the contribution to the area of positively charged nitrogen by intercalated ammonium ions in oxidized HOPG substrates cannot be ruled out, XPS results suggest that in both cases (i.e. pillar and honeycombs) the polymer is in the emeraldine salt (conductive) form. This observation is supported by AC impedance measurements discussed in chapter 4.

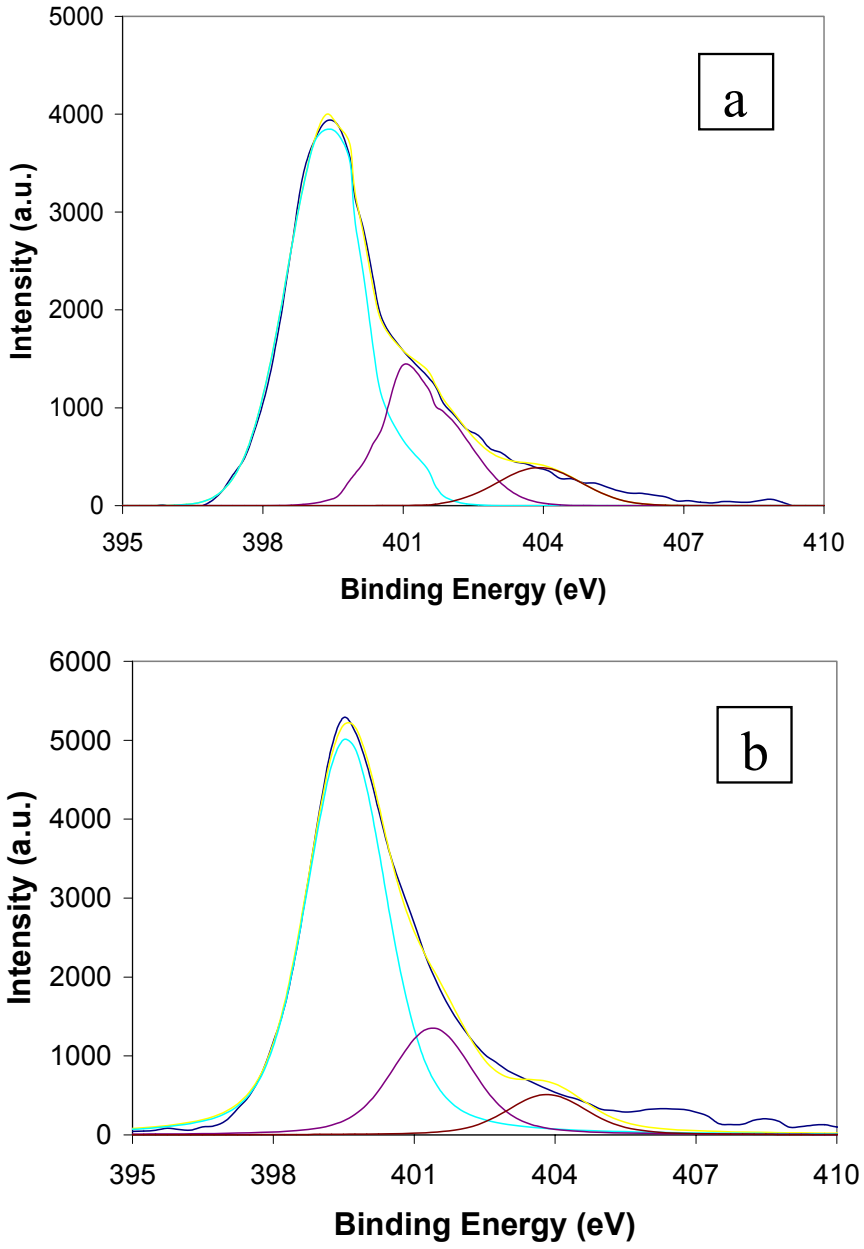

Figure 3.4. X-ray photoelectron spectroscopy data for: a) PANI honeycomb, and b) PANI nanopillars shown in Figures 3.2c, and 3.2a, respectively. Three nitrogen environments can be observed by deconvolution of the N_{1s} peak.

In order to assess the role of the surfactant in driving the partition of the monomer to the solid-liquid interface, and to confirm that the polymerization was occurring preferentially at the surface of the graphite, two control experiments were performed. For the first control sample (Figure 3.5a), the conditions for the admicellar polymerization of aniline were duplicated with the exception that no surfactant was added. The randomly deposited material observed in Figure 3.4a is consistent with polymerization in solution followed by deposition on the surface, or a combination of precipitated and surface-grown polyaniline. No evidence of sphere removal is found in Figure 3.5a indicating that the polymer grows over the spheres and is not removed when the spheres are removed. Solution polymerization occurs according to visual observation with and without added surfactant. Hence, the pattern in Figure 3.5a is not surprising; rather intriguing is the fact that this pattern is not seen when surfactant is adsorbed. With admicellar polymer at the surface, solution-polymerized material is apparently not able to stick to the graphite, and is probably removed in the water wash. When graphite containing adsorbed 504 nm spheres is dipped in a solution of already-formed polyaniline, a featureless, thick polymer films is observed as shown in Figure 3.5b. The absence of pattern replication in Figures 3.5a and 3.5b thus confirms the role of the surfactant in localizing the monomer to the solid-liquid interface, and the fact that the polymerization occurs preferentially at the graphite surface in TAAP.

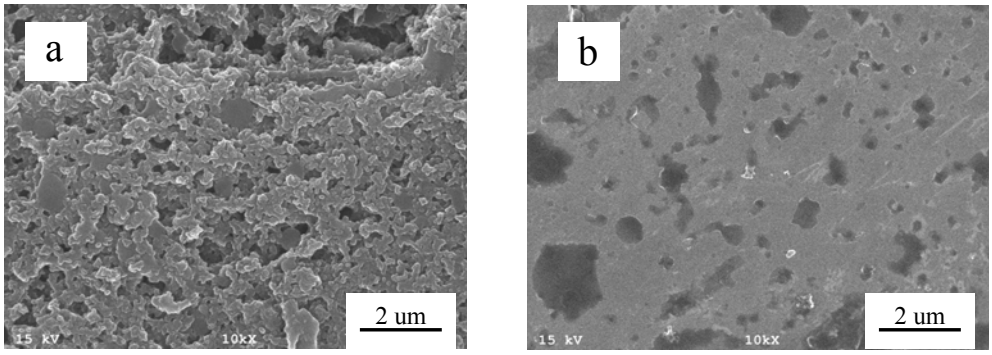

Figure 3.5. Control samples: a) Oxidative polymerization of aniline (no surfactant added) on HOPG previously masked with a close-packed monolayer of 504 nm latex spheres. b) The result of dipping the same substrate into a solution containing solution polymerized polyaniline after 24h.

Figure 3.6 shows the result of using a latex sphere pattern, but instead of admicellar polymerization, a protein is adsorbed to a glass substrate. Fluorescence micrographs in Figure 3.6 appear very similar to AFM images published by Garno et al., who performed similar experiments with protein and adsorbed latex spheres. Garno et al., however, added polymer and latex spheres at the same time and formed films by an evaporative process simultaneously, and in some cases it appears as if polymer adsorbed to the surface underneath the spheres. In our case, the spheres were adsorbed first followed by the addition of protein, and the protein does not appear to go underneath the spheres.

Protein pattern characteristics are shown in Table 3.2. In the case of protein adsorption, there are two restrictions concerning the size of the honeycomb. First, there is a critical sphere size that will allow polymer diffusion

through the interstitial site, roughly given by 0.155*sphere diameter.[34] The second restriction is defined by a limit given by the interaction of the sphere with the adsorbed protein, as well as the repulsion associated with the disruption of the protein chain from its normal adsorbed configuration if it comes too close to the sphere.

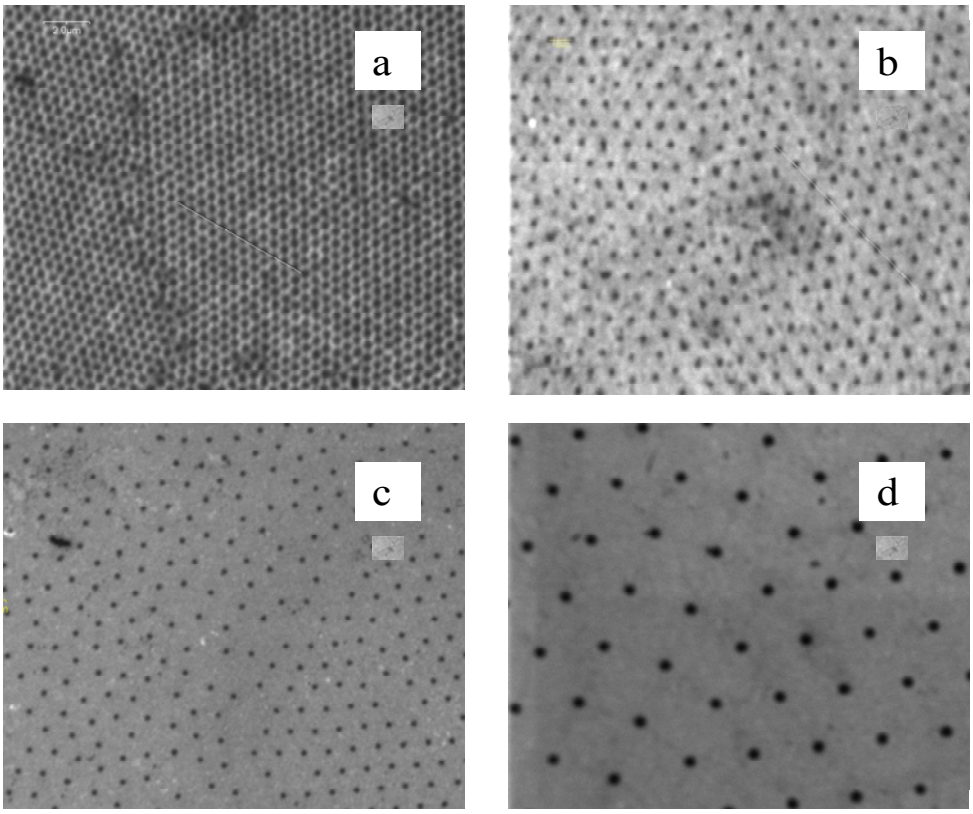

Figure 3.6. Optical micrographs of fluorescently tagged protein (light in photograph) adsorbed on glass after removal of latex sphere template: a) 560 nm, b) 1010 nm, c) 1920 nm, and d) 5430 nm spheres. The dark holes correspond to washed-away latex spheres. IgG (20 ug/ml) was used for figures a) and b). Fibrinogen (50 ug/ml) was used in figures c) and d).

Table 3.2. Protein Pattern Characteristics.

	Fibrinogen (Rg= 14.2 nm) [36]		**Bovine Serum Albumin (Rg= 7.2 nm)** [36]		**IgG (Rg=3.0 nm)** [37]	
Sphere diameter (nm)	Hole diameter* (nm)	Separation distance (nm)	Hole diameter* (nm)	Separation distance (nm)	Hole diameter* (nm)	Separation distance (nm)
560	210	14.4	200	12.6	160	6.4
1010	350	24.7	310	18.5	300	17
1920	510	28.4	380	13.2	350	10.9
5430	1820	143	2130	196	2250	219

*after sphere removal.

The closest approach distances in Table 3.2 assume that the protein has a 5 nm height; studies elsewhere have shown that adsorbed protein height is on the order of a few nm.[1,35] Honeycomb walls are clearly much thicker in the adsorption case as evidenced by comparison of Figures 3.2 and 3.6. For the nominal 500 nm spheres, wall thickness for the admicellar polymer and the adsorbed protein are 65 nm and 350 nm respectively. Wall thicknesses similar to the latter value were found by Garno et al., for the protein adsorbed concurrently with the spheres instead of sequentially.[1] The wall thickness for the electropolymerized material is intermediate between these two values: 150 nm (with a height of ~100 nm) for 600 nm spheres.[2] Moreover, for a given sphere nominal size, the separation distance between the polymer and the sphere is much larger in TAAP compared to adsorption. In addition, it is important to note the increase in apparent separation distance with sphere size in the adsorbed protein case, which is probably due to an increase in the contact area between the sphere and the surface as the sphere size increases due to deformation of the latex particles; this type of deformation has been observed before. The other interesting observation with respect to Table 3.2 is the dependence of the hole diameter on the radius of gyration. If sphere/protein interactions were totally unimportant, then the diameter of the hole should scale with the radius of gyration (R_g). The scaling relationship holds qualitatively except for the largest spheres; the latter result

suggests that sphere-polymer interactions can be important in the polymer adsorption case as well.[36,37] A more complete description of the characteristics of these adsorbed protein structures, along with other adsorbed protein structures will appear in a later publication.[38]

There are significant advantages of TAAP vs. other lithographic techniques. First, TAAP will work on any surface, rough or smooth, of any surface chemistry, if a surfactant (cationic, anionic, or nonionic) can be found to form aggregates on the substrate of interest. Second, nearly any monomer can be used in admicellar polymerization;[12-19] if hydrophilic monomers were desired organic solvents could be used. Third, the size of the polymer is much smaller than the size of the template, which gives the opportunity for very small polymer nanostructures. In fact, as shown in Figure 3.7, it is possible to control this distance by changing the surfactant chain length. Using an alkyl surfactant with eight hydrophobic units instead of twelve allows for the polymer to fit underneath the spheres and form the honeycomb pattern with the expected parabolic wall height vs. position, instead of the pillars shown in Figure 3.2a and 3.2b. The high sensitivity of TAAP with surfactant chain length is attributed to the existence of a critical number of hydrophobic units in the surfactant molecule, which controls the surface-induced self-assembly of the surfactant at the solid-aqueous interface as proposed by a number of groups who have studied similar systems.[39-43]

Moreover, for this particular system the critical number of hydrophobic units is expected to be highly dependent on the surface charge of the spheres.

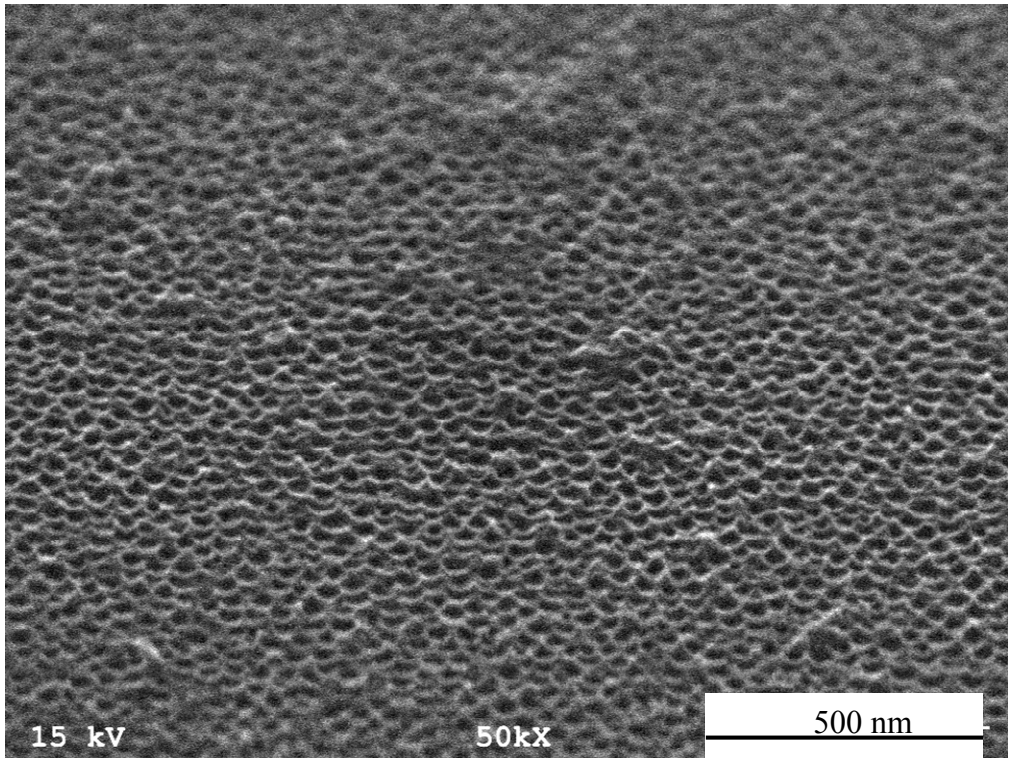

Figure 3.7. Honeycomb pattern produced by synthesis of polyaniline on graphite using 50 nm spheres as template and sodium octyl sulfate as surfactant.

IV. Conclusions

A simple method for fabricating polymeric nanostructures on solid surfaces has been reported. The method employs the interstitial sites of a 2-D self-assembled crystal of latex spheres. The size and shape (honeycomb vs. pillars) of the nanostructures formed was dependent upon the size of the spheres utilized and the method of polymer deposition. The fact that this method could be utilized to form nanoscale structures of both protein and conducting polymers suggests that this is a generic patterning technique which could be extended to a number of substrates and polymers.

V. References

1 Garno, J.C.; Amro, N.A; Wadu-Mesthrige, K.; Liu, G.Y. *Langmuir* **2002**, 18, 8186.

2 Han, S.; Briseno, A.L.; Shi, X., Mah, D.A.; Zhou, F. *J. Phys. Chem. B* **2002**, 106, 6465.

3 Cassagneau, T.; Caruso, F. *Adv. Mater.* **2002**, *14*, 1837.

4 Park, K.H.; Lee, S.; Koh, K.H.; Lacerda, R.; Teo, K.B.K.; Milne W.I. *J. Appl. Phys.* **2005***,* 97, Art. No. 024311

5 Kuo, C.W.; Shiu;,J.Y.; Chen, P. *Chem. Mater.* **2003,** *15,* 2917.

6 Weekes, S.M.; Ogrin F.Y.; Murray, W.A. *Langmuir* **2004**, *20*, 11208.

7 Segalman, R.A. *Matl. Sci. Eng. R-Reports* **2005,** *48*, 191.

8 Goran, M.; Lennox, R.B. *Nano Letters* **2001**, *1*, 735.

9 Seo, I.; Pyo, M.; Cho, G.J. *Langmuir* **2002**, *18*, 7253.

10 Thurn-Albrecht, T.; Schotter, J.; Kastle, C.A.; Emley, N.; Shibauchi, T.; Krusin-Elbaum, L.; Guarini, L.; Black, C.T.; Tuominen, M.T.; Russell, T.P. *Science* **2000**, *276*, 2126.

11 Park, M.; Harrison, C.; Chaikin, P.M.; Register, R.A.; Adamson, D.H. *Science* **1997**, *276,* 1401.

12 Wu, J., Harwell, J. H., and O'Rear, E. A. Langmuir 1987, 3, 531.

13 Matarredona, O.M., Mach, K., Rieger, M.M., and O'Rear, E.A. *Corrosion Science* **2003**, 45, 2541.

14 Buofi, S., and Gandini, A. *Cellulose* **2002**, 00, 1.

15 Le, D.V., Kendrick, M.M., and O'Rear, E.A. *Langmuir* **2004**, 20, 7802.

16 Castano, H., O'Rear, E.A., McFetridge, P.S., and Sikavitsas, V.I. *Macromol. Biosci.* **2004**, 4, 785.

17 Yuan, W-L., O'Rear, E.A., Grady, B.P., and Glatshofer, D.T. *Langmuir* **2002**, 18, 3343.

18 Dong, J., and Mao, G. *Colloid Polym. Sci.* **2005**, 284, 340.

19 Salgaonkar, L.P., and Jayaram, R.V. *J. Colloid and Interf. Sci.* **2005**, 291, 92.

20 Kuramoto, N., and Genie, E. M. *Synthetic Metals* **1995**, 68, 191.

21 Funkhouser, G. P., Arevalo, M. P., Glatzhofer, D. T., and O'Rear, E. A. *Langmuir* **1995**, 11, 1443.

22 Kitiyanan, B., O'Haver, J. H., Harwell, J. H., and Osuwan, S. *Langmuir* **1996**, 12, 2162.

23 Wu, J., Harwell, J. H., and O'Rear, E.A. *J. Phys. Chem.* **1987**, 91, 623.

24 Kim, B-J., Oh, S-G., Han, M-G., and Im, S-S. *Langmuir* **2000**, 16, 5841.

25 Haba, Y., Segal, E., Narkis, M., Titelman, G. I., and Siegmann, A. *Synthetic Metals* **1999**, 106, 59.

26 Kim, B-J., Oh, S-G., Han, M-G., and Im, S-S. *Synthetic Metals* **2001**, 122, 297.

27 Wanless, E.J, and Ducker, W.A. *J. Phys. Chem.* **1996**, 100, 3207.

28 Brash, J. L., and ten Hove, P. *Thromb Haemost* **1984** 51, 326.

29 Lee, S. H., Ruckenstein, E. *J. Colloid Interface Sci.* **1988**, *125*, 365.

30 Norde, W., and Fabier, J. P. *Colloids Surf.* **1992**, 64, 87.

31 Schaaf, P., Dejardin, P., Johner, A., and Schmitt, A. *Langmuir* **1992**, 8, 514.

32 (a) Kim, B. J.; Oh, S. G.; Han, M. G.; Im, S. S. *Langmuir* **2000**, 16, 5841. (b) Kang, E. T.; Neoh, K. G.; Tan, T. C.; Khor, C. S. H.; Tan, K. L. *Macromolecules* **1990**, 23, 2918.

33 Han, M. G.; Cho, S. K.; Oh, S. G.; Im, S. S. *Synth. Met.* **2002**, 126, 53.

34 0.155*sphere diameter is the largest sphere that can fit within the interstitial sites of hexagonally packed spheres.

35 Seitz, R.; Brings, R.; Geiger R. *Appl. Surf. Sci.* **2005**, 252, 154.

36 He, L.; Niemeyer, B. *Biotech. Prog*. **2003**, 19, 5444.

37 Cser, L.; Gladkikh, I.; Kozlov, A.; Nezlin, R.; Ogievetskaya, M.; Ostanevich, Y. *FEBS Letters* **1981**, 259, 635.

38 Patel, K.; Marquez, M.; Grady, B.P.; Schmidtke, D.W.; to be submitted.

39 Tiberg, F., Brinck, J., and Grant, L. *Current Opinion in Colloid and Interf. Sci.* **2000**, 4, 411.

40 Grant, L.M., and Ducker, W.A. *J. Phys. Chem. B* **1997**, 101, 5337.

41 Patrick, H.N., Warr, G.G., Manne, S., and Aksay, I.A. *Langmuir* **1997**, 13,

4349.

42 Grant, L.M., Tiberg, F., and Ducker, W.A. *J. Phys. Chem. B* **1998**, 102, 4288.

43 Holland, N.B., Ruegsegger, M., and Marchant, R.E. *Langmuir* **1998**, 14, 2790.

Chapter 4. Factors Affecting the Synthesis of Polymeric Nanostructures from Template Assisted Admicellar Polymerization

I. Introduction

The ability to engineer surfaces, and more precisely, to create chemical patterns at the nanometer scale with high accuracy and reproducibility has inspired a great research effort in the past few years because of the number of potential applications in the fields of chemistry,[1-3] catalysis, [4,5] biotechnology,[6-11] medical diagnosis,[12,13] and microelectronics.[14-17] As discussed in chapter 1, a number of methods are capable of forming sub-micron and nanometer size polymeric structures on a surface. The most industrial important of these is photolithography, and its related analogues, x-ray or e-beam lithography.[18-20] Other methods include micro-contact printing,[21] step-and-flash imprint lithography,[22] molecular self-assembly,[23-27] dip-pen[28] and scanning probe nanolithography (SPL)[29]. One benefit of these techniques is the ability to create very small feature sizes in complex shapes and arrays, with high-fidelity of reproduction. However, major drawbacks are the high cost of the equipment and the need for highly skilled personnel, as well as the long processing times (sometimes tens to thousands of hours depending on the process and application).

As demonstrated in chapter 3, template assisted admicellar polymerization (TAAP), a technique that relies on the use of surfactant aggregates adsorbed on a surface to concentrate monomer at the surface prior to polymerization, not only is facile and inexpensive, but also has the advantage that patterns with dimensions significantly smaller than the original template can be transferred over large areas (i.e. in the order of cm^2) of the substrate with relatively few defects. In particular, chapter 3 discusses template assisted admicellar polymerization of nanometer-scale polyaniline (PANI) pillars and honeycombs on highly ordered pyrolytic graphite (HOPG), and compares the resulting nanostructures with similar patterns formed via polymer adsorption. The separation distance between the nanostructure and the sphere template is explained in terms of the role of sphere-surfactant interactions in forming nanostructures significantly smaller than the original template. This current chapter is aimed at providing a better understanding of the factors affecting the synthesis of polymeric nanostructures from TAAP for three different monomers: aniline, pyrrole and methyl methacrylate, and three different surfaces: highly ordered pyrolytic graphite (HOPG), gold, and SiO_2. Among the parameters discussed are the effect of monomer and surfactant concentration, surfactant chain length, polymerization time and temperature, and solution ionic strength.

Previous publications such as the work by Chang and Wu on chemically synthesized PANI films on indium tin oxide substrates,[30] and Zhang et al.[31] on

the synthesis of polypyrrole nanostructures in solution (not surface-bounded) have discussed some of these effects. Lekpittaya et al. have also addressed the effects of polymerization media on the preparation of conductive polymer-coated fabrics via admicellar polymerization for three different monomers: aniline, pyrrole and thiophene.[32] However, none of these publications dealt with the formation of highly ordered nanostructures on templated substrates. This chapter demonstrates that control of the TAAP process allows the synthesis of different nanostructures, including polymer nanopillars, nanorings, "honeytubes" and honeycomb-type structures on various substrates.

II. Experimental

Materials. A 2.5 wt% aqueous dispersion of monodispersed polystyrene latex spheres, 504 nm in diameter, stabilized with a slight anionic charge from surface sulfate groups was purchased from Alfa Aesar. Pyrrole (Aldrich, 98%) was purified by passing through an activated alumina column at least 2 times before use. Aniline (Aldrich, 99%) was distilled under reduced pressure. The inhibitor was removed from methyl methacrylate (Aldrich, 99%) by passing the monomer several times through a column packed with hydroquinone monoethyl ether (MEHO)/ hydroquinone (HQ) inhibitor remover (Aldrich). All monomers were

kept cool in the dark before use. Hydrochloric acid, tri-n-octylphosphine oxide (TOPO, 98%), aniline hydrochloride (AnHCl, and sodium chloride were purchased from Merk. Ammonium peroxydisulfate (APS, 98%), sodium octyl sulfate (C8-sulfate, 98%), sodium decyl sulfate (C10-sulfate, 98%), and sodium dodecyl sulfate (SDS, 98%) were from Aldrich. Alkyl sulfate surfactants were recrystallized from ethanol prior to use. Sodium octanesulfonate (C8-sulfonate, 99%), sodium decanesulfonate (C10-sulfonate, 99%), and sodium dodecanesulfonate (SDSn, 99%) were from Avocado Research Chemicals Ltd. Highly-Ordered Pyrolytic Graphite (HOPG), monochromator ZYB grade (5 mm x 5 mm sheets) was purchased from Advanced Ceramics, and used freshly cleaved. Thermally oxidized silicon (SiO_2) wafers were kindly supplied by the Center for Nanophase Material Science at Oak Ridge National Laboratory, and used as received. Gold substrates were prepared in a two-step process: First, thin glass slides (13 mm in diameter) were thoroughly cleaned with soap, chromic acid, and methanol, and subsequently rinsed with double deionized (DI) water following each washing step. Clean glass slides were dried and stored separately in a dry container. In the second step, the glass slides were sputter-coated with a 30 nm chromium layer followed by a 100 nm gold layer.

Substrate Masking. Nanosphere lithography has been chosen because it provides a simple, relatively inexpensive, yet effective method for templating small structures, with the advantage that feature size can be easily changed by changing

the sphere size. In this work, a slight variation of the Langmuir-Blodgett (LB) technique has been used to produce well-ordered monolayers of latex spheres (500 nm in diameter) on a surface by allowing the particles to self-assemble at the air-liquid interface in the presence of a spreading agent (in this case SDS surfactant), and then transferring the monolayer to the substrate of interest through a simple dip-coating process. More details on this process can be found in chapter 2.

In the case of thermally oxidized SiO_2 wafers, enhanced sphere monolayer coverage was achieved by precoating the substrate with a monolayer of the hydrophobic agent tri-n-octylphosphine oxide (TOPO). Gold-coated glass slides were precoated with a monolayer of SDS to improve sphere wetting in order to render more uniform colloidal latex monolayers. In order to avoid premature lift-off of the spheres during the admicellar polymerization step, a stronger adhesion between the latex spheres and the substrate was achieved through a heat treatment at 100^{o}C (the Tg of PS latex colloids is ca. 90^{o}C) for 5 min. The heat-treated, templated substrates were cooled prior to the surfactant adsorption and polymerization. It is important to point out that surface preconditioning is not expected to interfere with surfactant adsorption during the admicellar polymerization step.

Admicellar Polymerization. The general sample preparation procedure is relatively simple; in a typical experiment the templated substrate is contacted with

5 mL of the monomer/surfactant solution for 6h (adsolubilization period). Upon addition of 100 uL of the initiator solution (5.4 mM APS), the sample is allowed to polymerize for 12h (except for those experiments in which the effect of polymerization time is evaluated for time periods ranging from 6h to 48h). At the end of the polymerization, excess monomer and surfactant are rinsed off with DI water, and the template is removed by dissolution in toluene for 7 days. All samples are kept in a desiccator until further characterization. The details of individual experimental subsets are described below.

To study the effect of monomer concentration on the morphology of polypyrrole nanostructures synthesized on HOPG, aqueous solutions of pyrrole/C12-sulfonate with a fixed surfactant concentration of 5.4 mM (equivalent to 45 % of the CMC with no monomer present), and varying monomer concentrations corresponding to a 1:1 and 1:2 monomer:surfactant ratio were prepared. Another set of experiments was designed in which the pyrrole concentration was fixed at 2.7 mM and the effect of surfactant chain length was evaluated for a series of sodium alkyl sulfonate surfactants. In the first case, the surfactant concentration was fixed to 5.4 mM, which corresponds to 4 %, 13 %, and 45 % of the CMC of the C8, C10, and C12-sulfonate surfactants, respectively. For the second case, the surfactant concentration was increased to 45 % of the CMC for each surfactant system. The third case evaluated the effect of increasing

the solution ionic strength by adding 1 mM NaCl to each sulfonate system, while keeping the surfactant concentration at 45 % of the CMC.

The effect of polymerization time on the morphology of PANI structures on HOPG was evaluated by preparing a series of 5.4 mM aniline/SDS solutions (pH = 2), and polymerizing at room temperature for different periods of time in the range of 6h to 48h. Another experiment was designed to evaluate the effect of temperature on TAAP. In this respect, PANI nanostructures with different morphologies (nanorings and nanopillars) were synthesized on three different substrates (HOPG, gold-coated glass, and thermally oxidized SiO_2 wafers) via low temperature (i.e. 16^{o}C) TAAP of a 5.4 mM AnHCl/SDS solution for 12h. In this case, the choice of AnHCl instead of aniline was to ensure equimolar concentrations of anilium and chlorine ions in solution. Note also that the Kraft temperature of the surfactant (16^{o}C for SDS), is in principle the lowest temperature at which the admicellar polymerization could be carried out without surfactant precipitation; however, this point is arguable since it is well known that in the presence of organic impurities (in this case aniline monomer), the Kraft point may be shifted toward lower temperatures. In any case, none of the samples polymerized at 16^{o}C showed evidence of precipitate formation, thus confirming the fact that all the surfactant was either in solution or adsorbed at the solid-liquid interface.

Polyaniline and polypyrrole honeycomb-type structures were also synthesized on gold-coated glass and silicon wafers via room temperature TAAP of 5.4mM AnHCl/SDS, and 2.7 mM pyrrole/5.4 mM C12-sulfonate solutions, respectively. Three different samples were prepared for each monomer/surfactant system: SiO_2 wafer with and without surface pretreatment, and SDS-precoated gold-coated glass. The adsolubilization and polymerization periods were 6h and 12 h, respectively.

Non-conducting PMMA nanostructures were prepared via room temperature TAAP of a 5.4 mM MMA/SDS solution on various substrates including HOPG (both thermally treated and untreated), as well as gold-coated glass and SiO_2 wafers precoated with a monolayer of SDS and TOPO, respectively. All samples, except the untreated HOPG substrate, were subjected to a thermal treatment for 5 min at 100^oC to improved adhesion of latex spheres to the substrate prior to the polymerization.

Finally, multiple TAAP's were carried out on different substrates. A total of four different samples were prepared: The first sample consisted of a PANI honeycomb prepared via TAAP of a 5.4 mM AnHCl/SDS solution on a gold-coated glass slide precoated with a monolayer of SDS as described previously. The sample was let to dry for 1 day, and then it was subjected to a second admicellar polymerization, for which a solution of 2.7 mM pyrrole/C12-sulfonate was used instead. The second sample was prepared according to the procedure

described above, but HOPG (no surface pretreatment) was used as the substrate instead of gold-coated glass. The third sample resembles the first sample in the sense that gold-coated glass was chosen as the substrate, but the order in which the monomer were polymerized changed: first a Ppy honeycomb was formed on the substrate, and then the admicellar polymerization of aniline was carried out in the final step. For the last sample, a nonconducting PMMA honeycomb was formed on HOPG via TAAP of a 5.4 mM MMA/SDS solution. Then, PANI and Ppy layers were subsequently admicellar polymerized on top on the substrate containing the PMMA honeycomb (first PANI and then Ppy). All samples were subjected to a 6h adsolubilization period, followed by polymerization for 12h at room temperature. Where the polymer formed, e.g. in the holes of the honeycomb or on top of the honeycomb depends on where surfactant adsorbs and will be discussed in the Results and Discussion section.

Instrumentation. Scanning electron microscopy (SEM) imaging of polymeric nanostructures on various substrates (i.e. HOPG, gold, and SiO_2 wafers) was performed using a field emission scanning electron microscope (SEM, JEOL-6300F, Peabody, MA). The SEM was operated with an accelerating voltage of 15kV. Despite the benefits of sample coating in getting sharper SEM images, no coating was applied to the PANI or poly(pyrrole) samples in order to preserve them for the AC impedance measurements.

Raman spectroscopy was performed using a Jovin Yvon-Horiba Laboratory Raman apparatus equipped with a CCD detector and with three different laser excitation sources having wavelengths of 633 nm (He-Ne laser), 514 nm, and 488 nm (Ar laser). The instrument was operated using Jovin Yvon-Horiba software. All spectra were recorded at 80 scans/min.

AC impedance spectroscopy experiments were performed using a current-sensing AFM (Digital Instruments, Nanoscope IIIa), equipped with a Solartron 1260 gain/phase analyzer and a 1296 electrochemical interface. The procedure involves an AFM cantilever tip (100 nm in diameter, from WiTech), subjected to laser ablation in order to increase its contact area with the substrate, and subsequently coated with gold for enhanced electrical conduction. The final tip diameter after laser ablation is ca. 1 um. The electrically conducting, blunted surface of the AFM tip serves as a contact electrode for measuring the AC impedance response of discrete regions on the sample surface, while keeping the load force between the tip and the surface constant. This method thus provides a convenient way to determine the electrical conductivity through the synthesized polymer nanostructures, in the direction perpendicular to the underlying substrate. AC impedance data collected over a range of 1 Hz to 1 MHz was used to generate the corresponding Nyquist plots (Figure 4.1), in which the imaginary and real values of impedance are plotted as a function of frequency. Conductivity values for each sample were then calculated from Equation 4.1:

$$\sigma = \frac{h_{avg}}{z' A_e} \qquad \text{(Equation 4.1)}$$

Where σ [S/cm] is the conductivity, h_{avg} [cm] is the average film thickness, z' [ohms] is the value of real impedance obtained from the extrapolated intercept with the real axis of the Nyquist plot at high frequencies, and A_e [cm^2] is the effective area of conduction, calculated as the fraction of polymer (F) in contact with the cross sectional area (A_{tip}) of the blunted AFM tip (Equation 4.2). The fraction of polymer was estimated as the fraction of area covered by polymer as determined via SEM images.

$$A_e = A_{tip} F \qquad \text{(Equation 4.2)}$$

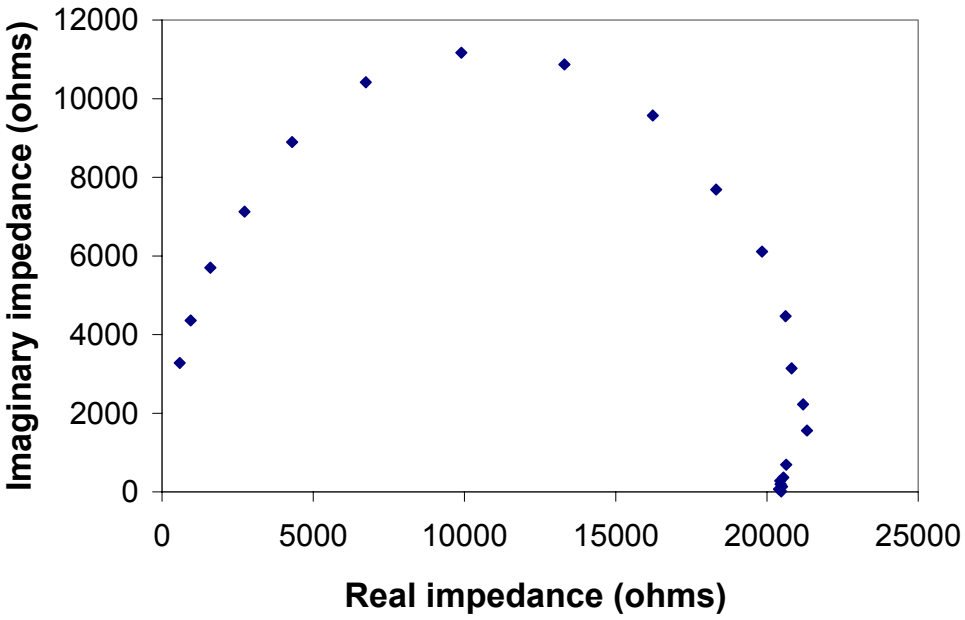

Figure 4.1. Nyquist plot for PANI honeycomb on HOPG.

III. Results and Discussion

Admicelle formation is well known to depend strongly on solution conditions (e.g. ionic strength, pH), surfactant concentration and chain length, presence of solute, and surfactant/substrate interactions, among other factors.[32] For this reason, admicellar polymerization, a process that involves the formation of surfactant surface aggregates to localize monomer to the surface prior to the polymerization, is also expected to be affected by the parameters that influence admicelle formation. Experimental results in this study demonstrate that the morphology and electrical properties of Ppy nanostructures synthesized via

TAAP on HOPG are strongly dependent on the monomer and surfactant concentration, the ionic strength of the solution, and the surfactant chain length.

The effect of monomer concentration was studied for aqueous solutions of pyrrole/C12-sulfonate with a fixed surfactant concentration of 5.4 mM (45% of the CMC), and varying monomer:surfactant ratios of 0.5:1 (Figure 4.2a), 1:1 (Figure 4.2b), and 2:1 (not shown). Comparison of Figures 4.2a and 4.2b indicates that when the surfactant concentration is fixed at 45% of the CMC, doubling the monomer concentration results in excess polymer formed in solution and subsequently precipitated onto the surface. A further increase of the monomer to a 2:1 monomer:surfactant ratio results in higher amounts of precipitated material. This observation seems reasonable when considering the adsolubilization capability of surface-bound surfactant aggregates, also defined as the excess concentration of a species at an interface due to the presence of admicellar aggregates.[33] Although monomer adsolubilization increases with surfactant concentration (up to the CMC)[34] and added electrolyte,[35] the monomer adsolubilization constant K_{ads}, defined as the moles of adsolubilized monomer per mole of adsorbed surfactant relative to the molar concentration of monomer in solution, is nearly independent of monomer concentration in the aqueous phase.[36] This means that for a given surfactant concentration above the critical aggregation concentration (CAC), a finite number of surfactant aggregates form on the surface of the substrate, which in turn sets a limit for the maximum amount of monomer

molecules that can potentially be adsolubilized in the core and/or the palisade regions of the surfactant aggregates. Further, even if the amount of adsolubilized monomer increased with increasing concentration in solution, the effect on the bulk monomer concentration would not be significant, since the surface area of the substrates is so small.

As demonstrated in chapter 3, spheres/surfactant interaction in TAAP strongly affects the morphology of nanostructures synthesized from TAAP, to the extent that either polymer pillars or honeycombs can be formed depending on the sphere/surfactant-monomer/substrate interaction. In this work, we pursued a better understanding of the role of the surfactant in driving the formation of polymer nanostructures via TAAP by studying the effect of surfactant chain length on the morphology of Ppy nanostructures synthesized on HOPG at a fixed pyrrole concentration (i.e. 2.7 mM), utilizing different sodium alkyl sulfonate surfactants with 8, 10, and 12 carbon atoms. Three sets of samples were evaluated: one in which the surfactant concentration was fixed to 5.4 mM, which corresponds to 45% (Figure 4.2a), 13% (Figure 4.2d), and 4% (Figure 4.2g) of the CMC respectively. For the second set of experiments, the admicellar polymerization was carried out at a fixed fraction of the CMC (i.e. 45%), for which the surfactant concentration in Figures 4.2d and 3g had to be increased to 19.4 mM (Figure 4.2e), and 63 mM (Figure 4.2h) for the C10 and C8-sulfonate surfactants, respectively. The last set of samples (Figures 4.2c, 4.2f, and 4.2i) was

designed to evaluate the effect of adding 1 mM NaCl, while keeping the surfactant concentration at 45% of the CMC measured without salt present.

The overall effect of surfactant chain length on the morphology of Ppy nanostructures formed on HOPG can be best appreciated by comparing the SEM images in rows 1, 2, and 3 of Figure 4.2, which correspond to various conditions of admicellar polymerization in the presence of C12, C10, and C8-sulfonate surfactants, respectively. Not surprisingly, the C12-sulfonate surfactant is more effective in driving the formation of honeycomb-type nanostructures compared to the C10 and C8-sulfonates. This observation may be explained in terms of the adsorption efficiencies (determined as the negative log of the equilibrium concentration of the surfactant in the liquid phase at the point of zero charge of the substrate), and CMC values for the series of alkyl sulfonate surfactants reported in Table 4.1. At a given concentration, the C12-sulfonate surfactant (i.e. the surfactant with the longest tail, the lowest CMC, and the higher adsorption efficiency), will have significantly more surfactant adsorbed, resulting in increased monomer adsolubilization capability, and honeycomb structures with less defects as confirmed by comparison of Figures 4.2a, 4.2d, and 4.2g (left column in Figure 4.2). Note the significant amount of irregularly-shaped Ppy on the surface of HOPG (Figure 4.2g), most likely precipitated from solution due to the high tendency of the C8-sulfonate to remain in the bulk, and the smaller size

of the palisade region in C8-sulfonate admicelles, which further limits monomer adsolubilization relative to the C10 and C12-sulfonate surfactants.[37]

If the above discussion regarding the effect of adsorbed surfactant and monomer adsolubilization capability is true, then improvements in the quality of the synthesized nanostructures should be observed when the admicellar polymerization is carried out at a fixed fraction of the CMC for each surfactant system. Indeed, vast improvements are shown when the surfactant concentration in Figures 4.2d and 3g is increased to 19.4 mM (Figure 4.2e), and 63 mM (Figure 4.2h) for the C10 and C8-sulfonate surfactants, respectively. In particular, when the concentration of C10-sulfonate was 13% of the CMC, both honeycomb patches and uncovered regions as shown in Figure 4.2d were observed throughout the surface of sample. When the concentration was raised to 45% of the CMC (Figure 4.e), a well-developed honeycomb sheet partially covered with solution precipitated polymer was observed. From these results it seems that increasing the C10-sulfonate concentration not only boosts admicelle formation as hypothesized, but also favors the competing polymerization in solution reaction. As shown later, salt can be added to favor admicellar polymerization over polymerization in solution. As expected, the effect of increasing the C8-sulfonate concentration from 4% to 45% of the CMC was far more drastic compared to the C10-sulfonate. As discussed earlier, at 4% of the CMC (Figure 4.2g) mostly irregularly-shaped Ppy is observed on the surface of HOPG, but at 45% of the CMC (Figure 4.2h)

honeycomb patches form, indicating the partition of more pyrrole monomer from the bulk to the HOPG surface, almost certainly due to an increase in the number of surfactant surface aggregates. Furthermore, the effect of added salt can be appreciated in Figures 4.2c, 4.2f, and 4.2i, which correspond to admicellar polymerizations carried out in the presence of 1 mM NaCl for C12, C10, and C8-sulfonate concentrations equivalent to 45% of their CMC's. In particular, there is a significant reduction in the amount of precipitated material observed in Figures 4.2f and 4.2i, relative to Figures 4.2e and 4.2h. Although it is true that that more monomer is incorporated into admicellar aggregates as a result of an increase in the monomer adsolubilization constant with added electrolytes as demonstrated by Funkhouser et al, in the percent reduction of monomer in solution is expected to be negligible due to the fact that the amount of monomer on the surface is very small. This effect is likely due to the interference of NaCl with the pyrrole polymerization mechanism in solution.

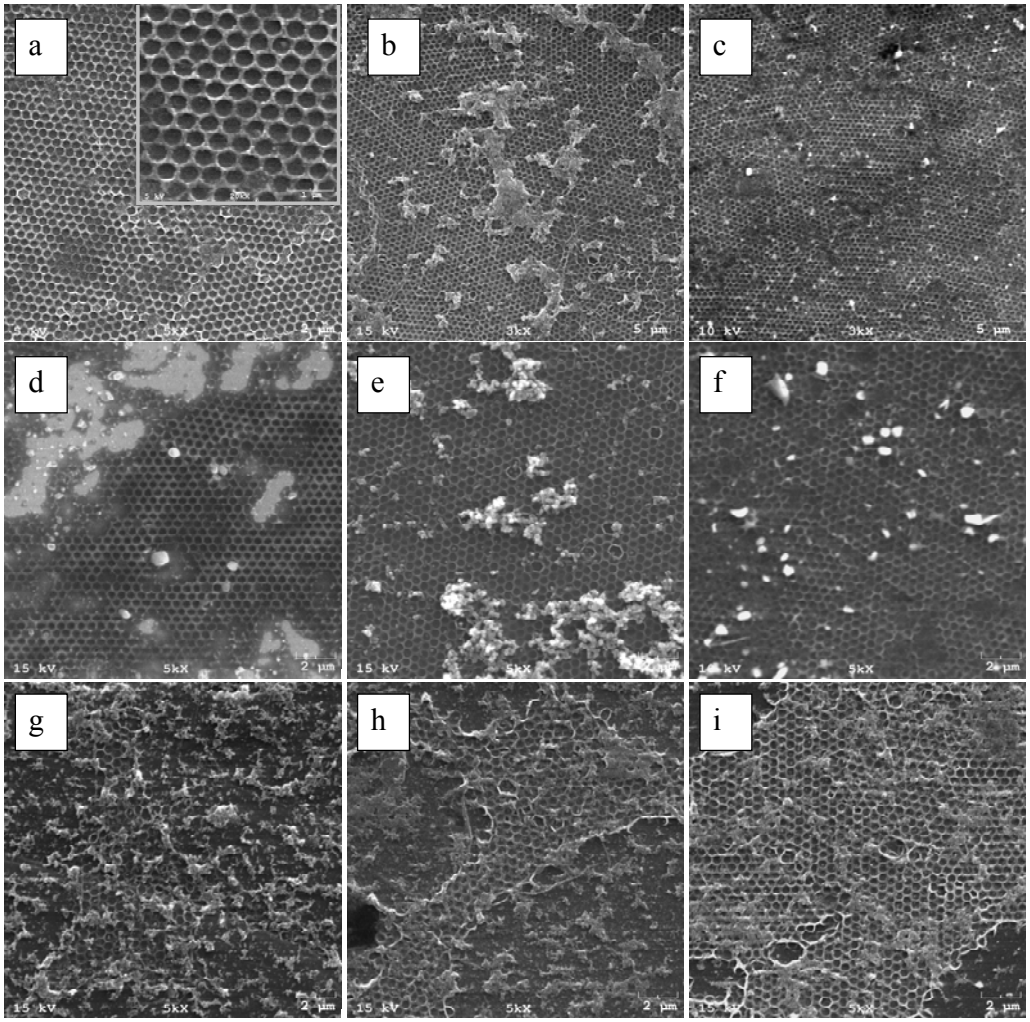

Figure 4.2. TAAP of pyrrole on HOPG substrates previously templated with a monolayer of close-packed latex spheres (500 nm in diameter), under various conditions of polymerization: (a) 2.7 mM pyrrole/5.4 mM C12-sulfonate. The inset in (a) shows a magnified image of the honeycomb structure; (b) 5.4 mM pyrrole/5.4 mM C12-sulfonate (45 % CMC); (c) 2.7 mM pyrrole/5.4 mM C12-sulfonate/1mM NaCl; (d) 2.7 mM pyrrole/5.4 mM C10-sulfonate (13 % CMC); (e) 2.7 mM pyrrole/19.4 mM C10-sulfonate (45 % CMC); (f) 2.7 mM pyrrole/19.4 mM C10-sulfonate/1mM NaCl; (g) 2.7 mM pyrrole/5.4 mM C8-sulfonate (4 % CMC); (h) 2.7 mM pyrrole/63 mM C8-sulfonate (45 % CMC); (i) 2.7 mM pyrrole/63 mM C8-sulfonate/1 mM NaCl. All samples were subjected to a monomer/surfactant adsolubilization period of 6h, followed by 12h admicellar polymerization at room temperature, and template removal.

Table 4.1. Adsorption efficiencies and critical micelle concentrations (CMC) of sodium alkyl surfactants used in this study. Surfactant concentration as a percentage of the CMC for a fixed surfactant concentration of 5.4 mM is also included for comparative purposes.

Sodium Alkyl Surfactant	Adsorption Efficiency[c]	CMC[a]/10^3 M	% of CMC[b]
C8-sulfonate	2.6	140	4
C10-sulfonate	3.8	43	13
C12-sulfonate	4.5	12	45
C8-sulfate	2.3	120	5
C10-sulfate	3.4	33	16
C12-sulfate	4.3	8.2	66

[a] in water at 25°C

[b] for a 5.4 mM surfactant solution

[c] On silver iodide at 20 ± 2°C, pH = 3, and total ionic strength = 1mM.[38]

Based on previous results for the synthesis of PANI nanostructures on HOPG (chapter 3), and the information reported in Table 4.1 for a series of alkyl sulfate surfactants, which correlates well with the trend observed for the adsorption efficiency and CMC values of alkyl sulfonate surfactants employed for the synthesis of Ppy nanostructures on HOPG; a experiment was designed to evaluate the effect of varying the polymerization time from 6h to 48h on the morphology of PANI nanostructures synthesized via TAAP of a 5.4 mM aniline/SDS solution (pH = 2) on HOPG substrates. As seen in Figure 4.3a, after

6h of polymerization the substrate is mainly covered by incipient honeycomb structures, thus indicating that the polymerization time was not long enough to allow sufficient monomer partition from solution to the unmasked sites on the substrate surface. This observation is further confirmed by the relatively shallow heights (ca. 45-60 nm) measured from the 45^{o} tilt view shown in the inset in Figure 4.3a. On the other hand, fully developed honeycomb structures (80 nm in height), with few defects are characteristically observed for samples polymerized for 12 h (Figure 4.3b). When the polymerization is let to proceed for 24 h, patches of fibrillar PANI form on top of a honeycomb layer as seen in Figure 4.3c. As the polymerization is allowed to proceed for even longer times (i.e. 48h), fibrillar PANI takes over the surface, completely burying the underlying honeycomb structure (Figure 4.3d). From these results, it seems that 12 h is the optimum time to completely fill the uncovered sites of the masked HOPG substrate without over saturating the surface with excess polymer. An additional comment can be made regarding the fibrillar morphology of the excess PANI in Figures 4.3c and 4.3d, which is likely the result of solution conditions significantly changing over time, thus affecting the morphology of the polymer formed in solution. In this respect, it is important to point out that the oxidative polymerization of aniline at surfaces has been found to precede the precipitation polymerization in the bulk volume of the aqueous phase due to the heterogeneous catalysis of the PANI-chain initiation afforded by a surface.[39,40] This explains why significant changes in the

morphology of PANI formed in solution are observed particularly at longer polymerization times.

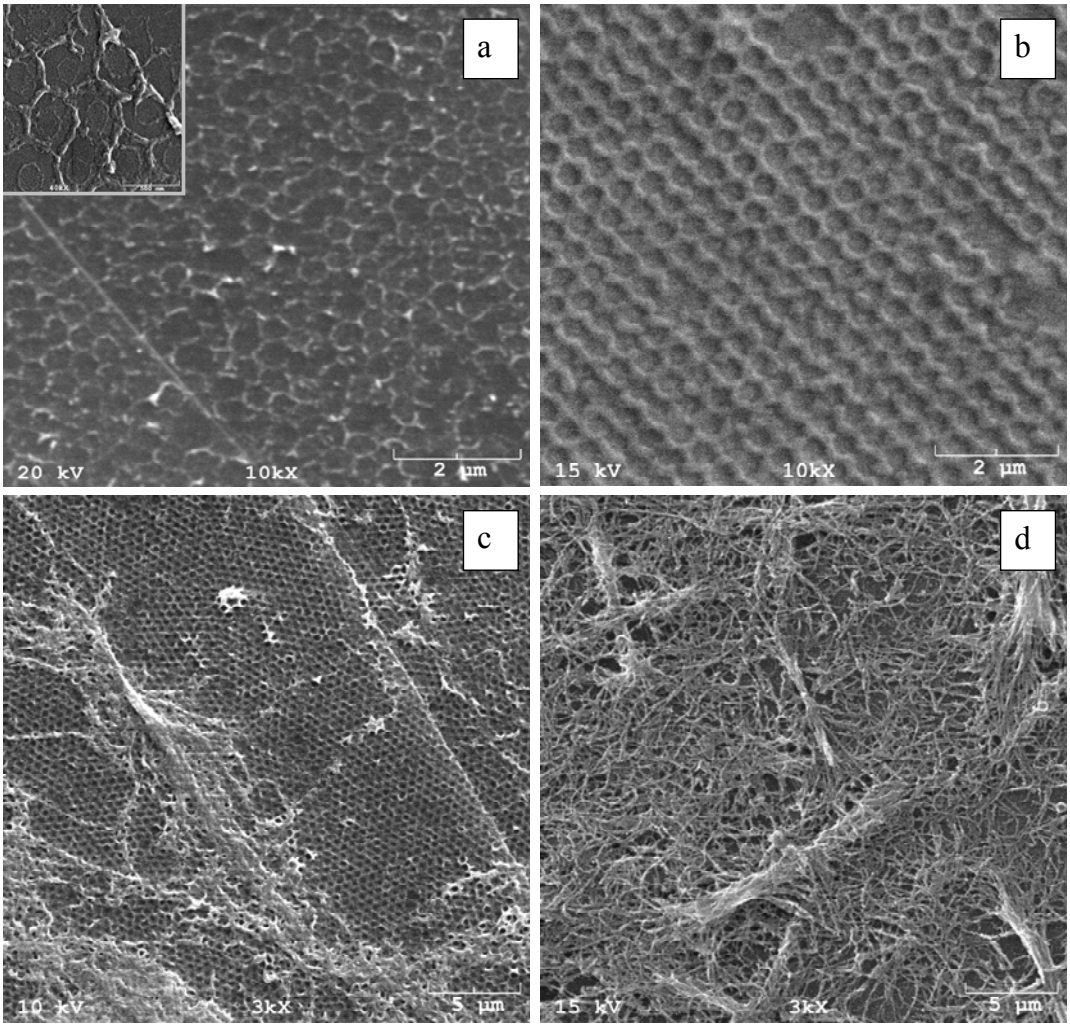

Figure 4.3. Effect of polymerization time on the morphology of PANI structures on HOPG prepared via TAAP of 5.4 mM aniline/SDS (pH = 2), at room temperature for: (a) 6h, (b) 12h, and (c) 24h, and (d) 48h. The inset in (a) shows the tilt view (45^{o}) of the incipient honeycomb structured formed after 6h of polymerization. All samples were subjected to a monomer/surfactant adsolubilization period of 6h. Images shown are after template removal in toluene.

In order to evaluate the effect of temperature on the morphology of PANI nanostructures synthesized from TAAP, the polymerization time was fixed at 12 h (i.e. the optimum time for the formation of PANI honeycombs with fewest defects on HOPG) and the polymerization was carried out at 16^{o}C (i.e. the Krafft temperature of SDS). The rationale for conducting the TAAP at the Krafft temperature of the surfactant was two-fold: to slightly increase SDS adsorption to the uncovered areas of HOPG,[41] and to regulate monomer partition from the bulk to the HOPG surface, thus providing an additional avenue to control the morphology of nanostructures prepared via TAAP. As shown in Figure 4.4, PANI nanostructures with different morphologies (nanopillars, nanorings) can be formed on various substrates (HOPG, gold-coated glass, and thermally oxidized SiO_2 wafers) via TAAP of a 5.4 mM AnHCl/SDS solution at 16^{o}C (Figures 4.4a-c). In order to explain these results it is necessary to take into consideration the water solubility and diffusion rate of aniline hydrochloride (AnHCl) as a function of temperature. As with most salts, the solubility of AnHCl increases with temperature (88.36 g and 107.35 g AnHCl/100 g H_2O at 15^{o}C and 25^{o}C, respectively),[42] hence monomer adsolubilization (a measure of monomer partition into admicellar aggregates) is expected to increase as the solubility of AnHCl in water is decreased at lower temperatures. Therefore at 16^{o}C, monomer molecules are more readily availability initially at the surface to form honeycomb structures.

However, both monomer diffusion and the rate of polymerization can be significantly slowed down at low temperatures. As a matter of fact, the diffusion rate of aniline,[43] and the rate of PANI growth via electrochemical polymerization[44] have been found to decrease 1.5% and 10% per °C reduction, respectively. As a result, interstitial PANI nanopillars as those observed on SiO_2 substrates (Figure 4.4c) are more likely to be formed at low temperatures because of a higher probability for the anilinium cation to partition to the center of interstitial sites, the loci with the lowest restriction to monomer flow. On the other hand, PANI nanorings observed on HOPG (Figure 4.4a), and gold-coated glass (Figure 4.4b), may be the result of a stronger interaction with the substrate, which can potentially drive the monomer from the interstices to the area where the sphere contacts the substrate via capillary forces.[45] As a final remark to emphasize the variations in morphology, the formation of PANI "honeytubes" occurs via rapid quenching of a sample that had been polymerized at room temperature which causes the PANI honeycomb sheet to roll up. Similar polymer "honeytubes" were previously reported in chapter 3.

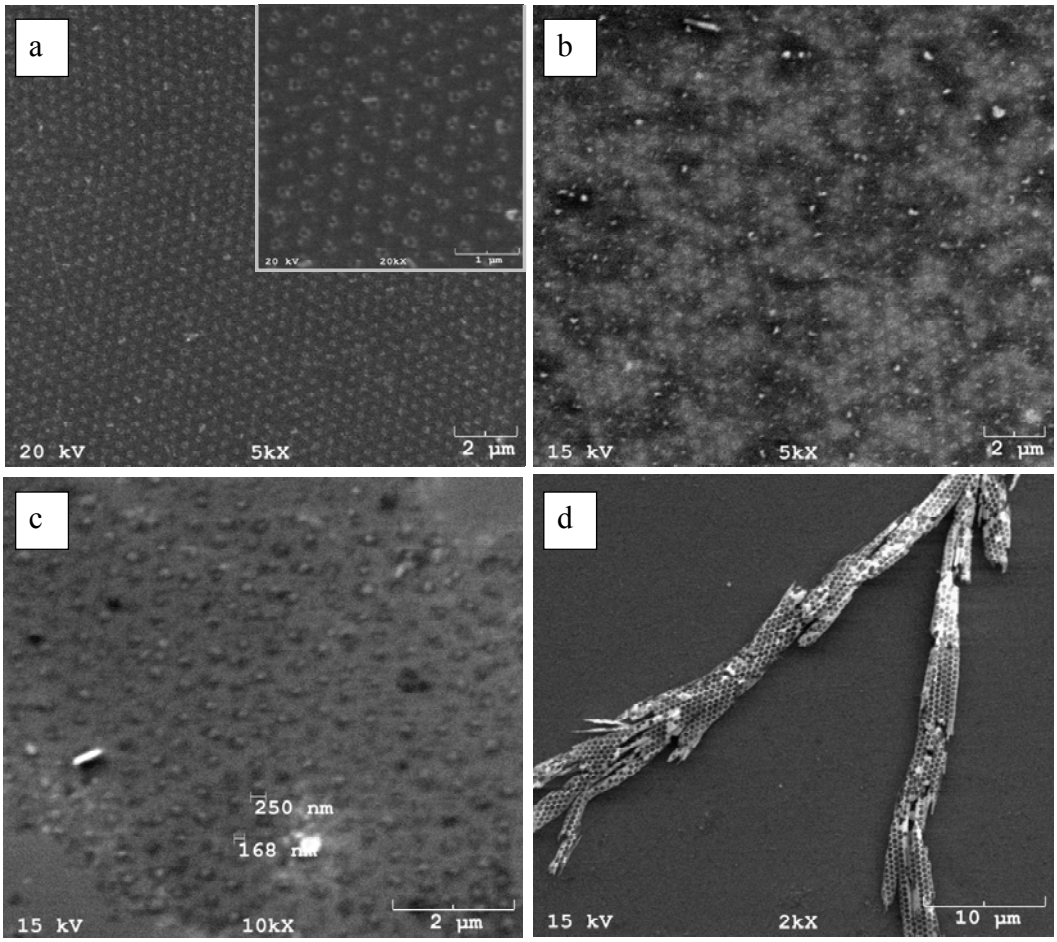

Figure 4.4. Temperature-controlled PANI morphologies (nanorings, nanopillars and "honeytubes") synthesized via TAAP of a 5.4 mM aniline/SDS solution (pH = 2), at 16^{o}C on various substrates: (a) PANI nanorings on HOPG. The inset in (a) shows a magnified image of the nanorings. (b) PANI nanorings on gold-coated glass. (c) PANI nanopillars on SiO_2, and (d) PANI "honeytubes" on SiO_2 obtained by rapidly quenching a sample that had been polymerized at room temperature. The adsolubilization and polymerization periods were 6h and 12 h, respectively. Images shown are after template removal in toluene.

As seen in Figure 4.5, PANI and Ppy honeycomb structures can also be synthesized on gold-coated glass and silicon wafers via room temperature TAAP of 5.4mM AnHCl/SDS, and 2.7 mM pyrrole/5.4 mM C12-sulfonate solutions,

respectively. In order to evaluate the effect of the hydrophobic/hydrophilic nature of the substrate, three different samples were prepared for each monomer/surfactant system: the first sample was a templated SiO_2 wafer without surface pretreatment (Figures 4.5a and 4.5d), the second was also a SiO_2 wafer coated with a monolayer of TOPO prior to the deposition of the PS latex spheres, and subsequently subjected to a heat treatment for 5 min at 100^{o}C to improve the adhesion of the latex spheres to the substrate, thus avoiding premature sphere lift-off during admicellar polymerization (Figures 4.5b and 4.5e). The third sample was a gold-coated glass slide precoated with a monolayer of SDS surfactant prior to sphere deposition, and subsequently subjected to the same heat treatment described above (Figures 4.5c and 4.5f). As observed in Figures 4.5a and 4.5d, neither PANI nor Ppy high a strong affinity with the untreated SiO_2 substrates. As a matter of fact, PANI seems to have a slightly higher tendency to form honeycomb-type structures on untreated SiO_2 compared to Ppy, possibly due to the fact that the admicellar polymerization of aniline, unlike that of pyrrole, is carried out under strong acidic conditions (pH = 2). Since the pzc of silicon oxide is between pH 2.5 and 3.0,[46] at the conditions of polymerization of aniline the SiO_2 is positively charged, which in turn may explain why the latex spheres (bearing sulfate groups on the surface) seem to be less susceptible to desorption during the polymerization step. The effect of precoating and thermally treating the substrates can be appreciated by comparison of Figures 4.5a and 4.5b (PANI), and

4.5d and 4.5e (Ppy). From these results it is evident that premature sphere lift off during the admicellar polymerization step has been significantly reduced by: 1) rendering the substrate's surface more hydrophobic through the precoating step, 2) minimizing sphere surface charge nonhomogeneity by annealing,[47] and 3) increasing the mechanical adhesion between the spheres surface and the substrate by partially softening a fraction of the outer layer of the spheres, thus creating a "sticky" effect as in adhesive tapes.

Despite the obvious improvements attained from surface preconditioning of both gold-coated glass and SiO_2 wafers, HOPG seems to be, in general, the best choice of substrate for TAAP. Similar results have been found by Carswell on the synthesis of electrically conducting polymers via the use of adsorbed surfactant aggregates.[48] A possible explanation as to why TAAP seems to work best on HOPG substrates may be provided by considering the mechanism of admicelle formation at the graphite-water interface. As in the case of micellar aggregates in solution, the formation of surface-bounded surfactant aggregates is known to be driven by hydrophobic interactions. In particular, the formation of half-cylindrical surfactant aggregates at the graphite-aqueous solution interface has been shown to be templated by an ordered monolayer in which the surfactant molecules are disposed parallel to the graphite basal plane. Beyond a critical alkyl chain length, the ordered monolayer is so stable that surfactant adsorption becomes effectively irreversible.[49] This would explain not only why

nanostructures of better quality are obtained on HOPG compared to other substrates such as glass-coated glass and SiO_2, but also why the C12-sulfonate performed better than the C10 and C8-sulfonates in the study of the effect of varying the surfactant alkyl chain length on the morphology of Ppy nanostructures synthesized via TAAP on HOPG.

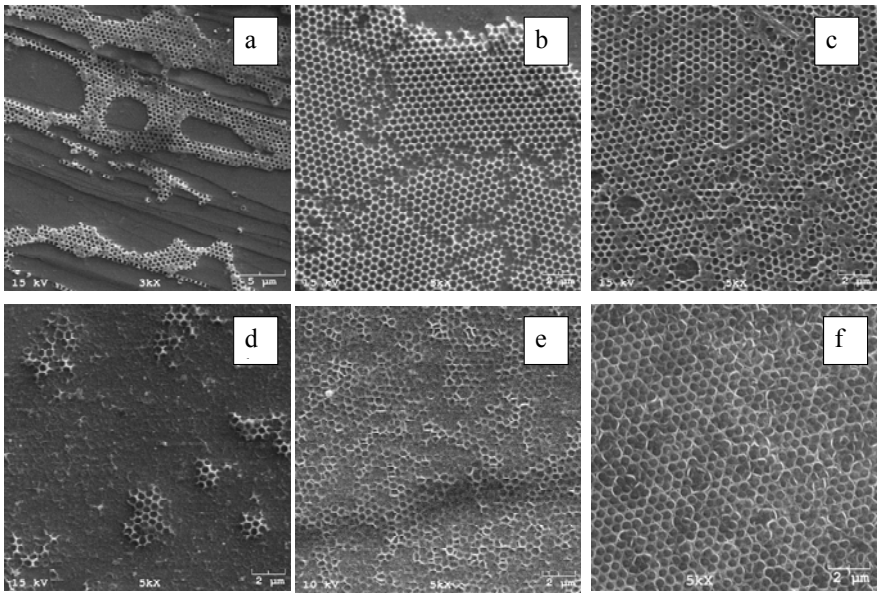

Figure 4.5. TAAP of aniline and pyrrole monomers on different substrates: (a) Low surface coverage PANI honeycombs on SiO_2 without surface pretreatment. (b) PANI honeycomb on SiO_2 precoated with a monolayer of TOPO. (c) PANI honeycomb on gold-coated glass precoated with a monolayer of SDS surfactant. (d) Ppy honeycombs on SiO_2 without surface pretreatment. (e) Ppy honeycomb on SiO_2 precoated with a monolayer of TOPO. (f) Ppy honeycomb on gold-coated glass precoated with a monolayer of SDS surfactant. PANI and Ppy samples were prepared from 5.4mM AnHCl/SDS, and 2.7 mM pyrrole/5.4 mM C12-sulfonate solutions respectively. All samples were subjected to a 6h adsolubilization period, followed by polymerization for 12h at room temperature, and template removal by dissolution in toluene.

In addition to PANI and Ppy nanostructures, non-conducting PMMA nanostructures were prepared via room temperature TAAP of a 5.4 mM MMA/SDS solution on various substrates including HOPG (both thermally treated and untreated), gold-coated glass, and SiO_2 wafers precoated with a monolayer of SDS and TOPO, respectively (Figure 4.6). All samples, except the untreated HOPG substrate, were subjected to a thermal treatment for 5 min at 100^{o}C to improved adhesion of latex spheres to the substrate prior to the polymerization, thus preventing premature sphere lift-off during the admicellar polymerization step. The effect of surface preconditioning can be appreciated by comparison of Figures 4.6a and 4.6b, which correspond to PMMA nanostructures formed on untreated and preconditioned (SDS precoated and thermally treated) HOPG substrates. The PMMA porous structure with variable pore sizes observed in Figure 4.6a could be an indication that the latex spheres are being pushed off the substrate by the strong affinity between the growing PMMA and the HOPG surface, resulting in template loss and disordered nanostructures. In comparison, the hexagonally ordered, fully-developed PMMA honeycomb shown in Figure 4.6b confirms the effectiveness of the surface pretreatment in keeping the spheres on the substrate until the end of the polymerization step. In this respect, it is important to point out that HOPG preconditioning was never required to preserve the sphere template during the polymerization of less hydrophobic monomers such as pyrrole or aniline. It seems that the growing PMMA nanostructure

reaches out to the contact area between the spheres and the substrate, competing with the latex spheres for adsorption sites on the substrate's surface. As a matter of fact, the thicker walls (ca. 250 nm) observed for PMMA honeycombs on HOPG and gold-coated glass (Figures 4.6b and 4.6c) compared to PANI or Ppy honeycomb walls (ca. 65 nm) confirm the ability of the growing PMMA to penetrate further underneath where the spheres touch, presumably because of a stronger interaction between the MMA monomer and the substrate.

An additional observation can be made regarding the thinner walls (ca. 100 nm) observed for PMMA honeycombs on SiO_2 (Figure 4.6d), compared to those formed on HOPG and gold-coated glass substrates (ca. 250 nm), which may be the result of a weaker interaction between MMA and the TOPO-coated SiO_2 wafer due to the high polarity of the phosphine oxide molecules. Furthermore, this weak interaction may also be the reason for the polymer flow evidenced in the inset in Figure 4.6d. Normally, PMMA would not be expected to flow at room temperature. However, there has been considerable experimental evidence for large reductions in the glass transition temperature (Tg) of PMMA thin films with decreasing film thickness[50] depending on the polymer-substrate interaction.[51,52] Hence, it is possible that at room temperature the thin PMMA honeycomb on SiO_2 may be able to flow, or the high energy SEM electron beam (15 kV) heated the sample enough to enable it to flow; neither could be true for either PANI or PPy. Another possibility is that either unreacted MMA monomer or dissolved PS

from template removal via dissolution in toluene may be the cause for the flow apparent in Figure 4.6d. To test the latter, Raman spectroscopy was conducted on all the PMMA honeycomb samples in Figure 4.6. Unfortunately, only the sample corresponding to the PMMA honeycomb on preconditioned HOPG (the sample with the thicker honeycomb walls-Figure 4.6b) had sufficient signal strength to allow the corresponding spectrum to be recorded (Figure 4.7).

Although the Raman signal recorded for the PMMA honeycomb (ca. 40 nm thick) shown in Figure 4.6b is very weak relative to the strong sp^2 carbon peak observed at 1583 cm^{-1} for HOPG, some characteristic peaks can be identified in the Raman spectrum shown in Figure 4.7. In particular, the peak observed at 1729 cm^{-1} corresponds to the C=O stretching of the C-COO group, while that at 1452 cm^{-1} is attributed to the C-H vibration of the α-CH3 group. The absence of a band at 1639 cm^{-1}, which is typically assigned to the C-C stretching mode of residual MMA monomer, discards the possibility of flow due to either residual MMA or oligomeric PMMA.[53] On the other hand, the assignment of the series of weak bands between 950 cm^{-1} and 1050 cm^{-1} is not trivial, as both PMMA and polystyrene (PS) show characteristic peaks in this region. Nonetheless, the presence of residual PS from the dissolution of latex spheres can also be ruled out due to the absence of a peak around 1600 cm^{-1}, which is characteristically observed in the Raman spectrum of PS samples.

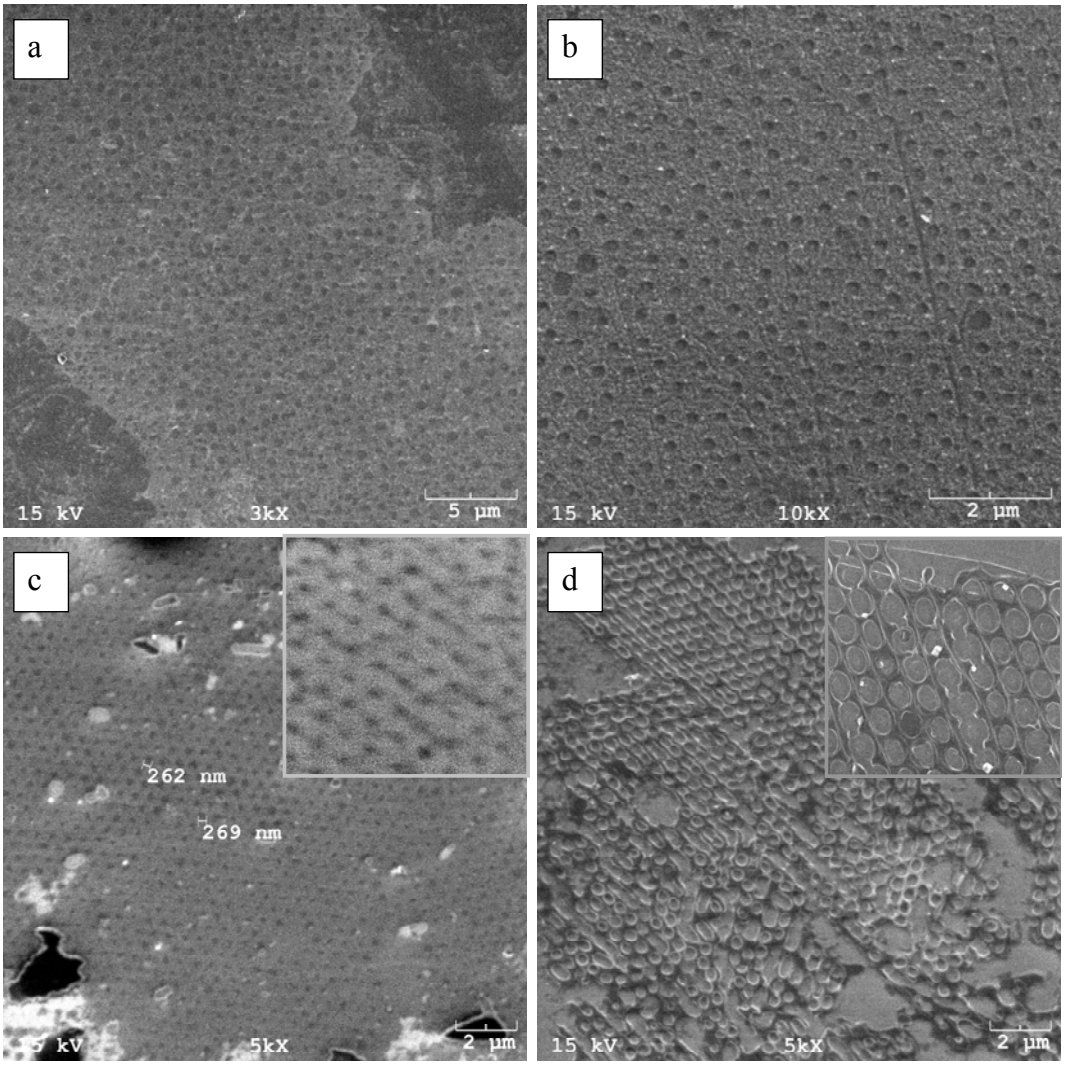

Figure 4.6. Non-conducting PMMA nanostructures prepared via room temperature TAAP of a 5.4 mM MMA/SDS solution on various substrates: (a) HOPG-no heat treatment, (b) HOPG, (c) gold, and (d) SiO_2 thermally treated for 5 min at 100^{o}C to improved adhesion of latex spheres to the substrate prior to the polymerization. The insets in Figures (c) and (d) are zoom images of the corresponding samples. The adsolubilization and polymerization periods were 6h and 12 h, respectively. All images shown are after template removal via dissolution in toluene.

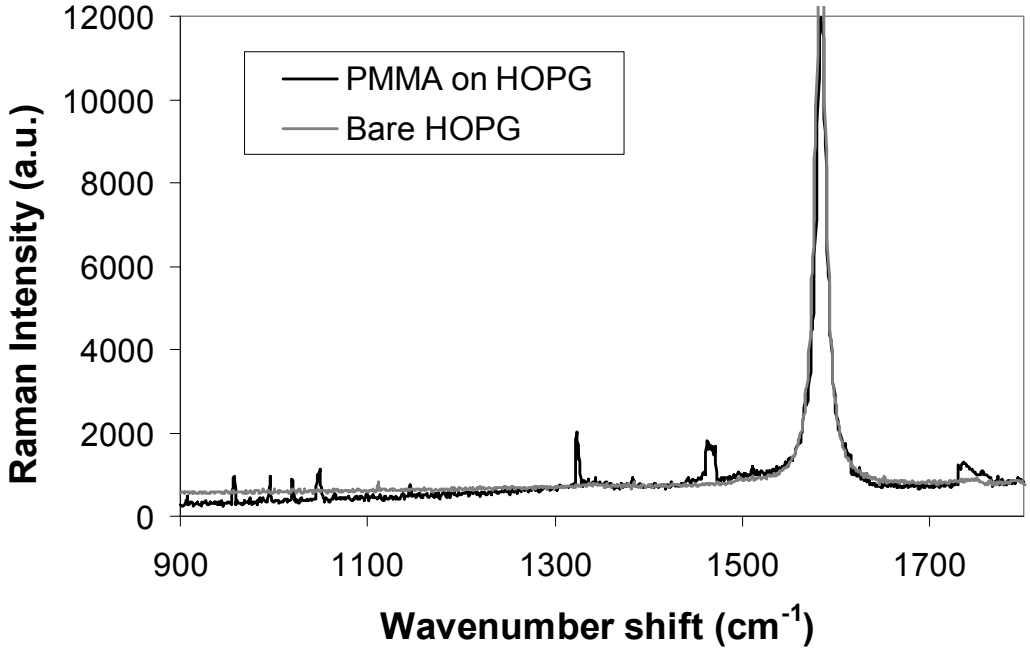

Figure 4.7. Raman spectra of HOPG substrates before (gray line) and after (black line) room temperature TAAP of a 5.4 mM MMA/SDS solution for 12h.

Although the images in Figure 4.8 are the result of preliminary studies, and more work needs to be done in order to find the optimum conditions for multiple TAAP sequences, the micrographs can be used to obtain information concerning the interaction of a given monomer/surfactant pair with the underlying substrate/templated polymer. For instance, the effect of substrate choice on the morphology of the resulting nanostructure can be appreciated by comparison of Figures 4.8a and 4.8b. When HOPG is used as the substrate (Figure 4.8b), the PANI honeycomb will template the growth of the Ppy honeycomb on top, which replicates almost exactly the shape of the underlying PANI honeycomb. If

instead gold-coated glass is used as the substrate, a thin-wall PANI honeycomb forms, and the pattern transfer capability is significantly reduced as evidenced by the top broken Ppy honeycomb patches observed in Figure 4.8a. At this point, we cannot be sure whether this effect is simply a size effect, e.g. the amount of surfactant adsorbed per unit area is inherently less on thinner walls, or a shape effect, i.e. the curvature of thinner walls is greater which in turn reduces surfactant adsorption. A schematic representation of the templating effect of thin vs. wall honeycombs in shown in Figures 4.9a and 4.9b, respectively.

The effect of changing the TAAP sequence for a given substrate (in this case gold-coated glass) can be appreciated in Figures 4.8a and 4.8c. As seen in Figure 4.8c, when Ppy is laid down on the surface first and the admicellar polymerization of aniline follows, the resulting morphology resembles pillar-like structures instead of the wall-templated honeycomb structures observed in Figure 4.8a. This observation, schematically illustrated in Figures 4.9a and 4.9c, indicates that pyrrole/C12-sulfonate adsorb preferentially to the PANI honeycomb walls, and aniline/SDS has more affinity towards the gold substrate than Ppy. A reasonable explanation for the former can be provided by considering the oxidation state of the PANI honeycombs. As demonstrated by XPS measurements in chapter 3, approximately 61% of the total nitrogen content in PANI honeycombs formed via TAAP corresponds to positively charged nitrogen ($-N^{+\bullet}-$). Conductivity values reported in Table 4.2 also support these findings.

Hence, it is reasonable to expect that the C12-sulfonate may be preferentially adsorbed to the walls of the positively charged PANI honeycombs through an ion pairing or ion exchange mechanism.[38,54] The adsorption of monomer/surfactant to the honeycomb walls does not rule out the possibility that some monomer/surfactant may also be adsorbed (although in less amounts) to the bare substrate.

Figure 4.8d shows the result of a triple TAAP process in which a thick-wall PMMA honeycomb has been first laid down on HOPG, and subsequently used as a template for two additional admicellar polymerization steps with aniline and pyrrole monomers, respectively. Although far from perfect, a layered nanostructure consisting of three sections with different chemistry and morphology has been synthesized from a relatively simple process. In particular, it is important to note the thinning of the honeycomb wall as the honeycomb nanostructure growths in the vertical direction. This observation, schematically illustrated in Figure 4.9d, is almost certainly the result of less surfactant adsorbed to the surface of honeycomb walls of decreasing size (PMMA > PANI > Ppy).

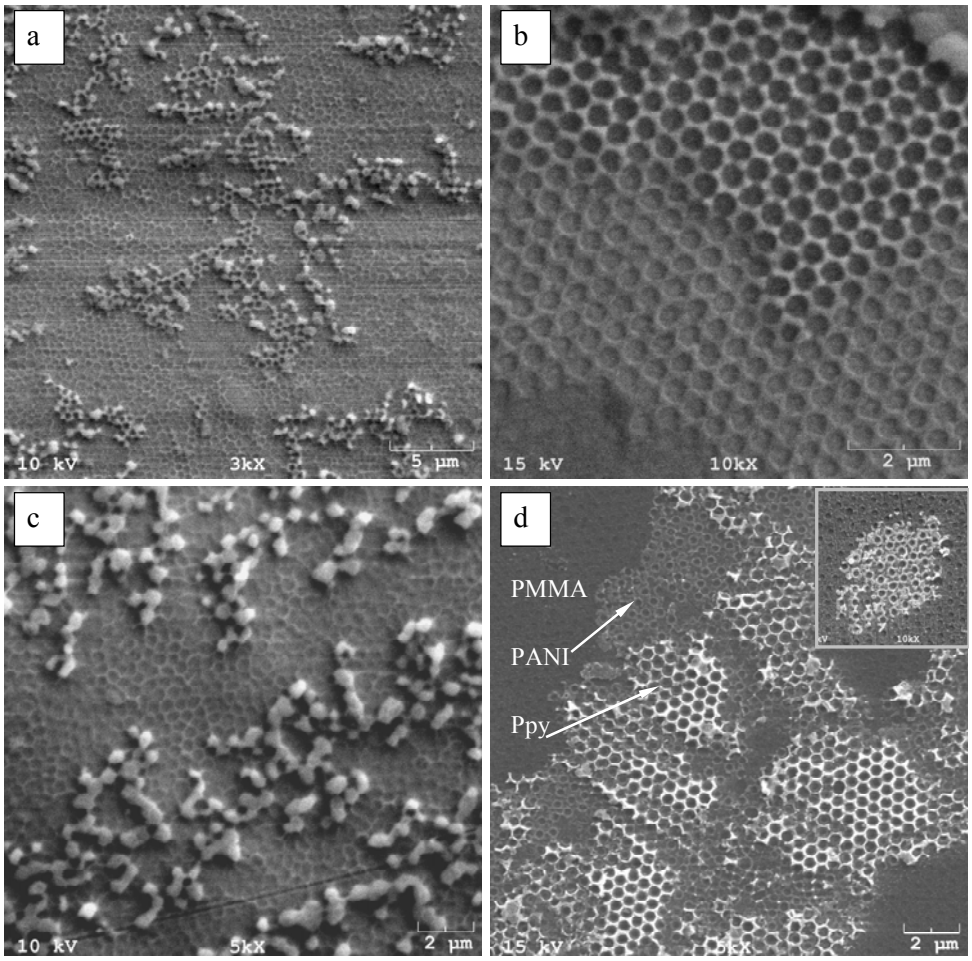

Figure 4.8. Layered polymer nanostructures via multiple TAAP on different substrates: (a) PANI honeycomb on gold-coated glass (TAAP 1), topped with fragments of a Ppy honeycomb (TAAP 2). (b) PANI honeycomb on HOPG (TAAP 1), topped with fragments of Ppy honeycombs (TAAP 2). (c) Ppy honeycomb on gold-coated glass (TAAP 1), partially covered by irregular fragments of PANI grown on top (TAAP 2). (d) PMMA honeycomb on HOPG (TAAP 1), with an overgrown PANI honeycomb patch (TAAP 2), topped with fragments of Ppy honeycomb (TAAP 3). The inset in (d) shows a magnified image of the underlying PMMA honeycomb (TAAP 1), and the overgrown PANI honeycomb (TAAP 2). 5.4 mM AnCl/SDS, 2.7 mM pyrrole/5.4 mM C12-sulfonate, and 5.4 mM MMA/SDS solutions were utilized for the synthesis of PANI, Ppy and PMMA nanostructures, respectively. All samples were subjected to a 6h adsolubilization period, followed by polymerization for 12h at room temperature, and template removal by dissolution in toluene.

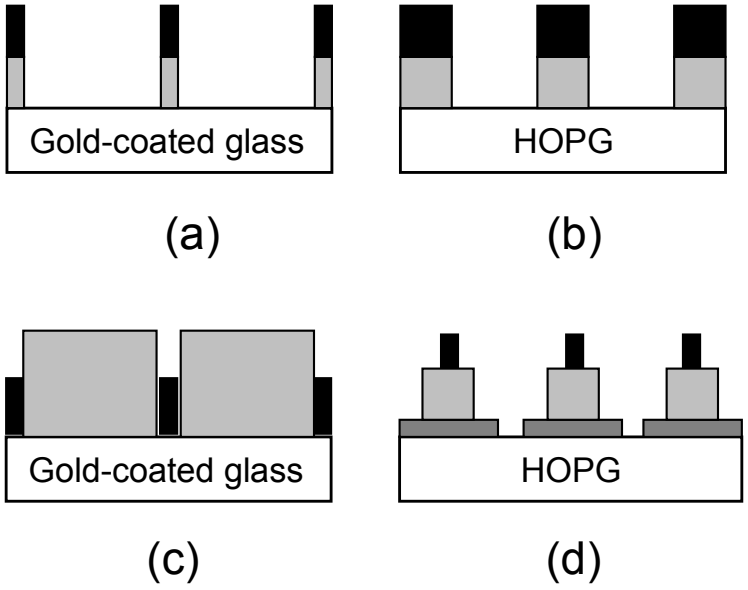

Figure 4.9. Schematics of layered nanostructures shown in Figure 4.9. Ppy is represented in black, whereas PANI and Side view, not drawn to scale.

The effect of nanostructure morphology, surface coverage and doping degree on the conductivity of PANI and Ppy nanostructures synthesized via TAAP was determined via AC impedance measurements using a current-sensing AFM apparatus. Conductivity results from AC impedance measurements are reported in Table 4.2.

Table 4.2. Electrical conductivity for PANI and Ppy nanostructures synthesized via TAAP.

Sample	Description	σ (S/cm)
1	50 nm PANI honeycomb on HOPG/high doping	3.2×10^{-3}
2	500 nm PANI honeycomb on HOPG/high doping	7.7×10^{-3}
3	500 nm PANI honeycomb on HOPG/low doping	1.1×10^{-3}
4	500 nm PANI honeycomb on HOPG/high doping/patchy (ca. 40 % surface coverage)	1.9×10^{-3}
5	500 nm PANI honeycomb on HOPG/ low doping/patchy (ca.70 % surface coverage)	7.7×10^{-5}
6	500 nm Ppy honeycomb on HOPG/C12-sulfonate (45 % CMC)	1.29×10^{-5}
7	501 nm Ppy honeycomb on HOPG/C10-sulfonate (45 % CMC)	4.97×10^{-3}
8	500 nm Ppy honeycomb on HOPG/C8-sulfonate (45 % CMC)	1.9×10^{-6}

The conductivity values reported in Table 4.2 are in agreement with literature values of electrical conductivity for PANI and Ppy thin films determined from AC impedance measurements.[55-58] These conductivity values are also consistent with the 61% doping degree and the presence of PANI in its emeraldine salt (conductive) as determined from XPS measurements in chapter 3. Several observations can be made from the data shown in Table 4.2:

With regards to the effect of template size on the measured values of electrical conductivity of PANI honeycombs on HOPG, it can be seen that when the same conditions of polymerization and doping are preserved but the template size is change (i.e. use 50 nm latex spheres instead of 500 nm spheres), the conductivity decreases slightly from 7.7×10^{-3} S/cm (sample 2) to 3.2×10^{-3} S/cm (sample 1). This is not surprising since the amount of PANI templated by the 50 nm latex monolayer is less than that templated by the 500 nm spheres. In addition, comparison of PANI samples with different doping degrees (samples 2 and 3) confirm the well-known fact that the electrical conductivity of PANI can be modified by adjusting the doping conditions. The conductivity decreases much more drastically (i.e. almost 2 orders of magnitude) in samples with different percentages of surface coverage (i.e. 40 and 70%). It is possible that different conduction mechanisms may be responsible for charge transport in samples 4 and 5; however, we do not currently have data to support this observation.

With respect to the conductivity of Ppy honeycombs synthesized on HOPG via TAAP using sulfonate surfactants with various alkyl chain lengths (samples 6 to 8), it can be seen that the values measured vary significantly depending on the surfactant used for the synthesis. As demonstrated earlier in this work, the morphology of Ppy nanostructures synthesized on HOPG via TAAP is a strong function of the surfactant used for the admicellar polymerization (Figure 4.2). As a matter of fact, for a fixed surfactant concentration (i.e. 45% CMC) the C12-sulfonate surfactant renders a honeycomb structure with few defects (Figure 4.2b), whereas the C8 and C10-sulfonate surfactant systems produce honeycombs with Ppy precipitated from solution (Figure 4.2e), and patchy honeycomb structures (Figure 4.2h), respectively. Then, it is reasonable to expect that the measured conductivity correlates with the morphologies observed in Figures 4.2b, 4.2e, and 4.2h. Results in Table 4.2 indicate that this is the case; the lowest conductivity measured (i.e. 1.9×10^{-6} S/cm) corresponds to the C8-sulfonate system, whereas a difference of almost two orders of magnitude was observed for the C10 and C12-sulfonate surfactant systems. This significant difference in the measured values of electrical conductivity for the C10 (4.97×10^{-3} S/cm), and C12-sulfonate (1.29×10^{-5} S/cm) surfactants may be due to the presence of excess Ppy as observed in Figure 4.2e. In general, caution must be exercised when interpreting conductivity data from samples with excess polymer precipitated from solution as these samples tend to have very rough surfaces on the scale of

the AFM tip (even after laser ablation), and this may cause varying amounts of interaction with the surface area of the tip. In an effort to obtain more accurate measurements (even in the presence of solution precipitated polymer), our group is currently working on measuring the electrical conductivity along the surface, rather than through the polymer film. It is expected that the polymer chains will lie parallel to the substrate's surface.[59] Hence, the values of electrical conductivity along the film surface are expected to be higher than those reported in Table 4.2.

IV. Conclusions

Template assisted admicellar polymerization (TAAP) is a rather simple, generic patterning technique which can be extended to a number of substrates and polymers. Its efficacy has been particularly demonstrated for the synthesis of both conducting (PANI and PPy) and non-conducting (PMMA) nanostructures on various substrates including HOPG, gold-coated glass, and SiO_2. The effect of various parameters such as monomer and surfactant concentration, surfactant chain length, solution ionic strength, polymerization time and temperature, and substrate choice on the morphology and electrical conductivity of the synthesized nanostructures was addressed. Control over these parameters allowed the synthesis of polymer nanopillars, nanorings, honeycomb-type structures and

"honeytubes". Preliminary results on the formation of layered polymer nanostructures via multiple TAAP's were also presented.

VI. References

1 Xu, H; Goedel, W. A. *Langmuir.* **2002**, 18, 2363.

2 Pork, S; Xia, Y. *Adv. Mater.* **1998**, 10, 1045.

3 Velev, O; Jede, T; Lobo, R; Lenhoff, A *Nature.* **1997**, 389, 447.

4 Kasemo, B; Johansson, S; Persson, H; Thormahlen, P; Zhdanov, V. *Top. Catal.* **2000**, 13, 43.

5 Barteau, M; Lyons, J; Song, I. *J. Catal.* **2003**, 216, 236.

6 Roco, M. *Curr. Opin. Biotechnol.* **2003**, 14, 337.

7 Curtis, A; Wilkinson, C. *Trends Biotechnol.* **2001**, 19, 97.

8 Holtz, J; Holtz, JS; Munro, C; Asher, A. *Anal. Chem.* **1998**, 70, 780.

9 Lee, K; Park, S; Mirkin, C; Smith, J; Mrksich, M. *Science* **2002**, 295, 1702.

10 Michel, R; Reviakine, I; Sutherland, D; Fokas, C; Csucs, G; Danuser, G; Spencer, N; Textor, M. *Langmuir* **2002**, 18, 8580.

11 Gu, J; Yam, C; Li, s; Cai, C. *J. Am. Chem. Soc.* **2004**, 126, 8098.

12 Lee, K; Kim, E; Mirkin, C; Wolinsky, S; *Nano Lett.* **2004**, 4, 1869.

13 Voros, J; Blatter, T; Textor, M. *MRS Bull.* **2005**, 30, 202.

14 Hoeppener, S; Maoz, R; Cohen, S; Chi, L; Fuchs, H; Savig, J. *Adv. Mater.* **2002**, 14, 1036.

15 Gerould, C. H. *J. Appl. Phys.* **1950**, 21,183.

16 Wang, Y; Juhue, D; Winnink, M; Leung, O; Goh, M. *Langmuir.* **1992**, 8, 760.

17 Hayashi, S; Kumamoto, Y; Suzuki, T; Hirai, T. *J. Colloid Interface Sci.* **1991**, 144, 538.

18 Moreau, W. M. *Semiconductor Lithography: Principles and Materials*; Pleanum Press: New York, 1988.

19 Brambley, D., Martin, B., Prewett, P. D. *Adv. Mater. Opt. Electron.* **1994**, 4, 55.

20 Xia, Y., Rogers, J. A., Paul, K. E., Whitesides, G. M. *Chem. Rev.* **1999**, 99, 1823.

21 Quist, A. P.; Pavlovic, E.; Oscarsson, S. *Anal. Bioanal. Chem.* **2005**, 381, 591.

22 Dickey, M.D.; Burns, R.L.; Kim, E.K.; Johnson, S.C.; Stacey, N.A.; Willson, C.G. *AICHE J.* **2005**, *51*, 2547.

23 Segalman, R.A. *Matl. Sci. Eng. R-Reports* **2005,** *48*, 191.

Guarini, L.; Black, C.T.; Tuominen, M.T.; Russell, T.P. *Science* **2000**, *276*, 2126.

24 Goran, M.; Lennox, R.B. *Nano Letters* **2001**, *1*, 735.

25 Seo, I.; Pyo, M.; Cho, G.J. *Langmuir* **2002**, *18*, 7253.

26 Park, M.; Harrison, C.; Chaikin, P.; Register, R.; Adamson, D. *Science* **1997**, *276,* 1401.

27 Cox, J; Eisenberg, A; Lennox, R. *Curr. Opin. Colloid Interface Sci.* **1999**, 4, 52.

28 Piner, R; Zhu, J; Xu, F; Hong, S; Mirkin, C. *IBM J. Res. Dev.* **1997**, 41, 159.

29 Liu, G-Y; Xu, S; Qian, Y. *Acc. Chem. Res*. **2000**, 33, 457.

30 Chang, S-S., Wu, C-G. *J. Phys. Chem. B* **2005**, 109, 18275.

31 Zhang, X., Zhang, J., Song, W., Liu, Z. *J. Phys. Chem. B* **2006**, 110, 1158.

32 Lekpittaya, P., Yanumet, N., Grady, B., O'Rear, E. *J. Appl. Polym. Sci.* **2004**, 92, 2629.

33 Wu, J., Harwell, J., O'Rear, E. A. *Langmuir* **1987**, 3, 531.

34 Asvapathanagul, P., Malakul, P., O'Haver, *J. Colloid and Interface Sci.* **2005**, 292, 305.

35 Funkhouser, G. P., Arevalo, M. P., Glatzhofer, D. T., O'Rear, E. A. *Langmuir* **1995**, 11, 1443.

36 Kitiyanan, B., O'Haver, J. H., Harwell, J. H., Osuwan, S. *Langmuir* **1996**, 12, 2162.

37 Dickson, J., O'Haver, J. *Langmuir* **2002**, 18, 9171.

38 Rosen, M. J. Surfactant and Interfacial Phenomenon; Wiley: New York, 1989.

39 Fedorova, S., Stejskal, J. *Langmuir* **2002**, 18, 5630.

40 Riede, A., Helmstedt, M., Sapurina, I., Stejskal, J. *Journal of Colloid and Interface Science* **2002**, 248, 413.

41 Wang, Z-N., Wu, Y-F., Wang, Z-W., Gao, Y-A., Li, G-Z., Zhang, G-Y. *J. Dispersion Science and Technology* **2004**, 25, 771.

42 House, E., Wolfenden, J. *J. Am. Chem. Soc.* **1952**, 74, 562.

43 Bard, A., Faulkner, L. Electrochemical Methods, Fundamentals and Applications; Wiley: New York, 1980.

44 Wei, Y., Sun, Y., Tang, X. *J. Phys. Chem.* **1989,** 93**,** 4878.

45 Winzer, M., Kleiber, M., Dix, N., Wiesendanger, R. *Appl. Phys. A* **1996**, 63, 617.

46 Iler, R. *The Chemistry of Silica: Solubility, Polymerization, Colloid and Surface Properties, and Bichemistry*., Wiley: New York, 1979.

47 Feick, J., Velegol, D. *Ind. Eng. Chem. Res*. **2004**, 43, 3478.

48 Carswell, A. *Adsorbed Surfactant at the Solid/Liquid Interface: Use of Adsorbed Surfactant Aggregates in the Synthesis of Electrically Conducting Polymers*. Ph.D. dissertation, University of Oklahoma, 2003.

49 Kiraly, Z., Findenegg, G. *Langmuir* **2005**, 21, 5047.

50 Roth, C., Dutcher, J. *J. Electroanalytical Chem.* **2005**, 584, 13.

51 Keddie, J., Jones, R., Cory, R. *Faraday Discuss.* **1994**, 98, 219.

52 van Zanten, J., Wallace, W., Wu, W-L. *Phys. Rev. E* **1996**, 53, R2053.

53 Bellamy, L. The Infrared Spectra of Complex Molecules, Vol. 1, 3rd ed; Chapman and Hall: London, 1975.

54 Somasundaran, P., Fuerstenau, D. *J. Phys. Chem*. **1966**, 70, 90.

55 Ou, R., Gerhardt, R., Samuels, R. *J. Polym. Sci. B : Polymer Physics* **2003**, 41, 823.

56 Dinh, H., Vanysek, P., Birss, V. *J. Electrochem. Soc.* **1999**, 146, 3324.

57 Van der Sluijs, M., Underhill, A., Zaba, B. *J. Phys. D: Appl. Phys.* **1987,** 20, 1411.

58 Zhang, J-L., Zhang, X-g., Xiao, F., Hu, F-P. *J. Colloid and Interface Sci.* **2005**, 287, 67.

59 Mitchell, G., Geri, A. *J. Phys. D. Apply. Phys.* **1987**, 20, 1346.

Chapter 5. Conclusions and Recommendations

I. Conclusions

This work demonstrated that the Langmuir-Blodgett (LB) technique can be used to produce ordered monolayers of latex spheres on a surface by allowing the particles to self-assemble at the air-liquid interface, and then transferring the structure to a substrate through a simple dip-coating process. In chapter 2, a correlation was found between the surface tension in the presence of latex spheres and the critical spreading agent concentration at which colloidal hexagonal arrangements occur at the air-liquid interface. Based on this observation, a simple, easy to automate surface tension method has been proposed to predict the optimal conditions for the formation of ordered monolayers of monodisperse spheres on a substrate from the LB deposition technique.

Surfactant-mediated ordered monolayers of latex spheres on highly ordered pyrolytic graphite (HOPG) were found to be the result of balanced thermodynamic and kinetic driving forces. On the one hand, the surfactant concentration must be high enough (i.e. slightly above the CMC of the latex-surfactant mixture) to effectively drive the spheres to the air-liquid interface; and on the other hand, the time for phase separation (sphere precipitation) decreases as the surfactant concentration is increased for a given sphere size. Other factors

such as solvent choice, sphere/substrate chemistry and surface charge homogeneity, humidity of the environment, and the rate of pulling vs. compression speed were found to significantly affect the assembly process, making very difficult (if not impossible) the formation of colloidal monolayers with cm^2-sized monocrystalline domains. As discussed in chapter 1, this is a common limitation to all the patterning methods that rely on particle lithography.

In chapter 3, polyaniline nanostructures were fabricated on HOPG via template assisted admicellar polymerization (TAAP), a technique that involves the use of surfactant surface aggregates to concentrate monomer to the surface prior to the polymerization. The resulting nanostructures were compared with similar patterns formed via polymer adsorption. The size and shape (honeycomb vs. pillars) of the nanostructures formed was dependent upon the size of the spheres utilized as the template, and the method of polymer deposition. The separation distance between the nanostructure and the sphere template was found to be consistently much larger for the TAAP-synthesized polymer compared to the adsorption case. These differences were explained in terms of the role of sphere-surfactant interactions in forming nanostructures significantly smaller than the original template.

In an extension to the work shown in chapter 3, an in-depth study of the factors affecting TAAP was presented in chapter 4 for three different monomers:

aniline, pyrrole, and methyl methacrylate; and three different surfaces: highly ordered pyrolytic graphite (HOPG), gold, and SiO_2. In general, the morphology and electrical conductivity of the synthesized nanostructures was found to depend strongly on monomer and surfactant concentration, surfactant chain length, solution ionic strength, polymerization time and temperature, substrate choice, and substrate preconditioning treatment. Control over these parameters allowed the synthesis of polymer nanopillars, nanorings, "honeytubes" and honeycomb-type structures. In addition, nanostructures consisting of layered polymer sections with different chemistry and morphology were synthesized, for the first time, via multiple TAAP's. The results were explained in terms of the amount of surfactant adsorbed as a function of the morphology and chemical affinity of the underlying substrate/polymer template.

II. Recommendations

In order to further exploit the potential of particle lithography, many challenges still need to be overcome. For instance, new methods or even modifications of existing ones must be evaluated in order to make possible the formation of defect-free, large colloidal monolayers with cm^2-sized monocrystalline domains. In particular, a modified version of Velev's controlled

spreading method discussed in chapter 1 (p. 33), in which surfactants are incorporated as spreading agents to aid in the formation of colloidal monolayers with large crystalline domains should be evaluated. Another possibility is to make further modifications to the custom-made Langmuir trough utilized in this study so that the ratio of the pulling speed to the compression speed can be precisely adjusted in small increments. It is also desirable that the device be equipped with a temperature-controlled stage, and a humidity-controlled chamber to regulate the evaporation rate of the sphere dispersion.

In general, latex particle size, particle size distribution and surface non-homogeneities have been recognized by the scientific community as some of the major limitations in advancing particle lithography. Hence, new synthetic routes for the reliable fabrication of monodispersed colloidal particles with homogeneous surface chemistries and charge distributions are much needed. It is also desirable to synthesize colloidal particles with a broad spectrum of surface chemistry choices, thus increasing their ability to interact with other substances and to carry out reactions in the interior and exterior surfaces of the particles. Furthermore, the formation of more uniform, defect-free colloidal monolayers should be greatly facilitated by the use of homogenous and atomically flat substrates.

As demonstrated in chapter 4, surface pretreatment can significantly reduce premature sphere lift-off during admicellar polymerization. Hence, a systematic study of different coating/heat treatments should be carried out in order to find the optimum conditions for enhanced surface coverage (close to 100 %) and for minimum premature sphere template loss. In addition, cleaner alternatives for template removal (e.g. mechanical removal using tape) are needed to avoid contamination of the underlying substrate. This is particularly true for the case of multiple TAAP's where the presence of redissolved PS from the latex spheres can significantly alter the surface chemistry of the underlying substrate and the resulting nanostructure. Alternatively, TAAP could be carried out on substrates masked via E-beam lithography. This will eliminate many of the limitations associated with using latex spheres as a template.

One of the outcomes of this study is a better understanding of the role of the surfactant in driving the formation of colloidal monolayers in the LB technique, and the formation of polymer nanostructures via TAAP. At this point, however, it is not clear how much surfactant adsorbs to the surface, or what is the morphology of the surfactant/monomer aggregate prior to polymerization. To address these questions adsorption isotherms in the presence of monomer and the sphere template should be measured for SDS and the C12-sulfonate surfactant. In addition, *in-situ* AFM studies, and computer simulation should be performed not

only to elucidate morphological changes during polymerization, but also as a mean to study surfactant confinement effects in templated structures at the nanometer scale.

Further characterization of structures synthesized via TAAP is needed. In particular, X-ray photoelectron spectroscopy (XPS) studies should be carried out on layered nanostructures formed via TAAP to confirm the chemical environment of each polymer layer. Gel permeation chromatography (GPC) and crystallographic studies should also be pursued in order to gain information about the molecular weight and crystallinity of the synthesized nanostructures. In addition, conductivity measurements across the surface of the film and through the film should be carried out to address the effect of the conditions of polymerization and spatial confinement on the electrical properties of nanostructures formed via TAAP.

Finally, given the flexibility of the TAAP process, many potential combinations of surfaces, surfactants, and monomers are available for further investigations. In particular, non-conducting honeycombs structures on conducting substrates should be tested as membranes for nanobattery applications. On the other hand, the building of biological sensors from conducting nanopillars and honeycombs is another area of future work.